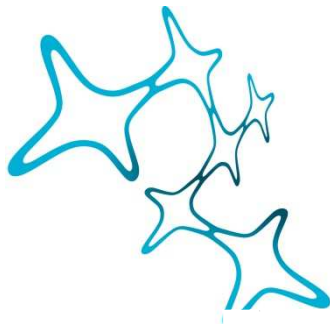


Pathomechanisms driving phase separation and aggregation of the fused in sarcoma protein in neurodegenerative diseases

Dissertation der Graduate School of Systemic Neurosciences
der Ludwig-Maximilians-Universität München



Graduate School of
Systemic Neurosciences

LMU Munich

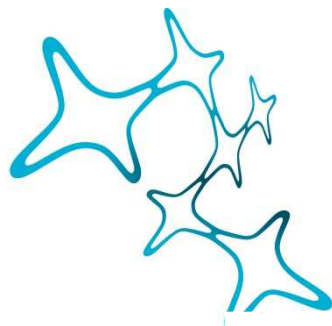


Mario Hofweber

July 2018

Pathomechanisms driving phase separation and aggregation of the fused in sarcoma protein in neurodegenerative diseases

Dissertation der Graduate School of Systemic Neurosciences
der Ludwig-Maximilians-Universität München



Graduate School of
Systemic Neurosciences

LMU Munich



Mario Hofweber

July 2018

This Ph.D. thesis was conducted and written under the supervision of Dr. Dorothee Dormann at the BioMedical Center (BMC) of the Ludwig Maximilians University Munich, Germany, in the time from the 2nd February 2015 to the 16th July 2018.

First reviewer and supervisor:	Dr. Dorothee Dormann
Second reviewer:	Prof. Dr. Dr. h.c. Christian Haass
External reviewer:	Prof. Dr. Edward Lemke
Date of submission:	18th July 2018
Date of defense:	5th December 2018

ABBREVIATION INDEX

ADMA	Asymmetric dimethylarginine
ALS	Amyotrophic lateral sclerosis
EWS	Ewing sarcoma
FTD	Frontotemporal dementia
FUS	Fused in sarcoma (also TLS)
G3BP1	Ras GTPase activating protein (SH3 domain) binding protein 1 (also G3BP stress granule assembly factor 1)
hnRNP	Heterogeneous ribonucleoprotein
HSP	Heat shock protein
IDP	Intrinsically disordered protein
LC	Low complexity
LLPS	Liquid-liquid phase separation
MAPT	Microtubule-associated binding protein Tau
MMA	Monomethyl arginine
NLS	Nuclear localization signal
PRMT	Protein arginine methyltransferase
PTM	Post-translational modification
PY-NLS	Proline (P) -tyrosine (Y) -NLS
RAN	GTP-binding nuclear protein Ran <u>or</u> repeat associated non-ATG (translation)
RBP	RNA-binding protein
RGG/RG	Arginine (R) – glycine (G) -glycine (G) / arginine (R) – glycine (G)
RNP	Ribonucleoprotein
SAM	S-adenosylmethionine
SDMA	Symmetric dimethylarginine
SG	Stress granule
TAF15	TATA binding protein-associated factor 15
TIA1	T-cell-restricted intracellular antigen 1
TDP-43	TAR DNA-binding protein of 43 kDa
TNPO1	Transportin 1 (also Karyopherin β 2)
UMA	Unmethylated arginine

INDEX

ABSTRACT	7
1 INTRODUCTION	8
1.1 ALS and FTD: late-onset neurodegenerative diseases.....	8
1.2 Genetic and neuropathological overlap of ALS and FTD	9
1.3 FUS and other FET family proteins.....	13
1.4 Nuclear import defects as a key pathomechanism in ALS and FTD.....	14
1.5 Nuclear functions of FUS.....	16
1.6 Physiological functions of FUS in the cytoplasm.....	18
1.7 Protein arginine methylation	19
1.8 Stress granules: protective messenger ribonucleoprotein (mRNP) granules.....	23
1.9 Phase separation of RBPs as driving force for protein aggregation	26
1.10 Aims of the Ph.D. project.....	36
2 RESULTS	39
2.1 The C-terminal RGG3-PY domain of FUS can undergo phase separation.....	39
2.2 The RGG3-PY domain and arginine residues are essential for phase separation of FUS	44
2.3 Phase transitions of FUS are suppressed by TNPO1 <i>in vitro</i>	49
2.4 TNPO1 exerts its chaperone function in cells independent of its nuclear import activity ...	54
2.5 Mechanisms contributing to the chaperone activity of TNPO1	57
2.6 Loss of arginine methylation promotes phase separation of FUS.....	61
2.7 Loss of arginine methylation alters droplet dynamics and promotes SG association of FUS...	65
2.8 Arginine methylation stabilizes RNA binding of FUS-RGG3-PY.....	67
2.9 ALS-associated FUS-P525L mutant impairs chaperone activity of TNPO1	69
3 DISCUSSION	74
3.1 Arginines in the RGG/RG motif are crucial for phase separation of FUS.....	74
3.2 Nuclear import receptors as chaperones	75
3.3 Possible mechanisms underlying the chaperone activity of TNPO1.....	78
3.4 Arginine methylations suppresses phase separation and SG association of FUS.....	80
3.5 Distinct mechanisms driving phase separation and SG association of FUS in ALS-FUS and FTD-FUS.....	81
3.6 Conclusion and Outlook.....	85
4 EXPERIMENTAL PROCEDURES	88
4.1 Cloning of cDNA constructs	88
4.2 Recombinant protein expression and purification	89
4.3 <i>In vitro</i> methylation.....	92

4.4	<i>In vitro</i> transcription	92
4.5	<i>In vitro</i> phase separation assays	92
4.6	Cell culture and transfection.....	94
4.7	Semi-permeabilized cell assay	94
4.8	Filter-binding assay	94
4.9	Electrophoretic mobility shift assay (EMSA).....	95
4.10	Immunostaining or Immunocytochemistry	95
4.11	Microscopy.....	95
4.12	Nuclear magnetic resonance (NMR).....	97
4.13	Isothermal Calorimetry (ITC).....	97
4.14	Quantification and analysis.....	97
5	APPENDIX.....	100
6	REFERENCES.....	104
7	PUBLICATION RECORD	123
8	ACKNOWLEDGEMENT	124
9	EIDESSTATTLICHE VERSICHERUNG/AFFIDAVIT.....	125
10	DECLARATION OF COPYRIGHT AND CONTRIBUTIONS	126

ABSTRACT

Nuclear depletion and cytosolic aggregation of the RNA-binding protein FUS are pathological hallmarks in a subset of patients suffering from frontotemporal dementia (FTD) and amyotrophic lateral sclerosis (ALS). Defective nuclear import of FUS by its nuclear import receptor Transportin (TNPO1) is a major pathomechanism contributing to the pathogenesis of ALS and FTD with FUS pathology (ALS-FUS, FTD-FUS). Mutations in the nuclear localization signal (NLS) of FUS that disrupt binding to TNPO1 are associated with ALS-FUS. In FTD-FUS patients, no such NLS mutations have been identified so far, but TNPO1 is aggregated and arginine methylation of FUS, which regulates FUS-TNPO1 interaction, is lost. Defective nuclear import of FUS causes an accumulation of FUS in the cytoplasm and, upon cellular stress, favors recruitment of FUS into stress granules (SGs), which have been proposed to be condensation sites for aberrant phase separation and aggregation of FUS. It is not clear which factors suppress phase separation and aggregation in healthy brains. Furthermore, it remains also ambiguous whether the loss of arginine methylation is involved in the aggregation process and which physiological roles arginine methylation of FUS plays. Thus, these questions were addressed in this Ph.D. thesis.

I could show that TNPO1 has a dual function towards FUS, namely it not only mediates nuclear import of FUS, but also acts as a FUS chaperone in the cytoplasm and thereby suppresses RGG/RG-driven liquid-liquid phase separation (LLPS), SG association and aggregation of FUS. The chaperone activity is specific to TNPO1, since other FUS RGG/RG domain interacting proteins or other importins are not able to suppress phase separation of FUS. ALS-associated FUS-NLS mutations impairing nuclear import of FUS furthermore reduce the chaperone activity of TNPO1. Moreover, I could demonstrate that arginine methylation also has a suppressive effect on LLPS and SG partitioning of FUS. Loss of arginine methylation, as seen in FTD-FUS patients, enhances phase separation and promotes SG recruitment of FUS. These data reveal two novel regulatory mechanisms of liquid phase homeostasis that suppress phase separation and SG recruitment of FUS and are impaired in ALS-FUS and FTD-FUS, respectively.

1 INTRODUCTION

1.1 ALS and FTD: late-onset neurodegenerative diseases

Amyotrophic lateral sclerosis (ALS) and frontotemporal dementia (FTD) are fatal, late-onset neurodegenerative diseases for which no curative treatments are available. ALS, also known as Lou Gehrig's or Charcot's disease, is the most common adult motor neuron disease caused by a progressive degeneration of upper and lower motor neurons. The neuronal death causes muscle weakness, atrophy and spasticity progressively affecting the patient's moving, swallowing, speaking and breathing abilities (Rothstein, 2009). Eventually, patients die of respiratory failure within 1-5 years of disease onset (Kiernan et al., 2011). While most ALS cases are considered sporadic (sALS), 5-10% of cases are familial (fALS), showing an autosomal dominant pattern of inheritance (Da Cruz and Cleveland, 2011).

After Alzheimer's disease (AD), FTD is the second most prevalent form of dementia in patients younger than 65 years. Hallmarks of the disease are selective degeneration of the frontal and temporal lobes hence the term FTLD (frontotemporal lobar degeneration) is commonly used to describe the neuropathology in FTD. Clinical characteristics of FTD are severe and progressive alterations in personality, behavior and/or language difficulties (Neumann et al., 2012; Rademakers et al., 2012). Clinically, FTD cases can be subdivided into behavioral variant FTD (bvFTD) and two forms of primary progressive aphasia: progressive non-fluent aphasia and semantic dementia (Gorno-Tempini et al., 2011; Rascovsky et al., 2011). In contrast to AD, memory is relatively well preserved at early stages of FTD, but with disease progression patients suffer from severe cognitive and physical decline and eventually die within 3-10 years of disease onset. Around 25-50% of all cases are classified as familial FTD (Rademakers et al., 2012; Rohrer et al., 2009; Seelaar et al., 2008).

ALS and FTD have been shown to have a large clinical overlap, since up to 15-20% of FTD cases exhibit clinical criteria for ALS and *vice versa*. While up to a third of FTD patients show motor neuron dysfunction, 30-50% of ALS patients suffer from cognitive defects (Lomen-Hoerth et al., 2002; Murphy et al., 2007; Wheaton et al., 2007).

1.2 Genetic and neuropathological overlap of ALS and FTD

Due to extensive studies in genetics and neuropathology of ALS and FTD, the molecular culprits for the clinical disease continuum have been largely uncovered (Ling et al., 2013; Van Langenhove et al., 2012). These studies have revealed that the clinical overlaps of ALS and FTD is also reflected in a genetic and neuropathological overlap:

The most common genetic cause of ALS and FTD is an abnormal GGGGCC hexanucleotide repeat expansion in a non-coding region of the *C9orf72* gene (DeJesus-Hernandez et al., 2011; Mackenzie and Neumann, 2016; Renton et al., 2011) (Fig. 1A). While healthy individuals typically carry 2-22 hexanucleotide repeats in the *C9orf72* gene, ALS/FTD patients can have hundreds or even thousands of repeats (DeJesus-Hernandez et al., 2011; Renton et al., 2011; van Blitterswijk et al., 2012).

Another genetic cause for ALS are mutations in the *TARDBP* gene (encoding for the TDP-43 protein) which have been associated with 4% of familial and 1.5% of sporadic ALS cases. So far, more than 38 ALS-linked *TARDBP* mutations have been identified (Mackenzie et al., 2010). Notably, most of the disease-linked mutations in TDP-43 have been identified in the prion-like C-terminal domain (Cushman et al., 2010; Fuentealba et al., 2010; Hock and Polymenidou, 2016; Lagier-Tourenne et al., 2010; Ling et al., 2013). In addition to mutations in TDP-43, cases with *C9orf72* repeat expansions also show TDP-43 pathology (Mackenzie et al., 2013). Other genetic causes for TDP-43-positive inclusion in FTD are mutations in the granulin gene (*GRN*) and in the valosin containing protein gene (*VCP*) (Mackenzie and Neumann, 2016) (Fig. 1A) which is implicated in autophagy (Ju et al., 2009). Based on the anatomical distribution, morphology and composition of inclusion, pathology in FTD-TDP is subdivided in four different patterns (type 1-4) (Mackenzie et al., 2010). Mutations in FTD seem to be quite rare, since only three different *TARDBP* mutations have been identified in patients so far (Mackenzie and Neumann, 2016; Mackenzie et al., 2010).

In 2009, mutations in *FUS* (Fused in sarcoma) have been identified in a subset of familial ALS (fALS) patients that are predominantly clustered in the C-terminal RGG3-PY domain (Kwiatkowski et al., 2009; Vance et al., 2009). Unlike in ALS-FUS patients, no *FUS* mutations in clinical FTD have been confirmed (Neumann et al., 2009; Rohrer et al., 2009; Snowden et al., 2011; Urwin et al., 2010) (Fig. 1A). The majority of cases with proven FTD-FUS pathology are sporadic (Urwin et al., 2010).

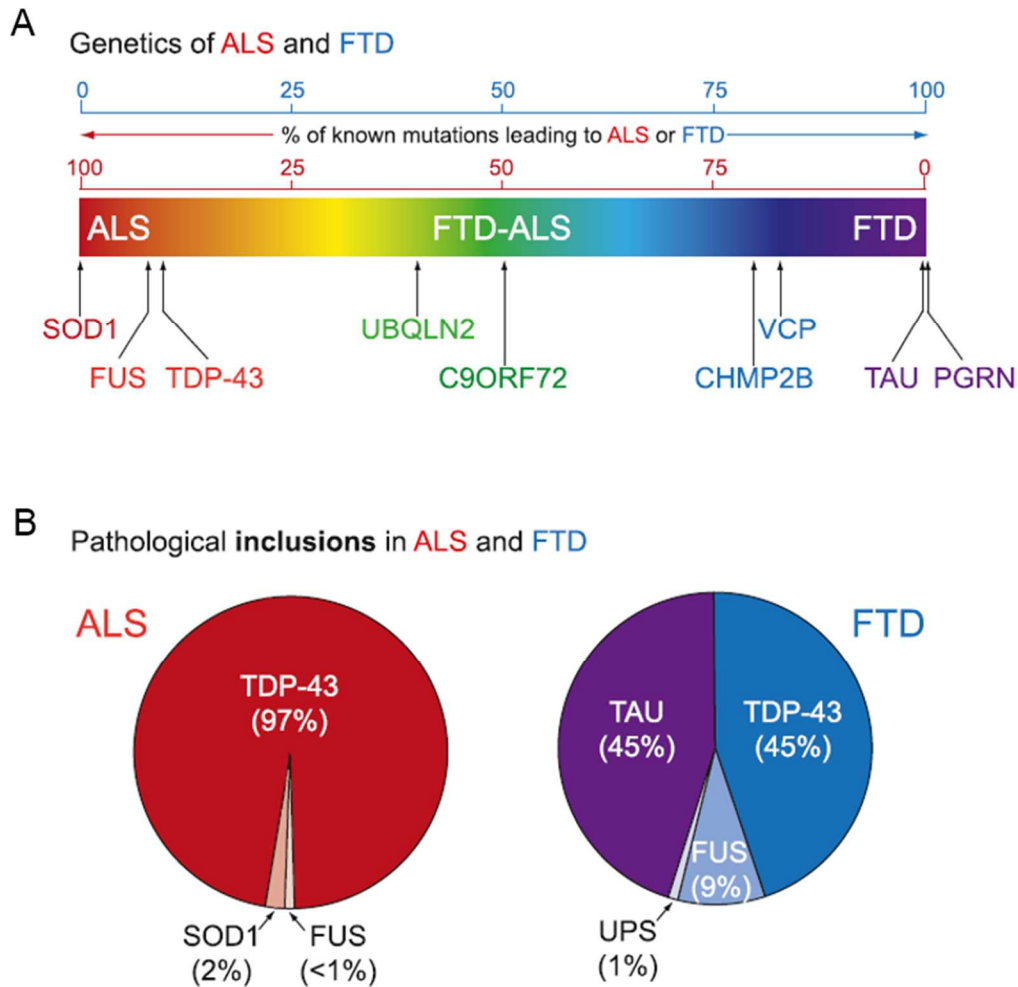


Figure 1: Disease continuum of ALS and FTD. A) ALS and FTD are the extreme ends of an overlapping disease spectrum sharing clinical symptoms (ALS in red and FTD in purple). Major genetic risk factors are delineated according to the likelihood of identified mutations to cause ALS or FTD. **B)** Distribution of the major accumulating protein in pathological inclusion in ALS and FTD. Inclusions of TDP-43 and FUS in ALS and FTD represent the neuropathological overlap of the two diseases. Figure reproduced from (Ling et al., 2013) with permission from Elsevier.

The molecular pathology of ALS and FTD is characterized by a nuclear depletion, cytosolic mislocalization and aggregation of RBPs in neurons and glia cells (Fig. 2). In 97% of all ALS cases and almost 50 % of FTD patients, pathological inclusions positive for TDP-43 have been identified (Arai et al., 2006; Neumann et al., 2006) (Fig. 1B). In addition to the above mentioned TDP-43 pathology, three different, not mutually exclusive, pathomechanisms have been proposed for *C9orf72* repeat expansions, (Gitler and Tsuiji, 2016): First, patients carrying *C9orf72* repeat expansions display repeat RNA foci that sequester RNA-binding proteins to the nucleus (Haeusler et al., 2014; Lee et al., 2013; Mori et al., 2013b), most likely leading to disturbances in RNA metabolism (Kwon et al., 2014). Second, both sense (GGGGCC) and antisense (GGCCCC) repeat RNA transcripts can be translated by

unconventional repeat associated non-ATG-initiated (RAN) translation, giving rise to five different dipeptide repeat (DPR) proteins, namely glycine-arginine (GR), proline-arginine (PR), glycine-alanine (GA), glycine-proline (GP) and proline-alanine (PA) (Ash et al., 2013; Gendron et al., 2013; Mori et al., 2013a; Mori et al., 2013b; Zu et al., 2013). Third, haploinsufficiency leading to reduced expression of *C9orf72* gene product is considered as a third possible mechanism how hexanucleotide repeat expansions in the *C9orf72* gene contribute to pathogenesis (Gitler and Tsuiji, 2016). In addition, a subset of ALS and FTD cases are characterized by cytoplasmic aggregation of FUS. ALS cases with FUS pathology are usually associated with FUS mutations which account for ~ 4% of familial and <1 % of sporadic ALS cases (Kwiatkowski et al., 2009; Mackenzie and Neumann, 2016; Vance et al., 2009). Pathological inclusions containing FUS were found in 5-10% of all FTD cases (Neumann et al., 2009) (Fig. 1B). FTD-FUS includes three distinct neuropathological subgroups: atypical FTLD with ubiquitin-positive inclusions (aFTLD-U), neuronal intermediate filament inclusion disease (NIFID) (Neumann et al., 2009) and basophilic inclusion body disease (BIBD) (Munoz et al., 2009). In very rare ALS cases, other RBPs, e.g. hnRNP-A1 and hnRNP-A2, have also been identified in pathological aggregates (Kim et al., 2013).

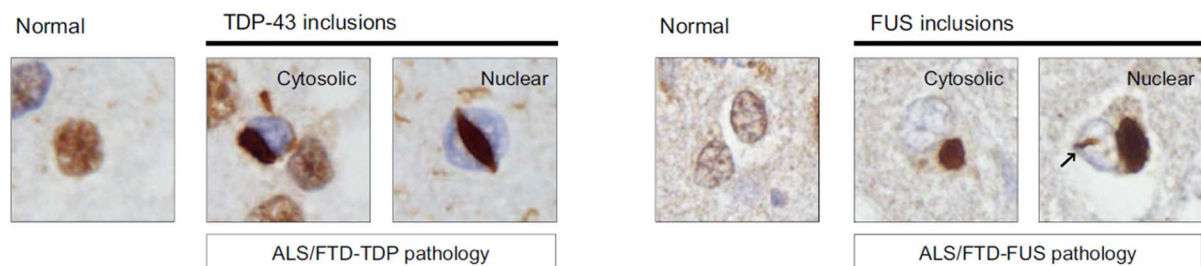


Figure 2: TDP-43 and FUS pathology in ALS/FTD. In healthy brains, FUS and TDP-43 are mainly localized in the nucleus (normal, left). Immunohistochemistry of TDP-43 and FUS showing characteristic depletion of diffuse nuclear localization and accumulation in cytosolic and rarely nuclear inclusions in *post mortem* brains of ALS and FTD patients (right, ALS/FTD pathology). Figure reproduced from (Ederle and Dormann, 2017) with permission from *John Wiley and Sons*.

Besides the above-mentioned characteristic nuclear depletion and cytosolic aggregation of the specific RBPs (Fig. 2), TDP-43 and FUS cases in ALS and FTD share other pathological features. First, TDP-43 inclusions have been reported to be positive for p62 and ubiquitin and TDP-43 is hyperphosphorylated (Arai et al., 2006; Neumann et al., 2006). Similarly, immunoreactivity for ubiquitin and p62 in inclusions is also a common hallmark of ALS-FUS and FTD-FUS (Baumer et al., 2010; Neumann et al., 2009; Seelaar et al., 2010). p62 facilitates autophagic degradation of

ubiquitinated proteins (Pankiv et al., 2007) and its aggregation may impair the ubiquitin-proteasome system (UPS) (Korolchuk et al., 2010). Second, pathological TDP-43 and FUS inclusion in ALS and FTD were shown to co-localize with various stress granule (SG) marker proteins, respectively. While co-localization of TIA1, PABP-1 and Staufen was found in TDP-43-positive inclusion in ALS patients, TDP-43 inclusion in FTD cases were shown to contain PABP-1 and eIF3 (Bentmann et al., 2013). Inclusions in both ALS-FUS and FTD-FUS have been demonstrated to be positive for PABP-1 and eIF4G (Baumer et al., 2010; Dormann et al., 2010), but cytoplasmic FUS aggregates immunoreactive for TIA1 have been found only in FTD-FUS patients (Fujita et al., 2008).

In addition to several pathological commonalities, there are also slight differences between ALS and FTD associated with the same RBP. In the cortex of FTD-TDP patients, TDP-43 is, in addition, proteolytically cleaved to C-terminal fragments that are highly aggregation-prone and co-deposited with the full-length TDP-43 protein (Arai et al., 2006; Neumann et al., 2006). Notably, in pathological inclusions in the cortex and hippocampus of FTD-TDP patients, full-length TDP-43 is less abundant than phosphorylated C-terminal TDP-43 fragments, whereas inclusions in the spinal cord of ALS-TDP patients contain mainly phosphorylated full-length TDP-43 (Hock and Polymeridou, 2016; Igaz et al., 2008). Moreover, co-labeling of FTD-TDP inclusions with the SG marker PABP-1 was only demonstrated in presence of full-length TDP-43 in spinal cord but not in hippocampal and cortex indicating that these converging observations may emerge from the fact that different brain regions have different TDP-43 species (Bentmann et al., 2013). Although pathological inclusions in both ALS-FUS and FTD-FUS patients contain FUS, the inclusions are characterized by a distinct protein composition (Dormann et al., 2012; Neumann et al., 2011; Neumann et al., 2012) (see section 1.4 for further details). In contrast to ALS with FUS mutations, co-deposition of two closely related proteins, namely Ewing sarcoma protein (EWS) and TATA-binding protein-associated factor 15 (TAF15), has been discovered only in FTD-FUS cases (Davidson et al., 2013; Neumann et al., 2011). Furthermore, the characteristic pattern of arginine methylation of FUS is lost (Dormann et al., 2012; Suarez-Calvet et al., 2016) and the nuclear import receptor Transportin (TNPO1) co-aggregates (Brelstaff et al., 2011; Davidson et al., 2013; Neumann et al., 2012; Troakes et al., 2013). These differences between ALS and FTD with FUS pathology indicate that both diseases develop from different pathomechanisms (Dormann and Haass, 2013).

1.3 FUS and other FET family proteins

FUS is a member of the FET protein family that also includes two other members, Ewing sarcoma protein (EWS) and TATA binding protein-associated factor 15 (TAF15) (Tan and Manley, 2009). The FET proteins have a homologous domain structure with an N-terminal transcriptional activation domain, several nucleic acid-binding motifs as well as a C-terminal PY-NLS (Fig. 3).

FUS, also known as translocated in liposarcoma (TLS), is a ubiquitously expressed DNA/RNA-binding protein with a length of 526 amino acids. FUS contains an N-terminal serine-tyrosine-glycine-glutamine-rich (SYGQ) domain which is commonly referred to as low-complexity (LC) domain due to its low-amino acid complexity. It is also termed “prion-like domain” due to its similarity to yeast prions (Alberti et al., 2009; Cushman et al., 2010). The SYGQ-rich domain is thought to mediate FUS aggregation (Burke et al., 2015; Kato et al., 2012; Murakami et al., 2015; Patel et al., 2015; Sun et al., 2011) and self-assembly of FUS (Yang et al., 2014) and is involved in transcriptional activation (Crozat et al., 1993; Rabbitts et al., 1993). The finding that translocation of the SYGQ-rich domain resulting in fusion to transcription factors, such as CHOP, gives rise to fusion oncogenes in human myxoid liposarcomas demonstrates its involvement in transcriptional activation.

Moreover, FUS harbors multiple domains with nucleic acid binding motifs that mediate both protein-RNA as well as protein-protein interactions. The first arginine-glycine-glycine rich domain (RGG1) is followed by a highly conserved RNA recognition motif (RRM) and two more RGG domains (RGG2 and RGG3) that flank a zinc finger (ZnF).

In addition, FUS contains a C-terminal non-classical NLS, composed of a proline-tyrosine NLS (PY-NLS) (Lee et al., 2006) and the preceding RGG3 domain (Dormann et al., 2012). The nuclear import receptor TNPO1, also known as Karyopherin β 2, binds to the NLS and mediates the import of PY-NLS-containing proteins from the cytoplasm into the nucleus (Lee et al., 2006).

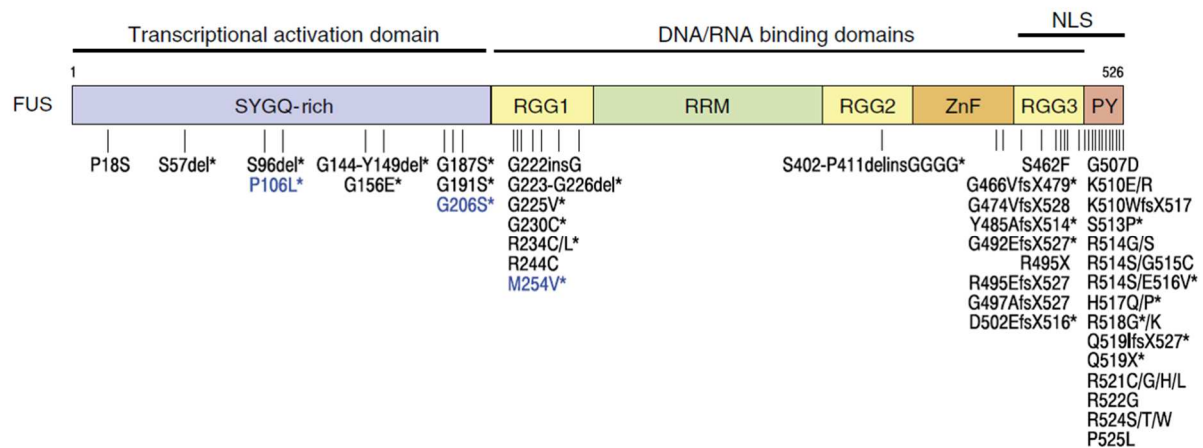


Figure 3: Domain structure and disease-associated mutations of FUS. FUS harbors a N-terminal prion-like serine-tyrosine-glycine-glutamine (SYGQ)-rich domain, three arginine-glycine-glycine (RGG)-rich domains, an RNA recognition motif (RRM), and a zinc-finger (ZnF) and a non-classical PY-nuclear localization signal (PY-NLS). The RGG3 domain together with the PY-NLS function as the protein's NLS, recognized by the nuclear import receptor Transportin (TNPO1). A number of dominant mutations in FUS have been identified in ALS (black) and rare FTD (blue) cases (including missense, deletions (del), insertions (ins), frameshifts (fs), and truncations (X)). Most disease-linked mutations cluster in the C-terminal NLS. Figure reproduced from (Dormann and Haass, 2013) with permission from *Elsevier*.

1.4 Nuclear import defects as a key pathomechanism in ALS and FTD

The pathology of a subset of ALS and FTD patients is characterized by a sequestration of RBPs, such as TDP-43 and FUS, from the nucleus into cytoplasmic inclusions in neurons and glia cells indicating nuclear import defects (Fig. 2).

Nuclear import of FUS is mediated by interaction of its C-terminal NLS with TNPO1 that translocates FUS across the nuclear pore complex into the nucleus. The FUS-NLS is composed of the PY-NLS and the neighboring RGG3 domain (Dormann et al., 2012). Cargo binding of TNPO1 in the cytoplasm and cargo release in the nucleus is regulated by the small GTPase Ran and its proteins regulating its GTP-bound state (Gorlich et al., 1996). In the cytoplasm, low levels of RanGTP allow tight binding of TNPO1 to cargoes containing a PY-NLS. In the nucleus, RanGTP binds TNPO1 with high affinity and mediates dissociation of the import complex (Lee et al., 2006).

1.4.1 Nuclear import defects in fALS-FUS

FUS mutations have been identified to cause familial ALS with FUS pathology. These ALS-associated mutations are mostly missense, nonsense or frameshift mutations in the C-terminal RGG3-PY domain (Dormann and Haass, 2013; Kwiatkowski et al., 2009; Vance et al., 2009) (Fig. 3). Cell culture studies showed that fALS-associated point mutations in the PY-NLS, e.g. R521G, R522G, R524S, P525L, show varying degrees of cytosolic mislocalization, ranging from slightly mislocalized for the R521G and R524S mutations (16 and 21% cytosolic, respectively) over an intermediate mislocalization for R522G (45%) to a very severe phenotype for P525L (65 %) (Dormann et al., 2010). With an early disease onset in the mid-twenties and a rapid disease progression, the P525L mutation causes an extremely aggressive form of fALS (Chio et al., 2009; Kwiatkowski et al., 2009). Hence, there is a correlation between the degree of cytosolic mislocalization of FUS with clinical symptoms, i.e. the more FUS is mislocalized the earlier and more severe the disease progresses (Dormann et al., 2010). Dormann and colleagues demonstrated that ALS-associated mutations in the NLS or complete deletion of the signal sequence drastically impair or disrupt TNPO1-mediated nuclear import of FUS (Dormann et al., 2012; Dormann et al., 2010). Mouse models carrying ALS-associated mutations or deletions of the NLS of FUS exhibit age-dependent degeneration of motor neurons (Devoy et al., 2017; Scekcic-Zahirovic et al., 2017; Sharma et al., 2016), demonstrating that impaired nuclear import of FUS indeed causes motor neuron degeneration. Together, these studies provide strong evidence that defective nuclear import of FUS is a key pathomechanism of ALS-FUS.

1.4.2 Observed defects in FTD-FUS

In contrast to fALS-FUS, no mutations have been identified in FTD-FUS cases so far (Neumann et al., 2009; Rohrer et al., 2009; Snowden et al., 2011; Urwin et al., 2010). Although pathological inclusions in both ALS-FUS and FTD-FUS patients are FUS-positive, they are completely distinct in protein composition (Dormann et al., 2012; Neumann et al., 2011; Neumann et al., 2012). Different from ALS-FUS, cytoplasmic inclusion in FTD-FUS do not only contain FUS, but also the other two members of the FET protein family, EWS and TAF15 (Neumann et al., 2011). Interestingly, the nuclear import receptor TNPO1 also shows nuclear depletion and co-aggregation in *post mortem* brains of FTD-FUS patients (Brelstaff et al., 2011; Davidson et al., 2013; Neumann et al., 2012; Troakes et al., 2013). This indicates that TNPO1-mediated nuclear import could be impaired in these patients, although a general defect in the TNPO1 import machinery seems unlikely as other PY-NLS containing TNPO1 cargoes, such as hnRNP-A1, are not altered. This points to further defects specifically affecting the FET family proteins (Neumann et al., 2011) (for details see section 1.7).

1.4.3 Nuclear import defects in TDP-43 proteinopathies and *C9orf72*-ALS/FTD

Nuclear import defects seem not to be exclusive for cases with FUS aggregates, but may also play an important role in ALS/FTD cases with TDP-43 pathology. TDP-43 is imported into the nucleus by the heterodimeric nuclear import receptor Importin α /Importin β 1, also known as karyopherin α / β 1 (Nishimura et al., 2010; Winton et al., 2008). A study of Nishimura and colleagues showed that knockdown of Importin β 1 and cellular apoptosis susceptibility protein (CAS, member of the karyopherin β family, also known as exportin-2), which recycles karyopherin α s back to the cytoplasm, results in cytoplasmic accumulation of TDP-43. Additionally, CAS and Importin α 2 levels are reduced in spinal cord and cortex of FTD patients showing TDP-43 pathology (Nishimura et al., 2010). Notably, aggregated TDP-43 sequesters components of the nucleocytoplasmic transport machinery, such as the nucleoporins Nup98, Nup214, and Nup358, and impairs nuclear protein import as well as mRNA export (Chou et al., 2018). Moreover, Kinoshita and colleagues showed that also in sporadic and SOD1-linked ALS cases nuclear importin β is significantly reduced (Kinoshita et al., 2009). Several recent studies in yeast and flies have linked the *C9orf72* repeat expansion with dysregulated nuclear transport (Boeynaems et al., 2016; Freibaum et al., 2015; Jovicic et al., 2015; Zhang et al., 2015). Unbiased genetic screens to identify modifiers of *C9orf72* toxicity revealed several factors implicated in nucleocytoplasmic shuttling as major toxicity modulators. Zhang et al. reported that Ran GTPase-activating protein 1 (RanGAP1) overexpression rescues *C9orf72* repeat expansion-induced toxicity while RNAi-mediated knockdown of RanGAP1 enhances toxicity. Furthermore, upregulation of importins rescues eye degeneration (Zhang et al., 2015). Concordantly, Boeynaems and colleagues demonstrated enhancement of degenerative eye phenotypes in *Drosophila* caused by poly-PR toxicity upon RanGAP1 downregulation (Boeynaems et al., 2016). Homologues of human TNPO1 (Kap104 in yeast, Trn in fly) were identified in these genetic screens. While overexpression of Kap104 was shown to suppress DPR toxicity in yeast (Jovicic et al., 2016), deletion of Trn in *Drosophila* increased eye degeneration (Boeynaems et al., 2016; Freibaum et al., 2015). In all, these studies provide strong evidence that dysregulation of nucleocytoplasmic transport may play a crucial role in disease initiation, causing nuclear loss of function and cytoplasmic gain of function of RBPs in ALS/FTD (Boeynaems et al., 2016).

1.5 Nuclear functions of FUS

FUS is a mostly nuclear RBP with multiple functions in DNA/RNA processing at the transcriptional and post-transcriptional level both in the nucleus and in the cytoplasm. Due to this plethora of functions, it seems obvious that its sequestration from the nucleus to cytoplasmic protein inclusions leads to

detrimental RNA processing defects and thus may contribute to the pathogenesis of ALS and FTD (Ederle and Dormann, 2017).

Originally identified as fusion oncogene, FUS was shown to be a potent transcriptional activator (Croizat et al., 1993; Rabbitts et al., 1993). The SYGQ-rich domain mediates FUS dimerization and subsequently binds transcriptionally active chromatin and thus regulates transcriptional initiation (Ratti and Buratti, 2016; Yang et al., 2014). Further studies revealed interactions with RNA polymerase II (RNAP II) and the TFIID complex, both components of the pre-initiation complex (PIC). FUS binds to and controls phosphorylation of the catalytic domain (CTD) of RNAP II on Serine 2 (Ser2) and thus regulates the activity of RNAP II (Bertolotti et al., 1996; Schwartz et al., 2012). Furthermore, FUS binding to ssDNA gene promoters also regulates gene expression (Tan et al., 2012). Importantly, ALS-associated mutations of FUS were reported to reduce transcriptional regulation by reduced binding to chromatin and RNAPII (Schwartz et al., 2014; Yang et al., 2014).

FUS is furthermore involved in splicing, not only by directly binding nascent pre-mRNAs, but also by interacting with essential components of the splicing machinery. One well-studied splice target of FUS is the pre-mRNA of the neuronal microtubule-associated binding protein Tau (*MAPT*) which has a complex alternative splicing regulation resulting in six different isoforms (Goedert and Spillantini, 2011). Multiple studies demonstrated that loss of FUS causes an increase in inclusion of exons 2, 3, and 10, respectively (Lagier-Tourenne et al., 2012; Orozco and Edbauer, 2013; Orozco et al., 2012; Rogelj et al., 2012). Since Tau-pathology is associated with FTD and other neurodegenerative diseases (Goedert and Spillantini, 2011), aberrant splicing of *MAPT* may contribute to neurodegeneration in cases with FUS pathology (Orozco and Edbauer, 2013). Importantly, FUS also binds to its own pre-mRNA and thus autoregulates its own expression, by repression of exon 7 splicing and subsequent degradation of the exon 7-skipped splice variant by nonsense-mediated decay (NMD) (Lagier-Tourenne et al., 2012; Zhou et al., 2013). FUS has been reported to be essential for assembly of spliceosomes by interacting with components of the spliceosome machinery, namely SMN proteins, U1 small nuclear ribonucleoprotein (snRNP) and the Sm-snRNP complex (Gerbino et al., 2013; Ratti and Buratti, 2016; Yamazaki et al., 2012). ALS-associated FUS mutations cause a dramatic reduction of nuclear Gems, severe splicing impairment, and reduce FUS binding to U1-snRNP (Ratti and Buratti, 2016; Sun et al., 2015; Tsuiji et al., 2013; Yamazaki et al., 2012; Yu et al., 2015). Since FUS interacts with both RNAP II and U1-snRNP, it is likely that FUS couples transcription and splicing (Yu and Reed, 2015).

In 1999, Baechtold and colleagues provided evidence that FUS is involved in DNA damage repair by demonstrating that FUS promotes D-loop formation and homologous recombination in the repair of

DNA double strand breaks (DSBs) (Baechtold et al., 1999; Ratti and Buratti, 2016). FUS knock-out mice were shown to have defective B-lymphocyte development, high genomic instability, elevated radiation sensitivity as well as defects in spermatogenesis (Hicks et al., 2000; Kuroda et al., 2000). Furthermore, interaction of FUS with factors involved in DNA damage repair, namely Poly-ADP-ribose polymerase 1 (PARP-1) and HDAC1, at sites of DNA damage is required for proper DNA damage response (Mastrocola et al., 2013; Ratti and Buratti, 2016; Rulten et al., 2014; Wang et al., 2013). Consequently, FUS depletion or FUS mutations causing reduced binding to PARP-1 and HDAC1 were shown to cause defects in DNA repair.

In addition, FUS also regulates processing of microRNAs (miRNAs) and long noncoding RNAs (lncRNAs). FUS, together with TDP-43, associates with the Drosha complex (Gregory et al., 2004). FUS binds to a precursor of miRNAs (pri-miRNAs) at sites of active chromatin and also recruits Drosha to these loci to stimulate pri-miRNA biogenesis (Morlando et al., 2012). Furthermore, FUS depletion causes reduced Drosha recruitment to sites of active transcription and thereby reduces biogenesis of miRNAs essential for neuronal functions, differentiation and synaptogenesis, e.g. of miR-9, miR-125b, and miR-132 (Morlando et al., 2012). Importantly, FUS also regulates biogenesis of miR141 and miR200a which in turn bind the 3'UTR of FUS mRNA and thus downregulate FUS protein synthesis (Dini Modigliani et al., 2014; Ederle and Dormann, 2017). The presence of ALS-linked mutations, e.g. a guanine-to-adenine substitution (G48A), in the 3'UTR seed sequence disrupt this auto-regulatory feed-forward loop (Dini Modigliani 2014). In addition to miRNAs, FUS is also interacting with diverse lncRNAs, such as *NEAT1*, which is necessary for paraspeckle formation. FUS regulates *NEAT1* levels and, together with TDP-43, is essential for proper paraspeckle assembly (Nishimoto et al., 2013; Ratti and Buratti, 2016; Shelkovernikova et al., 2013; Shelkovernikova et al., 2014). ALS-linked FUS mutations have been reported to sequester other paraspeckle proteins to cytosolic aggregates and disrupt paraspeckle assembly, suggesting a contribution to pathogenesis in ALS/FTD (Shelkovernikova et al., 2013).

1.6 Physiological functions of FUS in the cytoplasm

Although FUS is a mostly nuclear RBP with multiple nuclear functions, several studies reported that FUS also fulfills numerous tasks of mRNA regulation in the cytoplasm, including mRNA stability, trafficking, and mRNA translation (Bowden and Dormann, 2016; Ratti and Buratti, 2016). FUS was shown to interact with the 3'UTRs of various mRNA targets (Colombrita et al., 2012; Hoell et al., 2011; Lagier-Tourenne et al., 2012; Rogelj et al., 2012), although FUS knockdown had no effect on mRNA stability for bound targets like *Vps54*, *Taf15*, and *Nvl* in murine motoneuronal-like cells (Colombrita

et al., 2012; Ratti and Buratti, 2016). Recently, Udagawa and colleagues demonstrate that GluA1, a subunit of AMPA receptors, is downregulated due to decreased mRNA stability in FUS-depleted primary cortical neurons (Udagawa et al., 2015).

In 2005, two studies reported that FUS is localized in RNA granules that are transported to dendrites and presynapses of hippocampal neurons (Belly et al., 2005; Fujii et al., 2005). Upon mGluR5 stimulation, FUS was shown to enable mRNA transport into dendritic spines and to regulate spine morphology by transporting mRNAs encoding for β -actin and the actin-stabilizing factor *Nd1-L* (Fujii et al., 2005; Fujii and Takumi, 2005). Evidence for an involvement of FUS in local mRNA translation was provided when Yasuda and colleagues showed FUS co-localization with the tumor suppressor protein adenomatous polyposis coli (APC) in RNP complexes at cell protrusions and promotion of translation of APC-associated mRNA transcripts like *Kank2* and *Pkp4* (Yasuda et al., 2013). Remarkably, overexpressed or mutant FUS protein carrying ALS-linked mutations preferentially recruits APC-RNPs to cytosolic granules that are translationally active, showing that translation can take place in stress granule-like structures (Yasuda et al., 2013).

1.7 Protein arginine methylation

The three FET family members (FUS, EWS, TAF15) have been shown to undergo extensive asymmetric dimethylation at arginine residues in the RGG domains (Araya et al., 2005; Belyanskaya et al., 2001; Du et al., 2011; Hung et al., 2009; Jobert et al., 2009; Ong et al., 2004; Pahlich et al., 2005; Rappsilber et al., 2003). A remarkable difference in FTD-FUS pathology compared to ALS-FUS is that the state of arginine methylation of FUS is altered. Asymmetric dimethylation of FUS in healthy individuals and ALS-FUS patients is lost in FTD-FUS inclusions (Dormann et al., 2012; Suarez-Calvet et al., 2016) (detailed explanation of arginine methylation below). However, gene analysis of the responsible protein arginine methyltransferases (PRMTs) did not reveal any mutations or altered gene expression levels (Ravenscroft et al., 2013). Notably, inhibition of arginine methylation of FUS in HeLa cells and motor neurons rescues cytosolic mislocalization of ALS-associated FUS mutations (Dormann et al., 2012; Suarez-Calvet et al., 2016; Tradewell et al., 2012). Surprisingly, loss of arginine methylation of FUS, as seen in FTD-FUS patients, enhances binding affinity of FUS to TNPO1 *in vitro* (Dormann et al., 2012). Furthermore, TNPO1 co-aggregates in FTD-FUS inclusions, indicating that FUS binding to TNPO1 itself is not impaired (Jovicic et al., 2016).

Arginine methylation is a common post-translational modification (PTM) in mammals (Larsen et al., 2016) and is carried out by different members of the protein arginine methyltransferase (PRMT) family

(Bedford and Clarke, 2009). In addition to the PRMT family, there are other putative arginine methyltransferases like NDUFAF7 (Zurita Rendon et al., 2014). PRMTs catalyze the transfer of a methyl group from the methyl group donor *S*-adenosylmethionine (SAM) to the guanidino nitrogen atoms of arginine, resulting in methylarginine and *S*-adenosylhomocysteine (Fig. 4). In eukaryotes three forms of methylarginines have been identified, namely monomethylarginine (MMA), symmetric dimethylarginine (SDMA), and asymmetric dimethylarginine (ADMA) (Fig. 4). The nine members of the PRMT family can be subdivided into three groups according to the type of methylation mark they establish. Type I (PRMT1, PRMT2, PRMT3, PRMT4/CARM1, PRMT6, and PRMT8) and type II (PRMT5 and PRMT9) enzymes first establish the intermediate MMA and subsequently carry out the formation of ADMA or SDMA, respectively (Yang and Bedford, 2013) (Fig. 4). While for ADMA two methyl groups are added to one terminal nitrogen atom of the guanidine group, for SDMA the two methyl groups are added to one nitrogen atom each. PRMT7 is categorized as type III enzyme that only establishes MMA (Feng et al., 2013). Addition of a methyl group to an arginine residue eliminates one out of five potential hydrogen bond donors and causes a conformational change. Since arginine methylation increases bulkiness and hydrophobicity of a protein, protein-protein interactions can be affected both negatively and positively (Bedford and Clarke, 2009; Fuhrmann et al., 2015; Pahlich et al., 2006; Tripsianes et al., 2011; Yang and Bedford, 2013). Notably, the positive charge of arginine residues is not altered by the addition of methyl groups (Tripsianes et al., 2011). RGG/RG-rich motifs often play an important role in protein-protein interactions and nucleic acid binding and are the most common target motif for PRMTs (Guo et al., 2014; Thandapani et al., 2013; Wooderchak et al., 2008). Importantly, glycines next to arginines are supposed to facilitate the accessibility of arginines to the active site of PRMTs by increasing conformational flexibility (Blanc and Richard, 2017). In contrast to most other PRMTs, PRMT7 has been reported to favor RxR motifs neighboring lysines (Feng et al., 2013), and PRMT4 preferentially targets arginines in an proline-glycine-methionine (PGM)-rich surrounding (Yang and Bedford, 2013). Type I and II PRMTs harbor a central cavity and two opposing active sites forming head-to-tail homodimers (Zhang and Cheng, 2003). A highly conserved SAM binding pocket embedded in these active sites includes an E-loop essential for substrate recognition and methylation (Antonysamy et al., 2012). Remarkably, type III PRMT7 acts as a homodimer-like structure with two catalytic domains (Debler et al., 2016; Jain et al., 2016a).

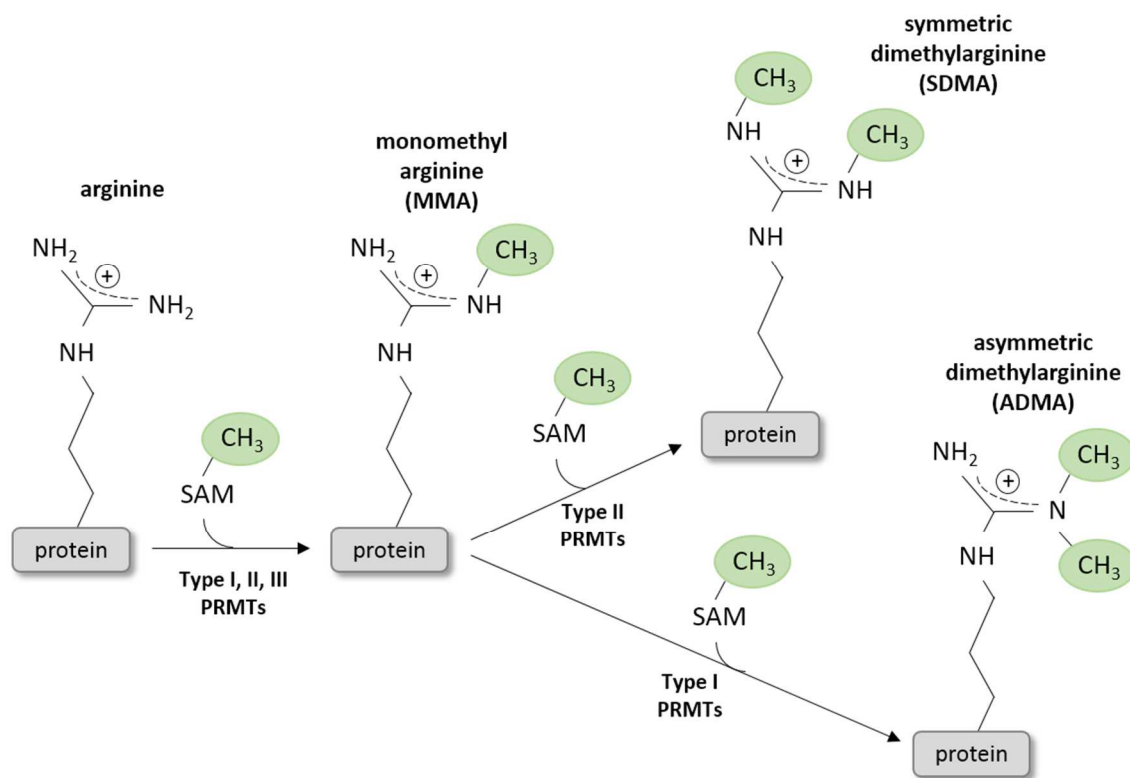


Figure 4: Different patterns of arginine methylation. Type I, II, and III protein arginine methyltransferases (PRMTs) are able to convert arginine to monomethylarginine (MMA) by transferring a methyl-group from S-adenosylmethionine (SAM) to one of the equivalent, terminal guanidino nitrogen atoms. Type II enzymes can subsequently catalyze the generation of symmetric dimethylarginine (SDMA) at different nitrogen atoms. The production of asymmetric dimethylarginine (ADMA) is catalyzed by type I enzymes where the two methyl groups are added to the same nitrogen atom of the guanidino group.

1.7.1 Protein arginine demethylation

For a long time, methylation of nitrogen atoms (*N*-methylation) was considered to be a very stable, irreversible post-translational modification. While the oxygen-dependent reversal of lysine methylation is well demonstrated by now, the existence of real arginine demethylases is still discussed controversially (Blanc and Richard, 2017; Yang and Bedford, 2013). In 2007, Jumonji C domain-containing protein 6 (JMJD6) was reported to be the first putative arginine demethylase (Chang et al., 2007). Two years later, JMJD6 was shown to be a lysine hydroxylase (Webby et al., 2009). Recently, JMJD6 was shown to demethylate the stress granule protein G3BP1 and thereby regulate stress granule (SG) dynamics by promoting SG formation (Tsai et al., 2017). Furthermore, certain Fe(II)- and 2-oxoglutarate (2OG) dependent JmjC-domain-containing demethylases (KDM3A, KDM4E, KDM5C) also possess methylarginine demethylation activity for histone and non-histone substrates *in vitro*

(Blanc and Richard, 2017; Walport et al., 2016). Nevertheless, further research is needed to clarify whether these enzymes are actual arginine demethylases or whether there are other enzymes that carry out this function.

1.7.2 Biological functions of arginine methylation

PRMTs have various histone and non-histone substrates, including numerous RBPs, and thereby play a key role in transcription, mRNA translation, signal transduction, DNA repair signaling, pre-mRNA splicing and nuclear import (Blanc and Richard, 2017; Yang and Bedford, 2013).

Among the multiple biological roles of arginine methylation, regulation of nucleocytoplasmic shuttling was the first uncovered function (Shen et al., 1998). RBPs are usually enriched in RGG, GAR, and PGM motives and thus prime targets for ADMA modification by the main type I enzymes PRMT1 and CARM1 (Bedford and Clarke, 2009; Tang et al., 2000). RBPs, like hnRNPs, shuttle between the nucleus and the cytoplasm. Initial yeast studies uncovered that deletion of the primary yeast type I PRMT, Hmt1/Rmt1, causes a nuclear accumulation of RBPs and Hmt1 overexpression enhances cytoplasmic localization of RBPs (Shen et al., 1998). The cold-inducible RNA binding protein CIRP2 identified in *Xenopus laevis* becomes hypermethylated by overexpression of xPRMT1, resulting in a cytoplasmic accumulation of CIRP2 (Aoki et al., 2002). In mammalian cells, hypomethylated Sam68 is cytosolically mislocalized (Cote et al., 2003). Interestingly, hypomethylation causes an accumulation of some RBPs in the nucleus, while others become enriched in the cytoplasm upon hypomethylation, and the mechanisms how arginine methylation regulates nucleocytoplasmic transport remain mostly elusive (Bedford and Clarke, 2009).

Nuclear import of FUS is also regulated by arginine methylation and this regulatory mechanism has been investigated in quite some detail: Chemical inhibition of methylation using adenosine dialdehyde (Adox) restores nuclear localization of FUS carrying an ALS-associated FUS-NLS mutation (Dormann et al., 2012; Tradewell et al., 2012) and of mutant EWS and TAF15 (Dormann et al., 2012). Similarly, PRMT1 knockdown revealed rescue of cytosolic mislocalization of NLS-mutated FUS and a restoration of nuclear localization (Dormann et al., 2012; Tradewell et al., 2012; Yamaguchi and Kitajo, 2012). Inhibition of arginine methylation causes enhanced TNPO1 binding to the unmethylated RGG3 domain of FUS compared to the methylated RGG3 domain and thereby results in improved TNPO1-dependent nuclear import of mutant FUS (Dormann et al., 2012).

As previously mentioned, another physiological function of arginine methylation is regulation of RNA binding. Studies on synthetic peptides corresponding to a RGG-rich region of nucleolin, which unwinds

dsDNA, showed that binding strength to RNA is not altered by arginine dimethylation, but unmethylated RGGs perturb the helical structure of RNA (Raman et al., 2001). Furthermore, poly(U) RNA binding activity of Sam68 and Sam68-like mammalian proteins (SLM-1/-2) was shown to be disrupted by arginine methylation (Rho et al., 2007). Hung et al. showed that arginine methylation of the REF/ALY mRNA export adaptor does not affect interaction with the actual export receptor TAP/NXF1 via its RG-rich motif, but reduces RNA-binding of REF/ALY and therefore also disrupts the transfer of RNA from REF/ALY to TAP/NXF1 (Hung et al., 2010). Recently, *in vitro* methylation of FUS was shown to interfere with its ability to bind to lncRNAs (Cui et al., 2018). Despite of these findings, the physiological roles of arginine methylation, particularly for FUS, remain ambiguous.

1.8 Stress granules: protective messenger ribonucleoprotein (mRNP) granules

As mentioned in a previous section, a vast number of ALS and FTD cases are characterized by a loss of TDP-43 or FUS from the nucleus and their cytosolic aggregation (Fig. 1 and 2). Interestingly, pathological aggregates of FUS and TDP-43 identified in ALS and FTD patients are often also positive for other RBPs, such as TIA1 and PABP-1, which are key components of stress granules (SGs) (Dormann et al., 2010; Liu-Yesucevitz et al., 2010). RBPs interact with mRNAs and thereby form messenger ribonucleoprotein particles (mRNPs). Translationally inactive mRNPs were reported to have the capability to assemble into higher order membrane-less mRNP granules, such as processing bodies (PB), neuronal transport granules, and stress granules (SGs) (Erickson and Lykke-Andersen, 2011). Importantly, SGs are cytosolic compartments that temporally sequester mRNA and associated RBPs in response to cellular stress or external stimuli and thereby keep the mRNA silenced and protected from degradation. Furthermore, mRNP granules are dynamic compartments that interact with each other and exchange components (Buchan et al., 2008; Kedersha et al., 2005). SGs form in response to various stress conditions, such as heat or cold shock, hypoxia, osmotic and oxidative stress, mitochondrial dysfunction, viral infection, or UV irradiation. Under these conditions, most mRNAs are silenced while mRNAs encoding molecular chaperones and repair enzymes, which are essential to deal with the stress, can escape SGs and get preferentially translated (Anderson and Kedersha, 2006). This makes SGs protective cell compartments and inhibition of SG formation under stress conditions was demonstrated to cause cell death (Hofmann et al., 2012). SGs are usually reversible cytoplasmic compartments that can disassemble upon stress recovery or can be cleared by autophagic degradation (Buchan et al., 2013). SGs typically contain various components, such as polyA-mRNA, 40S ribosomal subunits, polyA-binding protein (PABP), and various translational initiation factors of the eIF family (Buchan and Parker, 2009). Furthermore, SGs contain SG-nucleating RBPs, e.g. TIA1 and G3BPs, that

promote the formation of SGs by LC domain-driven self-assembly (Alberti et al., 2017; Cushman et al., 2010; Gilks et al., 2004), but also contain “passive client RBPs” that are simply recruited to SGs through their bound mRNAs (e.g. FUS, TDP-43, hnRNP-A1). Additionally, some SG-associated RBPs, such as Pumilio 2 and Staufen, play a role in translational silencing, while others are involved in mRNA localization or degradation (Anderson and Kedersha, 2008; Bowden and Dormann, 2016).

1.8.1 Stress granules as progenitors of pathological aggregates?

In addition to pathological FUS and TDP-43 inclusions in ALS and FTD being positive for several SG markers (e.g. TIA1, G3BP, PABP-1) (Baumer et al., 2010; Bentmann et al., 2012; Dormann et al., 2010; Fujita et al., 2008; McGurk et al., 2014), other protein aggregation diseases were also demonstrated to have SG pathology. Several SG markers have been identified in tau aggregates in FTD-tau and Alzheimer’s disease (Apicco et al., 2018; Vanderweyde et al., 2016; Vanderweyde et al., 2012) as well as in ALS cases linked to SOD1 aggregates (Lu et al., 2009). Thus, the presence of SG marker proteins in pathological aggregates in various neurodegenerative diseases suggests that SGs may be progenitors of such pathological inclusions. This view is further supported by recent studies linking altered SG dynamics caused by mutations in ALS/FTD-associated RBPs (e.g. hnRNP-A1/A2 and TIA1) to the formation of pathological aggregates in ALS/FTD (Kim et al., 2013; Mackenzie et al., 2017; Martinez et al., 2016).

Several studies demonstrated that ALS-causing point mutations in the NLS of FUS, which cause cytosolic mislocalization, drastically increase recruitment of FUS into SGs (Bentmann et al., 2012; Bosco et al., 2010; Dormann et al., 2010). These mutations cause altered TIA1 and G3BP1 binding as well as an increased number and size of SGs (Baron et al., 2013; Vance et al., 2013). These studies indicate that mutant FUS alters SG dynamics, possibly by recruiting and trapping additional SG components, and thereby contributes to ALS pathology (Bowden and Dormann, 2016; Dormann et al., 2010; Kwiatkowski et al., 2009; Vance et al., 2009; Vance et al., 2013).

In order to explain how nuclear FUS and TDP-43 accumulate in pathological inclusions, Dormann & Haass proposed a “two hit model” (Dormann et al., 2010) that has been modified to the “multiple hit theory” (Fig. 5). Accordingly, a first pathological hit is evoked by defective nuclear import causing nuclear depletion and a diffuse, cytosolic mislocalization of FUS (or other disease-associated RBPs) (step 1). Nuclear import defects of FUS can arise from mutations in the NLS that impair the binding of the import receptor TNPO1 (as observed in ALS-FUS) or from aggregation of TNPO1 (as observed in FTD-FUS). A second pathological hit, e.g. cellular stress, then evokes the recruitment of cytosolically

mislocalized FUS into SGs (Bentmann et al., 2012; Colombrita et al., 2009; Yang et al., 2015) (step 2). Persistent stress or other defects, e.g. genetic mutations, altered PTMs or defective protein quality control (PQC), as well as high local concentrations of FUS in SGs may induce aberrant SG dynamics and induce liquid-to-solid phase transition resulting in solidification of SGs (Note that the topic of phase separation and aberrant phase transitions will be discussed in more detail in section 1.9). This may lead to the formation of pathological aggregates as seen in ALS and FTD patients (step 3).

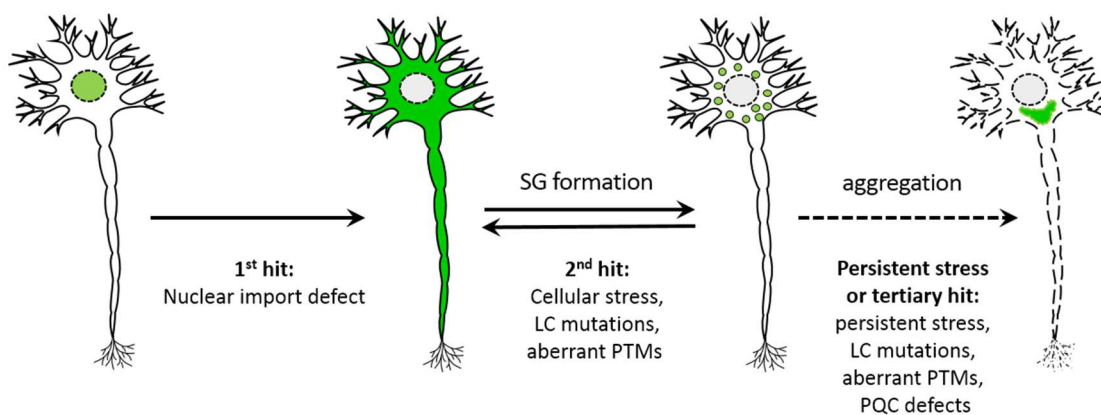


Figure 5: Multiple hit theory for pathological aggregation of FUS and other disease-linked RNA-binding proteins. The model postulates that a nuclear import defect is the first pathological hit causing cytosolic mislocalization of the normally nuclear FUS protein. Nuclear import defects may involve mutations in the NLS of FUS or mislocalization and aggregation of its nuclear import receptor TNPO1 (step 1). Cellular stress conditions act as a second hit and induce the formation of transient stress granules (SGs) driven by liquid-liquid phase separation (LLPS) of LC domain-containing RBPs and recruitment of mislocalized FUS into these SGs (step 2). Persistent stress, aggregation-promoting mutations, aberrant post-translational modifications (PTMs) or protein quality control (PQC) defects are believed to impair/reduce the dissolution of SGs and to cause liquid-to solid phase transition, leading to a solidification of FUS in SGs and ultimately to a conversion into pathological aggregates (step 3). Figure adapted from (Dormann and Haass, 2011) with permission from *Elsevier*.

Cytosolic mislocalization of FUS and TDP-43 and consequent depletion from the nucleus with subsequent accumulation of insoluble FUS in cytosolic aggregates may evoke neurodegeneration by either loss-of-function, toxic gain-of-function, or a combination of both (Sharma 2006, Harrison & Shorter 2017).

There are multiple mechanisms proposed how altered SG dynamics may contribute to neurodegeneration in RBP proteinopathies (extensively reviewed by (Bowden and Dormann, 2016)): First, solidification of SGs may cause persistent translational arrest of sequestered mRNAs. This mechanism is supported by studies showing that translational arrest mediated by phospho-eIF2 α

causes synaptic loss and neurotoxicity (Moreno et al., 2012) as well as death of hippocampal neurons upon brain ischemia (Jamison et al., 2008; Kayali et al., 2005).

Second, it may be possible that prolonged sequestration of regulatory RBPs, such as FUS, TDP-43, EWS, TAF15, in solidified SGs are toxic due to loss-of-function. Persistent trapping of FUS or TDP-43 in SGs may cause fatal impairment of the proteins functions in regulation of transcription and splicing, transcriptional regulation, DNA damage repair and mRNA localization and thus contribute to neurodegeneration (Bowden and Dormann, 2016; Lagier-Tourenne et al., 2012).

Third, Polymenidou and Cleveland proposed that mutant RBPs with prion-like domains may act as “seeds of neurodegeneration”, by inducing misfolding and trapping of their native counterparts into SGs (Polymenidou and Cleveland, 2011). Consistently, Vance and colleagues reported mutant FUS to bind to and recruit wild-type FUS to SGs (Vance et al., 2013). Prion-like domains are supposed to switch between two conformational states, namely an intrinsically unfolded and an aggregated state that forces its native counterpart by direct interaction into the same misfolded conformation. This process is supposed to be reinforced by high local protein concentrations in SGs. Furthermore, it seems likely that aggregated proteins may also induce misfolding and aggregation of dissimilar proteins, referred to as cross-seeding phenomenon. Strikingly, these seeding aggregates may be transferred from cell to cell and initiate misfolding and aggregation of native FUS and TDP-43 in neighboring cells (Polymenidou and Cleveland, 2011).

1.9 Phase separation of RBPs as driving force for protein aggregation

Intracellular compartmentalization is achieved by membrane-bound organelles such as the endoplasmic reticulum (ER), mitochondria and the Golgi apparatus. Divided by membrane boundaries, these compartments are functionally distinct from the rest of the cell by providing certain molecules at the proper time in the proper place. Nevertheless, another type of intracellular compartments has recently received a lot of attention, namely compartments that are not separated from the surrounding area by membranes and therefore are referred to as membrane-less organelles or biomolecular condensates (Banani et al., 2017; Weber and Brangwynne, 2012). Membrane-less organelles often contain RBPs and RNA and consequently are also referred to as RNP granules, e.g. processing bodies (PB), SGs, neuronal transport granules, germ granules and nucleoli. As previously described, RNP granules are involved in RNA metabolism, including splicing, mRNA storage and degradation. Both membrane-bound and membrane-less organelles play pivotal roles in

spatiotemporal control of biological processes by compartmentalizing biomolecules in the cell (Brangwynne et al., 2015).

1.9.1 Driving forces of phase separation and formation of membrane-less organelles

RNP granules are formed when certain biomolecules (RBPs, RNAs) separate from a cytosolic or nuclear pool of soluble molecules, forming condensed liquid phases in a less concentrated surrounding milieu (Fig. 6). Different from irreversible protein aggregates seen in neurodegenerative diseases, these physiological compartments have been demonstrated to be highly dynamic and exhibit liquid-droplet-like behavior including wetting surfaces, dripping in response to shearing and fusion into larger droplets/compartments upon contact (Brangwynne et al., 2009).

In 2009, a study in *C. elegans* demonstrated that germ (P) granules form by a mechanism called liquid-liquid phase separation (LLPS). Asymmetric localization of P granules to the posterior pole in the early embryo has been demonstrated to be based on spatiotemporally regulated LLPS structuring the cytoplasm (Brangwynne et al., 2009). Subsequently, phase separation was also shown to drive the assembly of nucleoli in *Xenopus* (Brangwynne et al., 2011) and SGs in yeast and mammalian cells (Kroschwald et al., 2015; Patel et al., 2015), indicating a general biophysical mechanism underlying the formation of membrane-less RNP granules in cells.

Phase separation not only drives the formation of membrane-less organelles, but is a ubiquitous phenomenon in nature. The most common examples are the different physical states that water can adopt, namely water vapor that condenses to liquid water that can further solidify into ice. In contrast to the molecules in vapor, transient hydrogen bonds formed in liquid water are permanently reorganized by thermal fluctuations allowing dynamic interactions between individual water molecules. In the frozen state, water molecules crystalize and stable hydrogen bonds hold the single molecules in place. Although phase transitions in this non-biological example are temperature-dependent processes, the propensity to undergo phase separation is primarily determined by the molecular properties (Weber and Brangwynne, 2012).

Although membrane-less compartments in cells have complex compositions containing multiple different proteins and RNAs, liquid-like compartments can be reconstituted *in vitro* using only one or two purified proteins that undergo LLPS (Fig. 6). These findings have provided evidence that in some cases a single protein may be necessary and sufficient to mediate the formation of membrane-less compartments by phase separation (Brangwynne et al., 2015). Major drivers of phase separation are

proteins harboring long stretches of intrinsically disordered regions of low amino acid complexity (so called LC domains), so called intrinsically disordered proteins (IDPs). The LC domains of IDPs show a preference for conformational disorder as well as inability to fold into defined three-dimensional structures (Brangwynne et al., 2015). Due to their high similarity to proteins in budding yeast forming prions, LC domains are termed prion-like domains (Alberti et al., 2009; King et al., 2012; Malinowska et al., 2013). IDPs can be subdivided into two groups. On the one hand IDPs that harbor mostly repetitive motifs of amino acids with polar sidechains (Q, S, G, N) as well as interspersed aromatic residues (F, Y), and on the other hand IDPs containing amino acids with positively charged side chains (mostly R), prominently found in repetitive RGG-rich domains. Most RBPs that are involved in formation of membrane-less, cytoplasmic RNP compartments are IDPs. Well-studied examples for this type of IDPs are FUS and hnRNP-A1. There is strong evidence that intracellular phase separation is driven by multivalent, low affinity interactions between LC domains that have a certain amino acid compositions (March et al., 2016; Shin and Brangwynne, 2017; Weber and Brangwynne, 2012). LLPS of hnRNP-A1 has been demonstrated to be promoted by lowering NaCl concentrations, indicating that LLPS of hnRNP-A1 is driven by electrostatic interactions between charged motifs (Molliex et al., 2015). Moreover, arginine-aromatic (cation- π) interactions between arginine residues in RG/GR motifs and aromatic FG/GF motifs were shown to contribute to phase separation of Ddx4 molecules (Nott et al., 2015). As hnRNP-A1 is also enriched in aromatic residues containing F and Y as well as arginine residues, it is likely that cation- π interactions may be another driving force of LLPS of hnRNP-A1 (Molliex et al., 2015). Additionally, interactions of dipoles (G, Q, N, S) and between aromatic residues (π - π stacking) are also considered to drive phase separation (Brangwynne et al., 2015; Lee et al., 2016). In summary, electrostatic interactions mediating long-range interactions complemented by short-range, directional interactions (including cation- π , π - π stacking, and interactions between dipoles) appear to give a hierarchical interplay between the different types of weak multivalent interactions driving LLPS of IDPs (Brangwynne et al., 2015). Besides weak multivalent interactions between disordered LC regions, modular binding domains and their multivalent ligands have been reported to drive phase separation (Li et al., 2012). Phase separation is a concentration-dependent process, in which a protein solution reaches a state of supersaturation, e.g. protein concentration beyond the phase transition boundary, and then forms liquid-like compartments with a much higher local concentration than the surrounding area. The level of molecular supersaturation can be modulated by changes in temperature, salt/proton concentration, changes in charge due to PTMs or mutations, pH or osmotic shocks as well as changes in the protein/RNA composition due to altered gene expression (Brangwynne et al., 2015). In addition to RBPs, even certain types of RNA have been demonstrated to undergo phase separation on their own (Jain and Vale, 2017; Saha and Hyman, 2017).

1.9.2 Phase separation and protein aggregation

A number of recent studies well demonstrated that FUS as well as other disease-linked RBPs, such as hnRNP-A1 and TDP-43, undergo reversible LLPS *in vitro* (Burke et al., 2015; Kato et al., 2012; Molliex et al., 2015; Monahan et al., 2017; Murakami et al., 2015; Patel et al., 2015). A number of studies suggested that LLPS and aggregation of FUS are mainly driven by its highly polar N-terminal SYGQ-rich domain (Burke et al., 2015; Kato et al., 2012; Murakami et al., 2015; Patel et al., 2015; Sun et al., 2011). Notably, full-length FUS undergoes LLPS at physiological concentrations which are considered to range between 1-10 μ M in HeLa cells (Patel et al., 2015). The FUS droplets formed *in vitro* initially have dynamic, liquid-like properties similar to cellular RNP granules such as SGs and recover quickly after photobleaching. However, droplet properties can change over time and liquid droplets can undergo an aberrant liquid-to-solid phase transition and form solid, fibrous aggregates *in vitro* (Molliex et al., 2015; Monahan et al., 2017; Patel et al., 2015) (Fig. 6). This liquid-to-solid phase transition is characterized by a conversion of liquid droplets to short cross- β fibrils (Burke et al., 2015; Kato and McKnight, 2017; Patel et al., 2015; Shorter, 2017) that are considered to be initially labile and reversible (Kato and McKnight, 2017) but eventually shift to solid, irreversible fibrils (Murakami et al., 2015; Patel et al., 2015; Shorter, 2017). As demonstrated by the work of Patel and Murakami and colleagues, LLPS and liquid-to-solid phase transition of FUS is driven in a concentration-dependent manner (Murakami et al., 2015; Patel et al., 2015) (Fig. 6), suggesting that high local FUS concentrations, as found in SGs, may promote aberrant phase transition of FUS to solid cytoplasmic aggregates and pathological protein inclusions (Bentmann et al., 2013; Bowden and Dormann, 2016; Li et al., 2013) (Fig. 5).

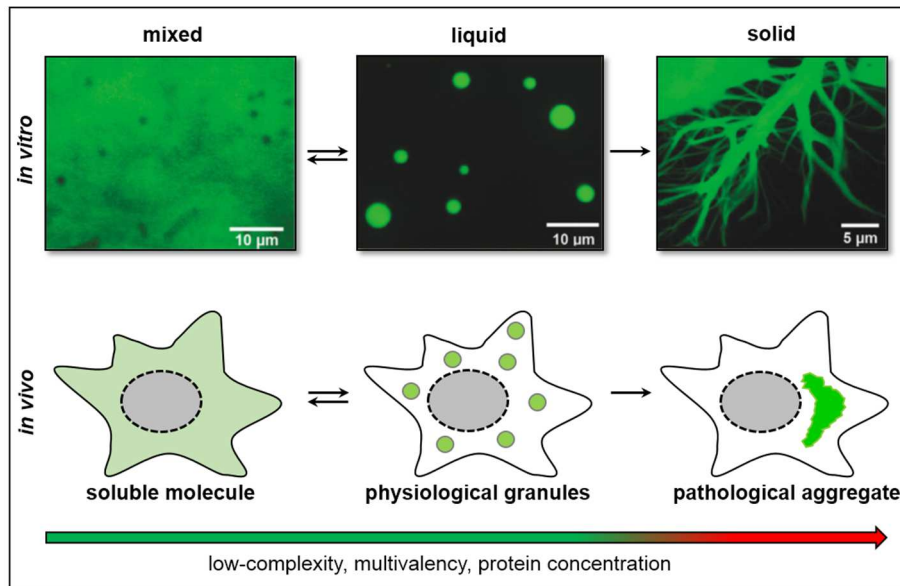


Figure 6: Phase separation drives the adoption of different material states of proteins with multivalent interaction domains or low complexity domains. When reaching a state of supersaturation, soluble proteins in the mixed phase (top panel left), such as purified FUS, undergo liquid-liquid phase separation (LLPS) forming protein droplets with liquid-like properties *in vitro*. LLPS causes a high local protein concentration in the droplets (top panel center) and a less-concentrated, surrounding solution. This process is driven by weak multivalent interactions between low-complexity domains or multivalent motifs as well as protein concentration. Importantly, each phase-separating protein has a specific saturation concentration where it crosses the phase boundary. LLPS is initially reversible and the protein can return to the mixed phase. If the molecular interactions get stronger or the local protein concentration further increases, the dynamic properties of the droplets change causing droplet solidification and formation of insoluble aggregates (top panel right). The conversion of liquid droplets to solid aggregates is referred to as liquid-to-solid phase transition. In cells, LLPS is considered to drive the formation of physiological RNP granules, including SGs and PBs (bottom panel center). Liquid-to-solid phase transition may further cause the formation of irreversible, pathological protein aggregates (bottom panel right). Figure adapted from (Alberti et al., 2017).

Multiple studies have demonstrated that disease-linked mutations in the LC domains of FUS, TDP-43 and hnRNP-A1 as well as hnRNP-A2 induce a faster transition from dynamic liquid droplets to solid aggregates, possibly by enhancing multivalent interactions and changed binding affinities of IDPs (Conicella et al., 2016; Kim et al., 2013; Lee et al., 2016; Molliex et al., 2015; Patel et al., 2015; Ryan et al., 2018). The phenomenon of liquid-to-solid phase transition may also occur in mRNP granules in cells, where IDPs are locally highly concentrated and disease-associated mutations further increase their aggregation propensity (Kim et al., 2013; Vance et al., 2013). Thereby, physiological mRNP dynamics may become dysregulated and form solidified mRNP granules and pathological aggregates as found in ALS, FTD and other proteinopathies (Bowden and Dormann, 2016; Elbaum-Garfinkle et al., 2015; Ramaswami et al., 2013) (Fig. 6). Furthermore, persistent SGs due to failure of the autophagy

machinery (e.g. caused by VCP or p62 mutations) or the UPS may also promote aberrant phase transition and be a key pathomechanism in ALS/FTD (Alberti and Hyman, 2016; Bowden and Dormann, 2016; Dormann and Haass, 2013).

1.9.3 Cellular determinants controlling RNP granule formation, aberrant phase separation and aggregation

As FUS is among the most abundant cellular proteins (Wisniewski et al., 2014) and was demonstrated to undergo LLPS and liquid-to-solid phase transition *in vitro* at physiological concentrations, certain protein quality control (PQC) mechanisms have to be in place to efficiently prevent or reverse aberrant phase transition in cells. There are different mechanisms present in the cell that regulate RNP granule dynamics and prevent the formation of pathological aggregates and fibrils (Alberti et al., 2017).

1.9.3.1 Adenosine triphosphate (ATP)

First, it may be possible that cells use energy sources to suppress aberrant phase transitions and formation of pathological aggregates (Brangwynne et al., 2015). Adenosine triphosphate (ATP) serves as energy source for biological reactions in the cell and has been shown to maintain the fluidity of intracellular compartments (Jain et al., 2016b). Recently, ATP as molecule has been reported to suppress LLPS of RBPs and to dissolve preformed droplets of FUS, hnRNP-A3, and TAF15. Therefore, ATP is able to function as a biological hydrotrope independently of its role as an energy source driving chemical reactions (Patel et al., 2017) around its physiological concentration between 5 and 10 mM (Traut, 1994). As ATP-dependent biological processes require only micromolar concentrations of ATP, its function as hydrotrope may explain millimolar concentrations of ATP present in cells. Curiously, ATP is even able to inhibit aggregation of boiled egg in a dose-dependent manner, possibly by stabilizing the native globular state (Patel et al., 2017).

1.9.3.2 Chaperones

Another aspect that appears to be involved in protein quality control in cells is active regulation by protein chaperones and RNA helicases that either clear preformed RNP granules or prevent formation or solidification of such. The first identified chaperone is the chromatin assembly factor nucleoplamin from *Xenopus* oocytes (Dingwall and Laskey, 1990) which is able to suppress undesired aggregation of

core histones upon DNA-binding (Jakel et al., 2002). The term chaperone was originally introduced in order to classify proteins with such nucleoplasm-like disaggregation activity. Currently, the term chaperone is commonly used for factors executing disaggregation activity like HSPs and importins (Jakel et al., 2002).

Studies on RNP granules in yeast under heat shock conditions revealed that deficiency in heat shock proteins (HSPs) such as HSP104 causes mislocalization of the P-body proteins Edc3 and Lsm4 resulting in their co-aggregation with misfolded proteins in SGs. Increased expression of HSP104 reduced the amounts of SG-localized Edc3, indicating that HSP104 can act as chaperone preventing protein aggregation (Kroschwald et al., 2015). Similarly, loss of the RNA helicase CGH-1/DDX6 in *C. elegans* induces polymerization of RNP granules to a solid state, indicating that this RNA helicase is able to modulate fluidity of RNP granules (Hubstenberger et al., 2013)

Recently, the chaperone function of several HSPs to encounter aberrant phase transition of SGs has been extensively studied. Mutant proteins, such as SOD1, have been shown to strongly decrease SG dynamics (Ganassi et al., 2016; Mateju et al., 2017). Furthermore, SGs positive for mutant RBPs have been shown to be enriched for ubiquitin and chaperones, such as HSP27 and HSP70, indicating that HSPs are specifically recruited into aberrant SGs containing mutant proteins (Ganassi et al., 2016; Mateju et al., 2017). Additionally, HSP27 recruitment to SGs upon heat shock is slightly delayed compared to poly-ubiquitin, indicating that HSP27 recruitment to SGs occurs in response to aggregation of misfolded proteins (Mateju et al., 2017). Remarkably, wild-type RBPs like FUS, TDP-43 and G3BP2 are depleted from SGs upon prolonged stress (Mateju et al., 2017). Since misfolded proteins are gradually recruited to SGs alongside with recruitment of chaperones while certain RBPs are depleted, SG composition changes over time. Moreover, inhibition of HSP70 was accompanied by a significant increase of SGs positive for misfolded SOD1, Ubc9TS, or poly-ubiquitinated proteins, denoting that HSP70 prevents both, formation and recruitment of misfolded proteins into SGs (Mateju et al., 2017). Aggregation of misfolded proteins significantly impairs SG disassembly alongside with HSP70 inhibition indicating that HSP70 mediates rapid SG disassembly (Ganassi et al., 2016; Mateju et al., 2017). Ganassi et al. (2016) uncovered that the chaperone holdase HSPB8 is recruited to SGs and in turn recruits the BAG3-HSP70 subcomplex that mediates disassembly of SG containing mutant proteins (Ganassi et al., 2016). On a molecular basis, HSPs suppress aggregation by binding exposed hydrophobic regions of folding and assembly intermediates and thereby ensure proper folding (Agashe and Hartl, 2000). Impaired PQC, possibly by defects in HSP chaperone activity, may cause the conversion of aberrant SGs into aggregates. To clear persisting aberrant SGs, cells have developed an

alternative clearance pathway that involves degradation by autophagy (Alberti et al., 2017; Ganassi et al., 2016; Mateju et al., 2017) (see section 1.9.3.3).

Notably, Jackrel and colleagues demonstrated that mutations of single residues of Hsp104 can cause a gain-of-function by potentiating its ability to dissolve TDP-43, FUS, and α -synuclein aggregates and thereby suppress proteotoxicity and even restore proper localization of the RBPs (Jackrel et al., 2014; Jackrel and Shorter, 2015, 2017; Yasuda et al., 2017). These potentiating missense mutations are restricted to the coiled-coil middle domain of Hsp104 (Jackrel et al., 2014) that possesses ATPase activity and disaggregase activity (Desantis and Shorter, 2012), and elevate its ATPase activity by ~2- to 4-fold indicating faster ATP binding and hydrolysis (Jackrel et al., 2014; Jackrel and Shorter, 2015). Engineering such enhanced protein disaggregases offers new therapeutic potential to encounter toxic protein aggregates (Jackrel and Shorter, 2015, 2017).

1.9.3.3 SG clearance by the autophagy machinery

In addition to molecular chaperones, also components of the UPS (ubiquitin proteasome system) and of the autophagy machinery are recruited to SGs. Among these are ubiquitin, HDAC6 (histone deacetylase 6) and VCP/p97 which is involved in the degradation of ubiquitinated proteins (Buchan et al., 2013; Kawaguchi et al., 2003; Kwon et al., 2007). Besides HSP-mediated disassembly of SGs, there is evidence for clearance of persisting SGs by autophagy mediated by VCP/p97. Inhibition of VCP activity by siRNA or by chemical inhibition causes decreased rates of SG clearance (Buchan et al., 2013). Autophagy is crucial for the removal of aggregated proteins that may have deleterious potential. Impaired autophagy is associated with numerous disorders including cancer and neurodegeneration (Yang and Klionsky, 2010). Furthermore, accumulation of p62 in SGs (Matus et al., 2014) further points to an essential role of autophagy in SG degradation (Alberti et al., 2017). Stress granules can be divided into physiological SGs and aberrant SGs containing misfolded proteins which recruit PQC factors and the autophagy machinery (Ganassi et al., 2016; Mateju et al., 2017). Furthermore, recent studies provide evidence for SG clearance by transport to the aggresome and degradation by the autophagy machinery (Ganassi et al., 2016; Mateju et al., 2017). Aggresome formation is dependent on SG-localized VCP and the VCP/p97-binding protein HDAC6 (Ju et al., 2008) that is furthermore involved in the recognition of misfolded proteins and their packaging into aggresomes (Kawaguchi et al., 2003). This tight link of SGs and aggresome formation indicates an important mechanism of cells to cope with an excess of aberrant SGs (Alberti et al., 2017) even though

the favored pathway of SG clearance is the chaperone-mediated disassembly of SGs and recycling of components upon stress release (see section 1.9.3.2) (Ganassi et al., 2016; Mateju et al., 2017).

In summary, SGs can be cleared by two pathways: first, by fast disassembly of dynamic SGs by molecular chaperones like HSP70 or second, by transport of aberrant SGs containing misfolded proteins to the aggresome that are eventually degraded by the autophagy machinery (Mateju et al., 2017). Many cases of age-related neurodegenerative diseases, such as ALS and FTD, arise from impaired SG dynamics leading to aggregate formation driven by aberrant phase transition of SG components. Additionally, mutations in genes encoding factors involved in SG clearance, such as HSPB8, BAG3, VCP/p97, or p62 cause functional impairment and promote conversion of aberrant SGs into aggregates (Alberti et al., 2017). Strikingly, mutations in VCP are causative for ALS and FTD cases with characteristic TDP-43 inclusions (Johnson et al., 2010; Neumann et al., 2007).

1.9.3.4 Posttranslational modifications (PTMs)

IDPs are characterized by their low amino acid complexity in the IDRs that allows the formation of weak multivalent interactions driving phase separation. The enriched amino acids in the IDRs are highly post-translationally modified, e.g. by phosphorylation, methylation, ubiquitination, glycosylation and SUMOylation. There is quickly growing evidence that PTMs are a key control mechanism in cells to regulate proper dynamics and composition of RNP granules (Wang et al., 2014) and control phase separation processes.

The best-characterized example for fine-tuning RNP granule dynamics and LLPS of RBPs is phosphorylation. Phase separation of tau protein is promoted by phosphorylation as seen under physiological and pathological conditions (Wegmann et al., 2018). Furthermore, single point-mutations, introduction of a phospho-mimicking, negatively charged residue, as seen for the ALS-linked G156E mutation in FUS, can severely alter dynamic properties of FUS droplets (Patel et al., 2015) and significantly increase its aggregation propensity *in vitro* and *in vivo* (Nomura et al., 2014). Beside these promoting effects of phosphorylation on phase separation, there is also an increasing number of studies demonstrating suppression of phase separation and aggregation by phosphorylation. P-granule disassembly in *C. elegans* embryo is regulated by phosphorylation of MEG-3 and MEG-4 proteins by MBK-2/DYRK kinase and granule formation is promoted and stabilized by MEG-3/4 dephosphorylation by PP2A^{PPTR-1/PPTR2} phosphatase (Wang et al., 2014). Hyperphosphorylation of TDP-43 at five C-terminal serine residues (379, 403, 404, 409 and 410) was confirmed in ALS and FTD-U inclusions and initially proposed to be a driving force towards the formation of aggregates (Hasegawa

et al., 2008). More recently, this assumption changed as Li et al. demonstrated with phosphorylation-mimetic mutations at these serine residues (S5D or S5E) that hyperphosphorylation of TDP-43 reduces its propensity to form aggregates as well as cytotoxic effects of C-terminal TDP fragments in neurites. In contrast to that, phosphorylation-deficient mutations to alanine (S5A) promote aggregation of TDP-43. In the same study, phosphorylation of TDP-43, and also ubiquitination, were furthermore shown to occur after aggregate formation (Li et al., 2011). Moreover, phospho-mimetic substitution at serine 48 (S48E) in the NTD of TDP-43 severely disrupts its ability to phase separate, but also impairs splicing activity (Wang et al., 2018a). Recently, phosphorylation of specific serine and threonine residues in the N-terminal LC-domain (SYGQ-rich) of FUS has been reported to suppress its phase separation and aggregation *in vitro*. Similarly, McKnight and colleagues earlier showed that *in vitro* phosphorylation at certain serine residues (S26, S42, S61, and S84) of the LC domain by DNA-PK reduces hydrogel retention (Han et al., 2012). The study by Fawzi and colleagues revealed that an even higher number of consensus serine/tyrosine sites in the LC domain of FUS (T7, T11, T19, S26, S30, S42, S61, T68, S84, S87, S117, and S131) can be phosphorylated by DNA-PK *in vitro* and in cells. As phosphorylation of serines and tyrosines causes a change from uncharged, polar residues in the LC domain to a net negative charge, this high number of possible phosphorylation sites interferes with FUS LC domain self-interaction and phase separation (Monahan et al., 2017) by electrostatic repulsion which disrupts tyrosine-mediated π - π stacking (Wang et al., 2018b). In contrast, the full-length FUS protein is practically unaffected in its phase separation behavior by the phospho-mimetic 12E substitution suggesting that LLPS behavior of full-length FUS is more complex involving the N-terminal RGG domains (Monahan et al., 2017). Phosphorylation of full-length FUS may change the cation- π interactions to electrostatic interactions (phosphorylated S/Y with positive R in RGG) and maintain LLPS. This is supported by the finding that phase separation of full-length FUS carrying the 12E substitution is disrupted by high salt while wild-type FUS is less affected (Monahan et al., 2017).

In addition to phosphorylation, there is currently increasing evidence emerging that also methylation, especially at arginine residues, has an important contribution to the regulation of phase separation. In contrast to phosphorylation where negative charge is added to an initially uncharged, polar amino acid, methylation does not alter the positive charge of arginines, but hydrogen bonding and local hydrophobicity is altered (Fuhrmann et al., 2015). Yamaguchi and Katajō demonstrated that SG formation related to truncated FUS lacking the PY-NLS (FUS-dC) is significantly reduced by conditional overexpression of PRMT1 in HEK293 cells. Furthermore, PRMT1-overexpression reduces the amount of detergent-insoluble FUS-dC aggregates (Yamaguchi and Kitajō, 2012). Comparison of unmethylated LC domain of Ddx4 (Ddx4^{N1}) with Ddx4^{N1} asymmetrically dimethylated at 5 to 6 arginines by PRMT1 revealed a significant suppression of Ddx4^{N1} droplet formation. The degree of droplet destabilization

corresponds to a lower phase separation temperature of 25 °C or a doubling in salt concentration (Nott et al., 2015). *In vitro* methylation of the hnRNP-A2 LC domain using recombinant PRMT1 reveals ADMA marks at four arginine residues (R191, R201, R216, R254), causing decreased phase separation of methylated hnRNP-A2 LC. Furthermore, Fawzi and colleagues also show that methylation of RGG disrupts the intermolecular contacts of R191, R201, and R216 with aromatic residues suggesting that arginine methylation reduces hnRNP-A2 LC phase separation by interfering with cation- π interactions (Ryan et al., 2018).

Arginine residues are not only post-translationally modified by methylation, but can be also converted into citrulline residues. Citrullination by peptidylarginine deiminases (PADs) causes a loss of positive charge and a conformational change (Anzilotti et al., 2010; Vossenaar et al., 2003). PAD4-mediated citrullination significantly reduced aggregation of TAF15, FUS, EWSR1, and hnRNP-A1 in cells. Furthermore, sodium arsenite treatment caused a significantly higher recruitment of FUS and TAF15 to SGs in MEF cells derived from Padi4-deficient mice (Tanikawa et al., 2018). Although the physiological role of citrullination remains mostly unclear, the observations by Matsuda and colleagues suggest that citrullination may suppress phase separation and aggregation by disrupting cation- π or electrostatic interactions formed by arginines as the positive charge is eliminated.

Poly(ADP-ribosylation) is a PTM catalyzed by poly(ADP-ribose) polymerase (PARP) enzymes in response to DNA damage. Poly (ADP-ribose) (PAR) rapidly recruits FUS to sites of DNA DSBs by direct interaction with FUS-RGG2 (Mastrocola et al., 2013). Lukas and colleagues demonstrated that PAR induces intracellular accumulation of FUS, EWS, and TAF15 at sites of DNA damage *in vitro* and *in vivo* (Altmeyer et al., 2015). At the same time, Alberti and colleagues reported that PARP1/2 inhibition prevents FUS recruitment to DNA lesions and inhibition of a PAR-degrading enzyme (PARG) causes longer persistence of FUS at sites of DNA damage (Patel et al., 2015). This indicates that negatively charged PAR forms electrostatic interactions with the RGG2 domain driving liquid demixing at sites of DNA damage and thereby may allow immediate response to DNA breakage (Altmeyer et al., 2015) as FUS is recruited within seconds after PARP1 arrival (Patel et al., 2015).

1.10 Aims of the Ph.D. project

It has been shown that the interaction of FUS with TNPO1 is fine-tuned by methylation of arginines in the RGG3-PY of FUS (Dormann et al., 2012). Apart from this, only little is known about the physiological function of arginine methylation of FUS. So, it is unknown whether it affects other protein-protein interactions, RNA-binding or the phase separation properties of FUS. Furthermore, it

is still unclear whether the loss of FUS arginine methylation and the pathological deposition of TNPO1, as seen in FTD-FUS patients (Dormann et al., 2012; Suarez-Calvet et al., 2016), contributes to pathogenesis.

In order to shed light in these ambiguities, the following questions were addressed in my Ph.D. project:

1) Contribution of arginines to LLPS of FUS

Based on previous studies, it has been suggested that phase separation of FUS is mainly driven by the N-terminal SYGQ-rich domains (Burke et al., 2015; Kato et al., 2012; Murakami et al., 2015; Patel et al., 2015; Sun et al., 2011). A closer look at the sequence of FUS reveals that also the three RGG domains, which are the sites of arginine methylation, and the C-terminal NLS (RGG3-PY) are also highly disordered LC sequences, making them good candidates to contribute to phase separation of FUS. Therefore, the contribution of arginines in the RGG domains and of the RGG3-PY domain of FUS to LLPS of FUS were addressed in this thesis.

2) Effect of TNPO1 on LLPS and aggregation of FUS

A number of nuclear import receptors have been reported to suppress aggregation of highly basic ribosomal proteins and histones in the cytoplasm (Jakel et al., 2002). We speculated that the nuclear import receptor TNPO1 may exert a similar chaperone function towards its cargo FUS and suppress LLPS and aggregation of FUS. This may be of particular relevance, as TNPO1 is aggregated in FTD-FUS cases (Brelstaff et al., 2011; Davidson et al., 2013; Neumann et al., 2012; Troakes et al., 2013) and its binding to FUS is impaired in ALS-FUS patients due to FUS-NLS mutations (Dormann et al., 2012; Dormann et al., 2010). Thus, impaired TNPO1 function or binding may have a critical contribution to pathological aggregation of FUS in ALS and FTD. Therefore, one aim of this thesis was to address the impact of TNPO1 on LLPS and aggregation of FUS.

3) Effect of arginine methylation on LLPS and RNA-binding of FUS

RGG-rich motifs are a highly abundant sequence pattern in RBPs, including FUS, which has been shown to undergo extensive asymmetric dimethylation in its RGG domains *in vitro* and *in vivo* (Araya et al., 2005; Belyanskaya et al., 2001; Du et al., 2011; Hung et al., 2009; Jobert et al., 2009; Ong et al., 2004; Pahlich et al., 2005; Rappsilber et al., 2003). Beyond its involvement in regulating nucleocytoplasmic shuttling of FUS, little is known about the physiological and pathological functions of FUS arginine

methylation, e.g. whether it regulates phase separation or RNA/protein-interactions of FUS. As arginine methylation of FUS is lost in FTD-FUS patients (Dormann et al., 2012; Suarez-Calvet et al., 2016) and arginines may have a critical contribution to LLPS of FUS (see Aim 1), we speculated that arginine methylation may affect phase separation of FUS. Thus, another aim of this thesis was to study the role of arginine methylation in LLPS and RNA-binding of FUS.

2 RESULTS

DECLARATION OF COPYRIGHT AND CONTRIBUTIONS BY OTHER RESEARCHERS

This section of my Ph.D. thesis was prepared in parallel to the paper ‘Phase separation of FUS is suppressed by its nuclear import receptor and arginine methylation’ published in *Cell* (Hofweber et al., 2018). Thus, the data, structure and text of this Ph.D. thesis and the paper will partially overlap. Elsevier holds the copyright (2018) for this article published in *Cell* and permits the usage of text and figures in this dissertation.

Table 1: Summary of contributions to the result section by other researchers. Please note that Saskia Hutten contributed equally to Hofweber et al. 2018. These data are included in this Ph.D. thesis and comprise the pulldown assays, sedimentation assays and semi-permeabilized cell assays.

Figure 11D, E Figure 13B,C Figure 18B, C	Sedimentation assays conducted and quantified by Saskia Hutten
Figure 13D	Pulldown assays performed and quantified by Saskia Hutten
Figure 14B	TEM imaging conducted by Martina Schifferer
Figure 15A, B Figure 22C, D	Cytosolic anchoring of FUS performed and quantified by Saskia Hutten
Figure 15D, E Figure 19C, D Figure 22A, B	Semi-permeabilized cell assays conducted and analyzed by Saskia Hutten
Figure 16A, B	NMR experiments performed by Benjamin Bourgeois and Emil Spreitzer
Table 2	ITC experiments performed by Benjamin Bourgeois and Emil Spreitzer
Figure 16C, D, E Figure 20C, D Table 3	Radioactive filter-binding assays conducted and analyzed by Annika Niedner-Boblentz
Figure 20B	Electrophoretic Mobility Shift Assays (EMSA) performed by Annika Niedner

2.1 The C-terminal RGG3-PY domain of FUS can undergo phase separation

As previously mentioned, FUS contains multiple low-complexity (LC) domains characterized by low amino acid complexity. These LC domains include the very N-terminal SYGQ-rich domain as well as three C-terminal RGG domains that are highly enriched in repetitive RGG/RG motifs. Applying the amino acid sequence of FUS to the PONDR (Predictor of Natural Disordered Regions) algorithm yields a plot showing the degree of order/disorder of the protein (Fig. 7A). This demonstrates that the LC domains of FUS are highly disordered (Fig. 7A). Based on previous studies addressing phase separation

behavior of FUS, the prion-like SYGQ-rich domain was considered to be the main driver of phase separation of FUS (Burke et al., 2015; Kato et al., 2012; Murakami et al., 2015; Patel et al., 2015; Sun et al., 2011), but there is also evidence that the disordered C-terminal domains of FUS may also contribute to phase separation and aggregation (Boeynaems et al., 2017; Burke et al., 2015; Schwartz et al., 2013; Sun et al., 2011).

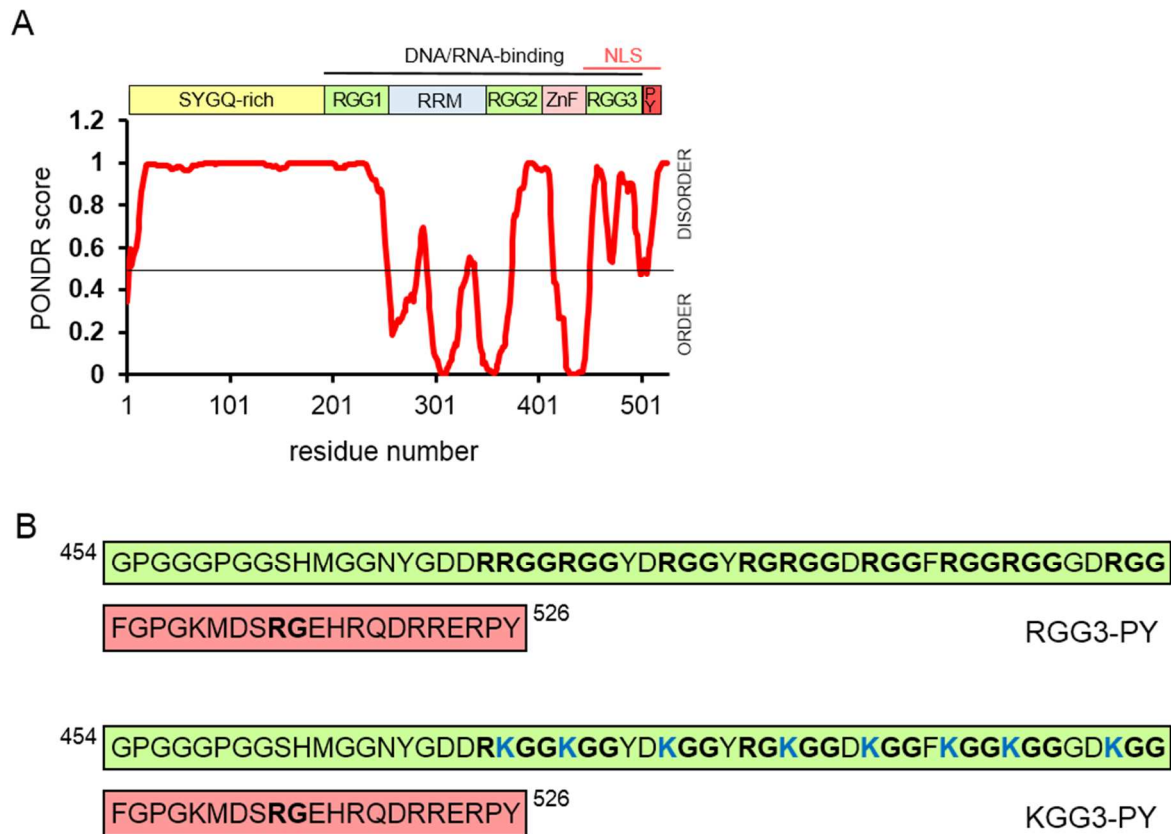


Figure 7: The RGG-rich motifs and PY-NLS of FUS are highly disordered. A) Schematic representation of the FUS domain structure and order/disorder plot predicted by the PONDR algorithm. A high degree of disorder is predicted for the SYGQ-rich domain, RGG1, RGG2 and RGG3-PY domain. **B)** Amino acid sequence of the isolated RGG3-PY domain (residues 454-526) (RGG3 in green, PY in red) demonstrating high enrichment of RGG/RG motifs (bold). In the KGG3-PY mutant, all arginines in RGG motifs are mutated to lysines (blue).

To test this hypothesis, I purified the C-terminal RGG3-PY domain of FUS (for sequence see Fig. 7B) from *E. coli* and examined its propensity to undergo phase separation *in vitro*. For affinity purification, the RGG3-PY domain was N-terminally His₆-Z-tagged, separated by a TEV protease cleavage site that allows proteolytic removal of the tag (Dormann et al., 2012) (Fig. 8A). Its disordered nature renders the RGG3-PY domain resistant to denaturation, allowing its purification from *E. coli* by boiling the bacterial pellet. This results in precipitation and removal of all folded proteins (Livernois et al., 2009),

while the RGG3-PY domain remains soluble. Noteworthy, the proteins were purified in a nucleic-acid free form, by incubation of the immobilized protein with Benzonase Nuclease (Sigma) and subsequent high salt washes (2M NaCl) (see Fig. 8B and 8C), as confirmed by 260/280 nm ratios of 0.6 - 0.8.

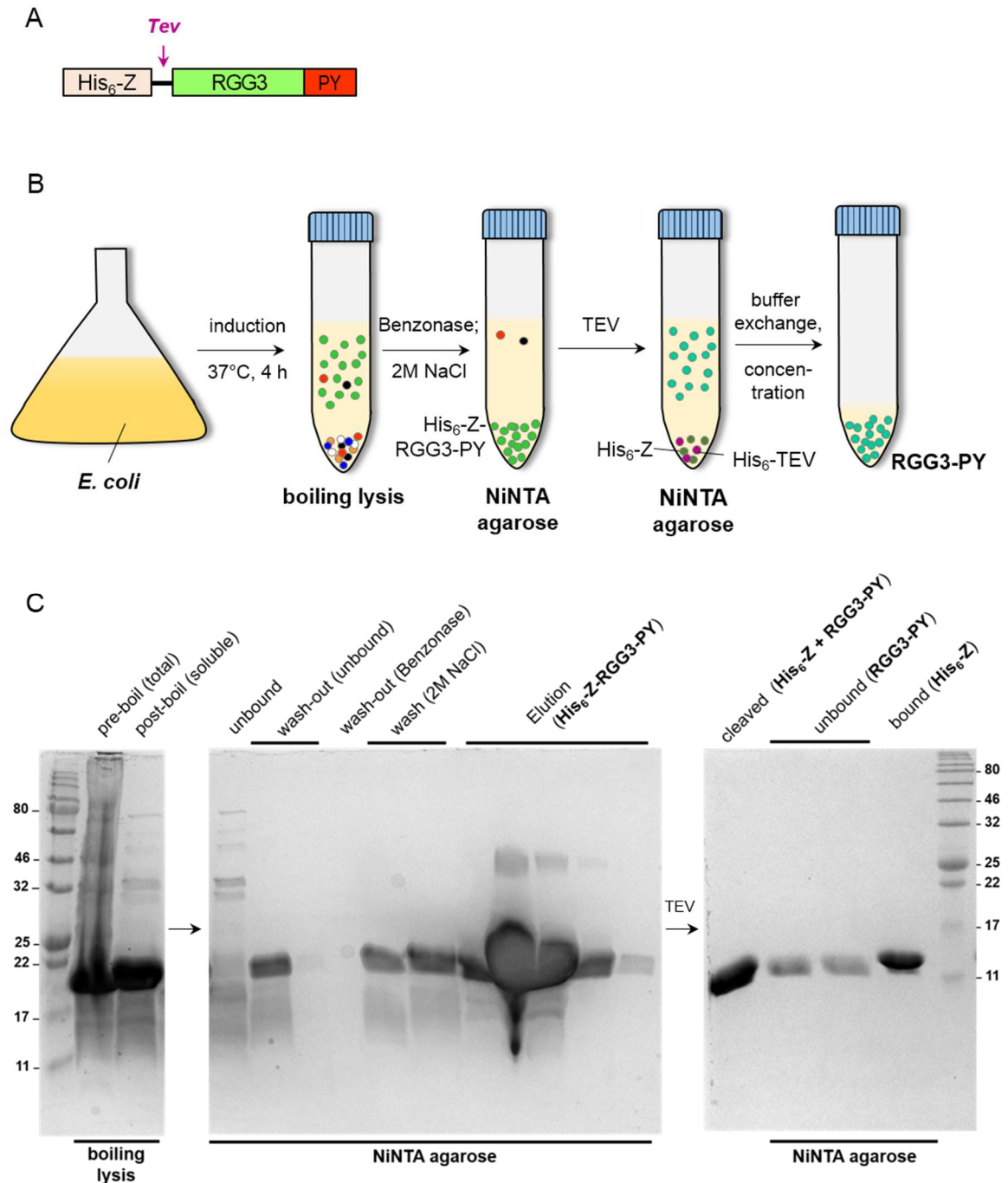


Figure 8: Purification of the C-terminal RGG3-PY domain. **A)** Schematic diagram of the purified protein (C-terminal RGG3-PY domain fused to an N-terminal His₆-Z-tag separated by a TEV protease cleavage site). **B)** Schematic representation of the workflow for purification of RGG3-PY domain of FUS. The resuspended bacterial pellet is subjected to boiling lysis allowing fast removal of most contaminating proteins while the disordered His₆-Z-RGG3-PY stays soluble during boiling. Immobilized on NiNTA agarose, the protein is subjected to Benzonase nuclease treatment and high salt washes (2M NaCl) in order to remove bound nucleic acids. Following

elution, His₆-TEV protease is added to the protein to remove the His₆-Z-tag. The liberated tag and His₆-TEV protease bind to NiNTA agarose and the untagged RGG3-PY remains in the supernatant. **C)** Exemplary SDS-PAGE gels visualizing the purification of RGG3-PY. Protein bands are visualized by Coomassie stain. Note, that the lanes are not loaded equally. Due to low amount used, His₆-TEV protease is not visible on the gel. Furthermore, untagged RGG3-PY and the liberated tag are of similar molecular weight (8-10 kDa) and therefore run on similar heights on the SDS-PAGE gel. Elution fractions have been pooled. Molecular weight markers (in kDa) are indicated on the left and right, respectively.

Initial experiments on phase separation of the RGG3-PY domain were performed with the His₆-Z-tagged RGG3-PY protein in presence of 150 mg/ml Ficoll. His₆-Z-RGG3-PY undergoes liquid-liquid phase separation in a concentration- and salt dependent manner (Fig. 9A and 9B). The fact that the His₆-Z-tag exhibits also some degree of disorder raised concerns about possible artifacts on phase separation. In order to eliminate this risk factor, the His₆-Z-tag was removed after elution from NiNTA by incubating the protein with His₆-TEV protease. By an additional Ni²⁺-affinity purification step, His₆-TEV and the liberated His₆-Z-tag as well as uncleaved His₆-Z-RGG3-PY were removed from the solution and untagged RGG3-PY remained in the supernatant (see Fig. 8B and 8C). In presence of substoichiometric amounts of RNA, RGG3-PY undergoes phase separation and forms liquid droplets in a concentration-dependent manner (Fig. 9C). Titrating different types of RNA, namely *in vitro* transcribed *MAPT* RNA (a known FUS target (Orozco et al., 2012)) and total RNA isolated from HeLa cells (data not shown), revealed that there is an optimal RNA-to-protein ratio resulting in a maximal degree of phase separation of RGG3-PY (Fig. 9D). In the case of *MAPT* RNA, the optimum ratio RNA:RGG3-PY was 1:50, which was used for subsequent experiments addressing the phase separation behavior of RGG3-PY (including Fig. 9C). Similar to the N-terminal SYGQ-rich domain of FUS (Burke et al., 2015; Murakami et al., 2015), RGG3-PY forms droplets in a temperature-dependent manner (Fig. 9E). At defined protein concentrations, phase separation of RGG3-PY can be enhanced by lowering the temperature and decreased with increasing temperature. Furthermore, droplet formation of RGG3-PY is promoted by lower salt concentrations and suppressed at higher salt concentrations (Fig. 9F), indicating that phase separation of this domain is driven by electrostatic interactions, most likely involving positively charged RGG/RG motifs.

In the end, the results obtained from untagged and tagged RGG3-PY showed similar trends (Fig. 9). Furthermore, removal of the tag has another advantage for subsequent protein analysis by Western blotting, namely that the Z-tagged protein is recognized by the constant region of IgGs causing unspecific signal for any antibody and therefore makes selective blotting of His₆-Z-RGG3-PY impossible. Furthermore, for initial tests the crowding agents Ficoll (Fig. 9A and 9B) or polyethylene glycol (PEG) (data not shown) were used to promote phase separation of His₆-Z-RGG3-PY, as described in a number of publications addressing phase separation of RBPs or DPR proteins (Boeynaems et al.,

2017; Murakami et al., 2015; Patel et al., 2015). Addition of crowding agents was sufficient to induce droplet formation of His₆-Z-RGG3-PY in absence of RNA, even though higher protein concentrations were required (Fig. 9A and 9B). Like in the case of the His₆-Z-tag, crowding agents were subsequently excluded to avoid artifacts and thus all experiments were repeated with untagged RGG3-PY in the absence of crowding agents.

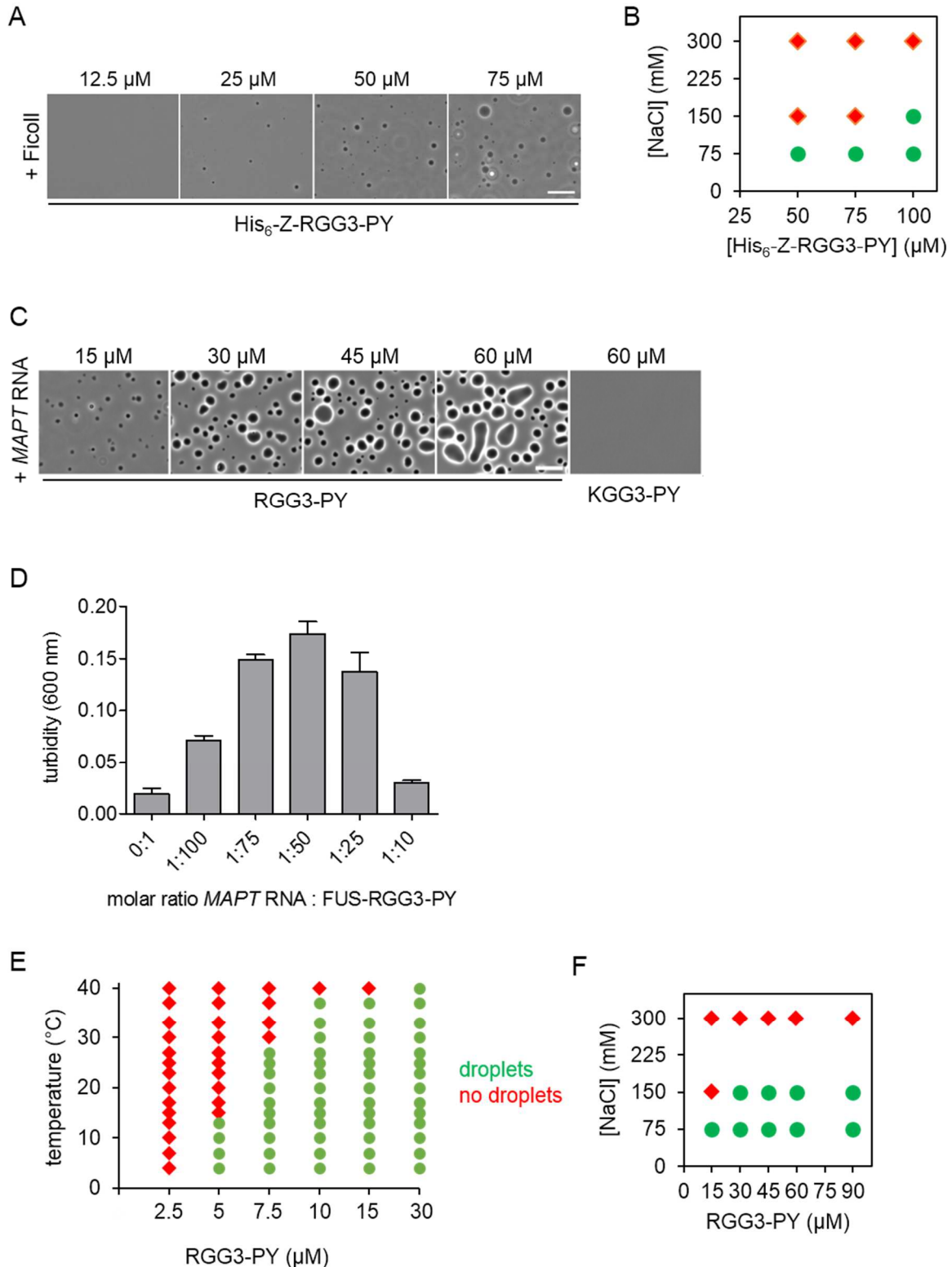


Figure 9: The C-terminal RGG3-PY domain of FUS undergoes LLPS. A) Droplet formation of His₆-Z-RGG3-PY at indicated concentrations in the presence of 150 mg/ml Ficoll. Images acquired by phase contrast microscopy. Scale bar, 10 μm. **B)** Phase diagram of His₆-Z-RGG3-PY in presence of 150 mg/ml Ficoll at different protein concentrations as a function of salt concentration. **C)** Addition of substoichiometric amounts of *MAPT* RNA (molar ratio 1:50) induces liquid droplet formation of RGG3-PY at indicated concentrations. The KGG3-PY mutant does not phase separate at 60 μM upon addition of *MAPT* RNA. Images acquired by phase contrast microscopy. Scale bar, 10 μm. **D)** Titration of substoichiometric amounts of *in vitro* transcribed *MAPT* RNA to RGG3-PY reveal maximal turbidity at a molar RNA-to-protein ratio of 1:50 which was used for all phase separation assays with untagged RGG3-PY. **E)** and **F)** phase diagrams of RGG3-PY as a function of temperature **E)** and salt concentration **F)** over protein concentration. Presence (green circles) or absence (red diamonds) of droplets were scored using phase contrast microscopy.

2.2 The RGG3-PY domain and arginine residues are essential for phase separation of FUS

In order to elucidate the influence of arginine residues on phase separation of RGG3-PY, we purified a mutant version, termed KGG3-PY, in which all eight arginines in RGG motifs of the RGG3 domain were mutated to lysines (K), thus maintaining the positive charge of the residues (for sequence see Fig. 7B). Remarkably, under conditions inducing large liquid droplets of RGG3-PY, mutant KGG3-PY does not phase separate at all and remains completely dispersed (Fig. 9C). Thus, arginines in the RGG3 motif are essential for LLPS of the RGG3-PY domain.

To address whether the C-terminal RGG3-PY as well as arginines in the RGG/RG motifs are also essential for phase separation of full-length FUS, human FUS was cloned into a vector encoding an N-terminal MBP-tag and a C-terminal His₆-tag (MBP-FUS-His₆ WT). Both tags were separated from FUS by TEV protease cleavage sites, allowing proteolytic removal of the tags by TEV protease (for scheme see Fig. 10A). Purification of MBP-FUS-His₆ proteins was demanding and required much effort for optimization. First, no bacterial expression constructs giving proper expression in *E. coli* were available. In particular, protein expression from some constructs could not be induced whereas others (both GST- or MBP-tagged at the N-terminus of FUS) could be induced, but the protein of interest did not bind to the respective affinity matrices. Eventually, an expression construct encoding MBP-FUS-His₆ WT, which could be successfully induced, was obtained from a collaborator and the protein of interest was binding to Amylose and NiNTA resins via the respective affinity tags. Second, good yields of soluble protein could be only obtained by very mild induction of protein expression at 12°C for at least 22 h in *E. coli*. Third, it was crucial to use optimized bacterial strains, such as Rosetta, that have tRNAs for rare arginine codons (AGA, AGG, CGA) and glycine codons (GGA) to improve protein

expression, since the bacterial expression construct for full-length, human FUS is not codon optimized. The N-terminal MBP-tag keeps the proteins soluble and also serves as an affinity tag for purification. Following sonification, tandem affinity purification using NiNTA and Amylose resin was performed (see Fig. 10B and 10C).

As a side note, the RGG3-PY domain in general and any full-length FUS proteins used in assays involving the addition of RNA were purified in a nucleic acid-free form. In contrast to RGG3-PY (see scheme in Fig. 8B), this was not straightforward for full-length FUS, as simple high-salt washes were not sufficient to remove nucleic acids and any nuclease treatments caused irreversible precipitation of the protein during purification. Furthermore, treatment of the bacterial lysates or purified proteins with polyethyleneimine (PEI) (0.1% w/v) or protamine sulfate (1% (w/v)) did not facilitate precipitation and removal of nucleic acids, but caused precipitation of the protein (not shown). Initially, purification of the double-tagged MBP-FUS-His₆ protein was performed via single-affinity purification yielding full-length FUS free of contaminating protein bands, but bound to nucleic acids. Surprisingly, tandem-affinity purification by itself yields soluble, nucleic acid-free FUS.

In addition to MBP-FUS-His₆ WT (hereafter referred to as MBP-FUS), I also cloned two mutant versions, a C-terminal deletion mutant where the RGG3-PY domain was deleted (Δ RGG3-PY) and a variant in which all arginines in RGG/RG motifs were mutated to lysines (all-KGG) (Fig. 10D). All MBP-FUS proteins were purified as described above. Besides plasmid sequencing, we performed Western Blot analysis of the WT and mutant MBP-FUS proteins using different FUS antibodies to confirm the protein identities. First, we used an anti-pan-FUS antibody (4H11) directed against a common epitope N-terminally of the RGG3 domain. It recognizes all three versions of FUS and confirmed a lower molecular weight of Δ RGG3-PY. Second, an anti-FUS-RGG3 antibody (14G1), which only detects MBP-FUS WT, was used to confirm the mutations (Fig. 10E).

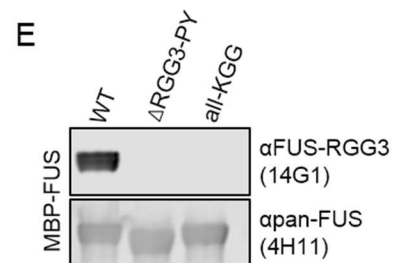
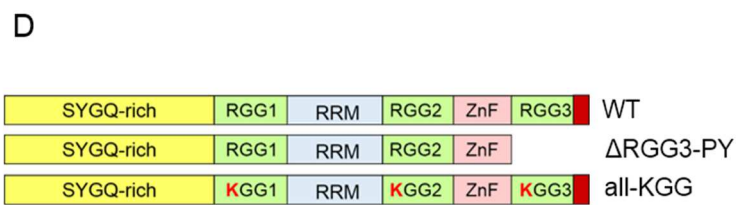
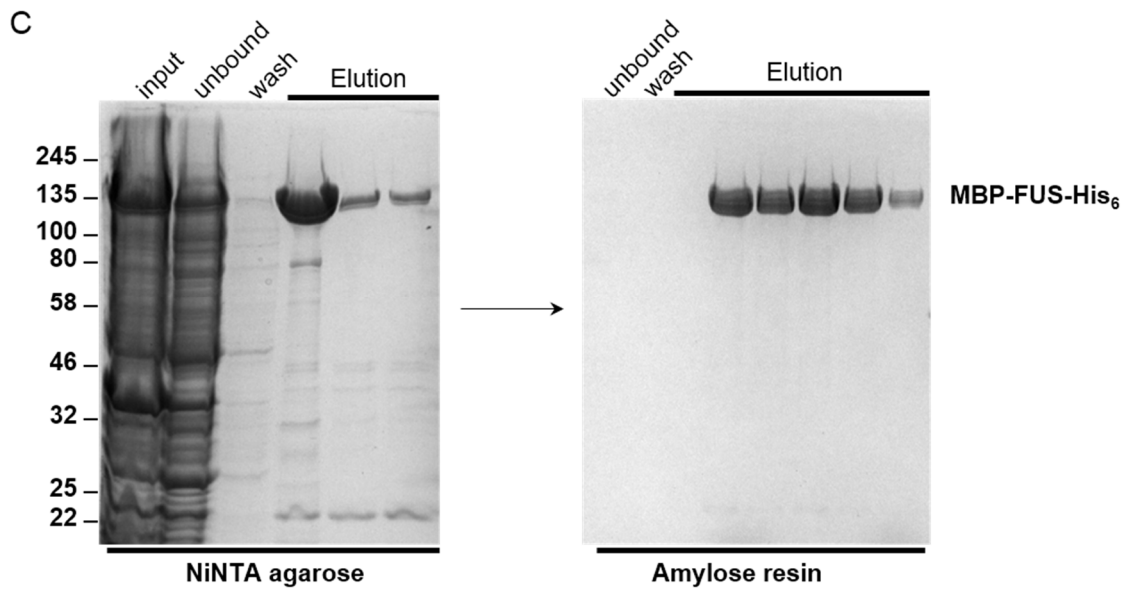
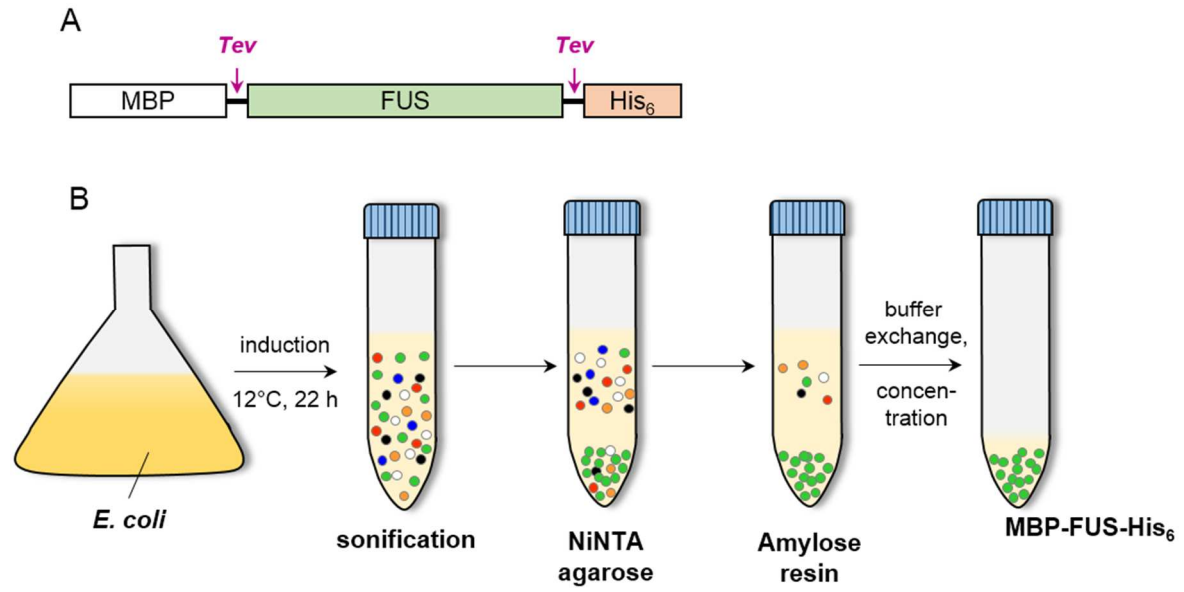


Figure 10: Purification of MBP-FUS-His₆ proteins. **A)** Scheme of MBP-FUS construct. Full-length FUS was N-terminally tagged with MBP to keep the protein soluble as well as C-terminally His₆-tagged. Both tags are separated from FUS by TEV cleavage sites and can be utilized for tandem-affinity purification. **B)** Schematic of the workflow for purification of all MBP-FUS-His₆ proteins. Induction of protein expression in *E. coli* was performed under very mild conditions at 12°C for 22h, in order to obtain soluble MBP-FUS. Following sonification, tandem-affinity purification using both affinity tags via NiNTA agarose and Amylose resin was performed. Pure MBP-FUS-His₆ proteins were buffer exchanged to IVM buffer and concentrated. **C)** Exemplary SDS-PAGE gels visualizing the purification of MBP-FUS-His₆ (WT). Protein bands are visualized by Coomassie stain. Note, that the lanes are not loaded equally. Elution fractions were pooled before buffer exchange. Molecular weight markers (in kDa) are indicated on the left. **D)** Schematic diagram of FUS full-length (WT), FUS with deletion of the RGG3-PY (Δ RGG3-PY), and a FUS mutant in which all RGGs in the RGG domains were mutated to KGGs (all-KGG). The three proteins are N-terminally tagged with MBP and C-terminally with His₆, as shown in the scheme in A). **E)** Western blots for verification of protein identities. Antibody specific for FUS-RGG3 (14G1) does not recognize mutant MBP-FUS proteins (Δ RGG3-PY and all-KGG). Equal loading demonstrated using an anti-FUS antibody that binds N-terminally of the RGG3 domain (4H11).

Upon liberation from the MBP-tag by proteolytic cleavage, full-length FUS (WT) starts to undergo liquid-liquid phase separation and forms liquid-like protein droplets (see scheme Fig. 11A) at physiological concentrations (1-10 μ M in HeLa cells (Patel et al., 2015)). In order to exclude that phase separation of FUS is induced simply by the presence of TEV protease independent of its proteolytic cleavage activity, recombinant MBP-FUS harboring a PreScission cleavage site was used. This protein only phase separates upon addition of PreScission protease, while addition of TEV protease does not induce its phase separation. Complementary, addition of PreScission protease is unable to induce phase separation of MBP-FUS containing a TEV cleavage site (Fig. 11B).

When a protein phase separates, the solution rapidly turns turbid and its optical density (OD) increases. The optical density can be measured at 600 nm and used as a quantitative readout for phase separation. When analyzed in such a turbidity assay, FUS WT shows a strong increase in turbidity, whereas turbidity of FUS Δ RGG3-PY reaches significantly lower turbidity values. The all-KGG mutant completely fails to phase separate and the solution remains clear (Fig. 11C). Furthermore, a sedimentation assay was performed, where protein samples are centrifuged and the partitioning of the protein into the pellet fraction is used as a measure for phase separation. Concordant with the turbidity measurements, FUS Δ RGG3-PY partitions significantly less into the pellet fraction in comparison to WT, and the all-KGG mutant remains almost completely in the supernatant (Fig. 11D, see Fig. 11E for quantification). Together, these results demonstrate that phase separation of FUS is not exclusively driven by the N-terminal SYGQ-rich domain (Burke et al., 2015; Kato et al., 2012; Murakami et al., 2015; Patel et al., 2015; Sun et al., 2011), as arginines in the C-terminal RGG/RG motifs and the RGG3-PY domain also have a crucial contribution to phase separation of FUS.

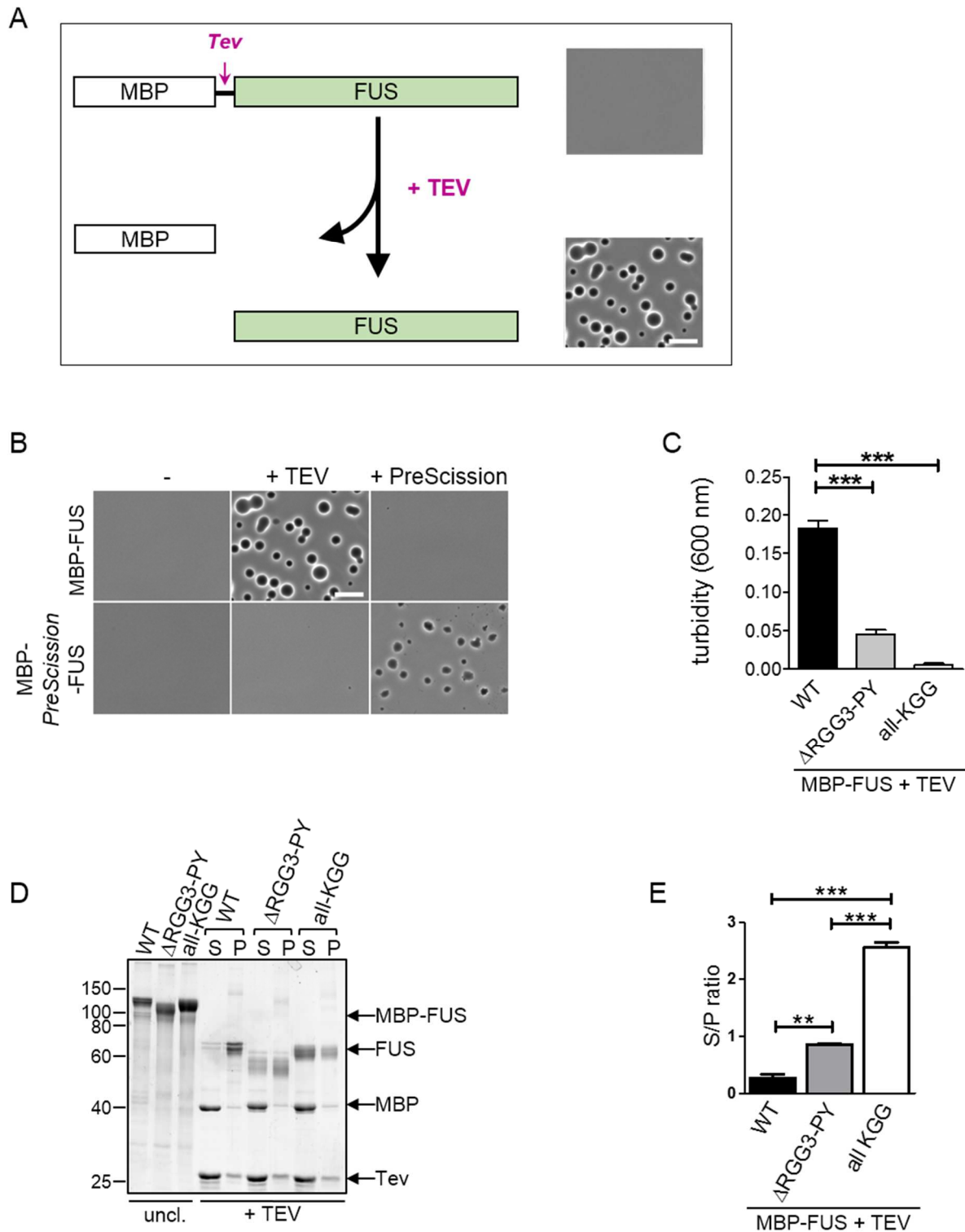


Figure 11: Arginines residues in the RGG/RG motifs crucially contribute to LLPS of full-length FUS. A) Schematic representation of TEV protease cleavage-induced phase separation of FUS. Addition of TEV protease to soluble MBP-tagged FUS causes proteolytic liberation of the MBP-tag (and His₆-tag, not shown in this scheme) and induces formation of liquid-like FUS droplets. **B)** TEV protease selectively induces phase separation of MBP-FUS harboring a TEV cleavage site by liberating the MBP-tag, but does not induce droplet formation of MBP-*PreScission*-FUS. Images acquired by phase contrast microscopy. Scale bar, 10 μ m. **C)** Turbidity assay for

quantitative comparison of TEV cleavage-induced phase separation of MBP-FUS-WT with the mutants MBP-FUS- Δ RGG3-PY and MBP-FUS-all-KGG (all proteins at 7 μ M). Phase separation of the C-terminal deletion mutant (Δ RGG3-PY) and the all-KGG mutant are strongly impaired in comparison to FUS WT. Values represent means \pm SEM (n=3). ***p < 0.001 by one-way ANOVA with Dunnett's multiple comparison test. **D)** Sedimentation assay for quantitative comparison of TEV cleavage induces phase separation of MBP-FUS-WT, MBP-FUS- Δ RGG3-PY and MBP-FUS-all-KGG (all proteins at 1 μ M). The mutant proteins are significantly less partitioned to the pellet fraction, confirming decreased phase separation compared to FUS WT. Proteins were detected by SyproRuby staining, molecular weight markers (in kDa) are indicated on the left. **E)** Quantification of the FUS band intensities in supernatant (S) and pellet (P) fractions is depicted as S/P ratio. Values represent means \pm SEM (n=3). **p<0.01 and ***p < 0.001 by one-way ANOVA with Bonferroni multiple comparison test.

2.3 Phase transitions of FUS are suppressed by TNPO1 *in vitro*

Several importin β -type nuclear import receptors have been shown to suppress aggregation of positively charged ribosomal proteins and histones in the cytoplasm (Jakel et al., 2002). As TNPO1 mediates nuclear import of FUS by interacting with the RGG3-PY domain (Dormann et al., 2012; Lee et al., 2006), which we have shown to be required for phase separation, we assumed that TNPO1 may fulfill a similar chaperone function towards its import cargo FUS. In order to test the hypothesis whether TNPO1 affects liquid-liquid phase separation of FUS, we cloned a C-terminally EGFP-tagged version of the previously used MBP-FUS, referred to as MBP-FUS-EGFP, and purified the protein analogously from *E. coli* (for scheme see Fig. 10B). This EGFP-tagged protein allowed us to visualize liquid droplets by fluorescence microscopy. EGFP-His₆ was fused to the C-terminus of FUS by a flexible 13-amino-acid linker (GAPGSAGSAAGSG), which according to Patel et al. (2015) maintains functionality of the FUS C-terminus (Fig. 12A). Similar to non-fluorescently labelled MBP-FUS, MBP-FUS-EGFP is soluble at physiological concentrations, but starts to phase separate upon proteolytic removal of the MBP-tag by TEV protease (Fig. 12B).

In order to test whether TNPO1 influences LLPS of FUS, equimolar amounts of recombinant TNPO1 or buffer only were added to MBP-FUS-EGFP-His₆ and formation of TEV cleavage-induced (+ TEV) FUS-EGFP droplets was visualized using confocal microscopy. Remarkably, FUS droplet formation is completely suppressed in presence of equimolar amounts of TNPO1 (Fig. 12B, see quantification of droplet area in Fig. 12C). Notably, half-molar amounts of TNPO1 are not sufficient to suppress droplet formation of FUS completely, but only suppress LLPS partially (approximately to fifty percent) (Fig. 12B), indicating that a 1:1 ratio of FUS:TNPO1 is needed for efficient suppression of LLPS. Furthermore, addition of TNPO1 to preformed FUS droplets causes an instantaneous dissolution of the droplets (Fig. 12D). These results show that TNPO1 is not only able to prevent, but also to reverse phase separation of FUS. In order to examine, whether this effect is specific to TNPO1, we added two other known FUS

interactors, namely PRMT1 that binds to FUS-RGG domains (Scaramuzzino et al., 2013; Tradewell et al., 2012) and an anti-FUS-RGG3-specific antibody (Suarez-Calvet et al., 2016) (direct binding confirmed in an *in vitro* binding assay, Fig. 13D), does not suppress phase separation of FUS to the same degree as TNPO1 (Fig. 12B, see Fig. 12C for quantification). Furthermore, the presence of the nuclear import receptor Importin 5 (Imp5), which is not a cognate import receptor of FUS and does not interact with FUS *in vitro* (Fig. 13D), is also not able to suppress phase separation of FUS (Fig. 12B and 12C).

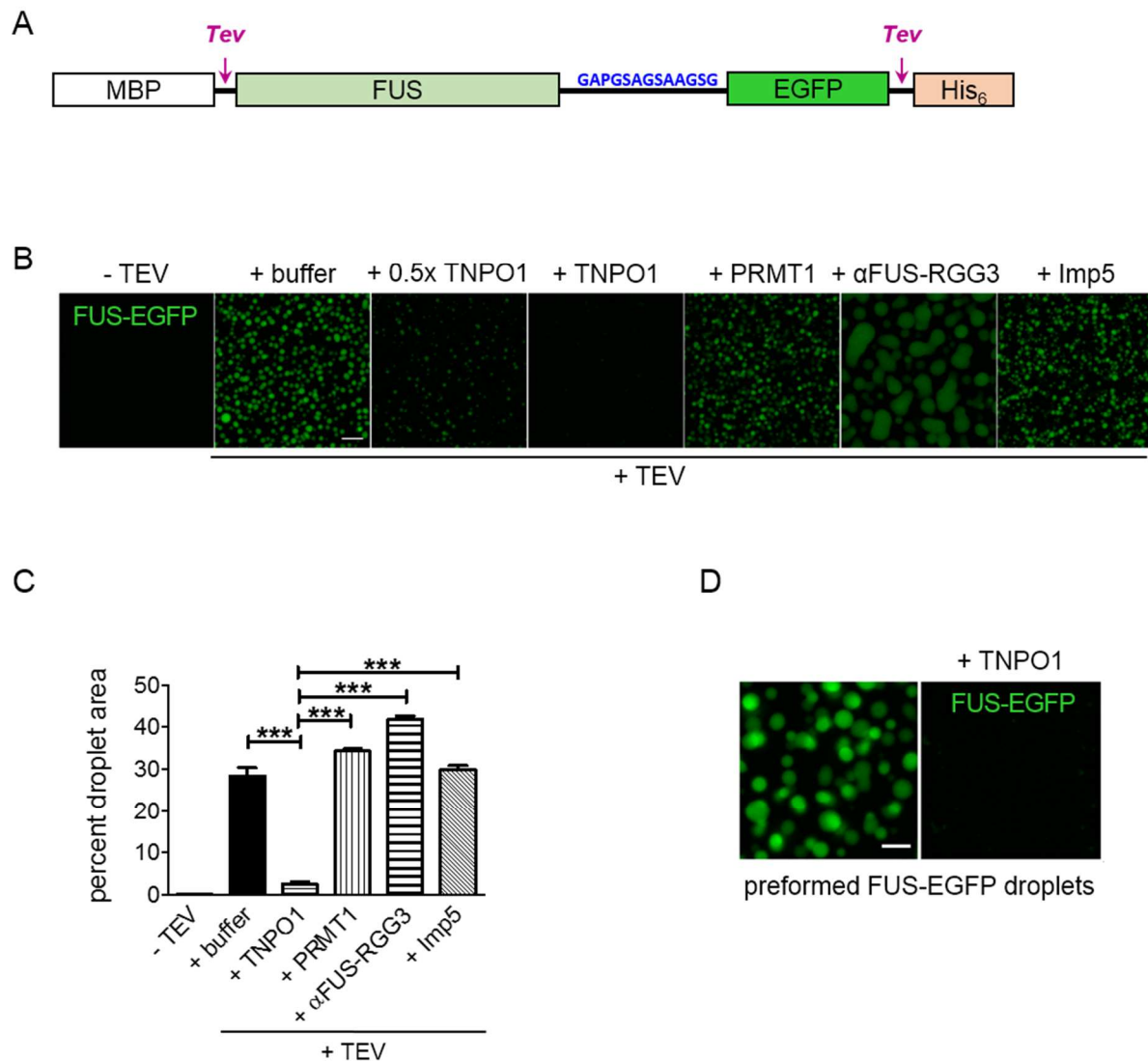


Figure 12: Transportin (TNPO1) suppresses and reverses droplet formation of FUS-EGFP *in vitro*. **A)** Scheme of MBP-FUS-EGFP construct. The construct is analogous to the MBP-FUS constructs and was purified as depicted in Fig. 10B. Instead of the C-terminal His₆-tag, it contains a C-terminal EGFP-His₆ separated by a 13 amino acid linker, to maintain functionality of the PY-NLS of FUS. **B)** Phase separation of MBP-FUS-EGFP induced by TEV protease cleavage is efficiently suppressed by equimolar amounts of TNPO1, but not by PRMT1, an antibody

specific for FUS-RGG3 (14G1) or by Importin 5 (Imp5). Note that the FUS-RGG3-specific antibody appears to increase the size of liquid FUS droplets, possibly by crosslinking two FUS molecules. Images were acquired by confocal fluorescence microscopy. Scale bar, 10 μm . **C**) Quantification of image area covered by FUS-EGFP droplets in percent. Values represent means \pm SEM (n=3). ***p < 0.001 by one-way ANOVA with Dunnett's multiple comparison test. **D**) Preformed droplets of FUS-EGFP (6 μM) dissolve instantaneously upon mixing with equimolar amounts of TNPO1. Changes in FUS-EGFP concentration and buffer conditions were obviated by using a highly concentrated stock of TNPO1 (140 μM) in droplet buffer. Scale bar, 5 μm .

Besides microscopic observation of droplet formation with subsequent quantification of droplet area, there are also other assays to monitor phase separation in a more quantitative way, namely the above described turbidity and sedimentation assays (Fig. 11C and 11D), for which non-EGFP-tagged FUS was utilized. To confirm our findings with EGFP-tagged FUS, we analyzed the effect of TNPO1 or control proteins on phase separation of MBP-FUS in a turbidity assay or sedimentation assay, respectively. In the presence of buffer, PRMT1, anti-FUS-RGG3 antibody or Imp5, respectively, the protein solution becomes turbid upon TEV protease-induced removal of the MBP-tag from FUS, whereas in the presence of TNPO1 the optical density of the solution remains low, comparable to the uncleaved and therefore dispersed MBP-FUS (Fig. 13A). Similarly, in a sedimentation assay, TEV cleavage causes quantitative partitioning of FUS into the pellet fraction after centrifugation, whereas FUS remains soluble in the presence of TNPO1. In contrast to TNPO1, PRMT1, the FUS-RGG3-specific antibody, and Imp5 are not able to keep FUS in the supernatant (Fig. 13B, see Fig. 13C for quantification).

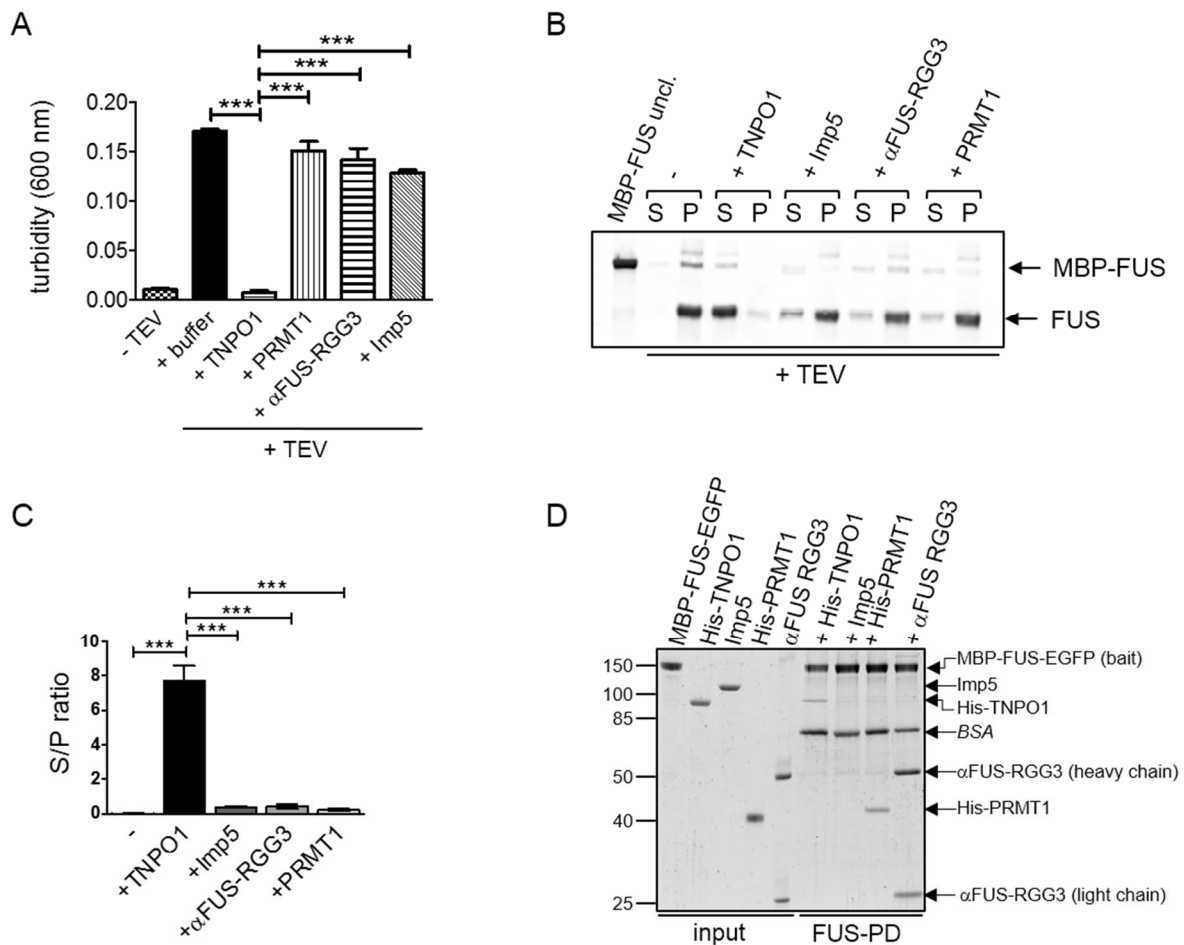


Figure 13: TNPO1 suppresses phase separation of FUS *in vitro*. **A)** Turbidity measurement for quantitative analysis of MBP-FUS phase separation in presence or absence of TNPO1 or various control proteins (PRMT1, Imp5 and anti-FUS-RGG3 antibody (14G1)). The MBP-tag of recombinant MBP-FUS (7 μ M) was cleaved by TEV protease in presence or absence of equimolar amounts of TNPO1 or various control proteins, respectively. Values represent means \pm SEM (n=3). ***p < 0.001 by one-way ANOVA with Dunnett's multiple comparison test. **B)** Sedimentation assay to quantify TEV cleavage-induced phase separation of MBP-FUS (1 μ M) in the presence or absence of equimolar amounts of TNPO1 or the control proteins PRMT1, Imp5 or anti-FUS-RGG3 antibody, respectively. **C)** Quantification of the FUS band intensities in supernatant (S) and pellet (P) fractions is depicted as S/P ratio. Values represent means \pm SEM (n=3). ***p < 0.001 by one-way ANOVA with Tukey's multiple comparison test. **D)** Pulldown (PD) assay to test direct interactions of MBP-FUS-EGFP with TNPO1 or indicated control proteins. Input and PD represent 5 % or 30 % of the sample, respectively. Protein bands are visualized by SyproRuby. Molecular weight markers (in kDa) are indicated on the left.

As recently reported in multiple studies, recombinant FUS can form solid aggregates and fibril-like structures *in vitro* through a liquid-to-solid state transition (Monahan et al., 2017; Patel et al., 2015). In order to study whether TNPO1 is not only able to prevent FUS droplet formation, but also to suppress the formation of FUS aggregates, *in vitro* "aging" assays were performed according to Patel

et al. (2015). Here, droplet formation of FUS-EGFP is induced by TEV protease cleavage and is followed by incubation for eight hours under mild agitation, leading to solidification and formation of large amorphous structures (Fig. 14A). The presence of equimolar amounts of TNPO1 suppresses droplet formation of FUS and consequently prevents the formation of large aggregates. In contrast, PRMT1 or Imp5, are not able to suppress the formation of amorphous aggregates (Fig. 14A). Notably, large amorphous aggregates form only when sample agitation is combined with pipetting up and down every hour. Otherwise, droplets only attach to each other and form chain-like structures. 90 min after TEV protease cleavage of MBP-FUS, we observed rod-like FUS fibrils by transmission electron microscopy (TEM). In line with the previously described assays, formation of FUS fibrils is completely suppressed in the presence of TNPO1 (Fig. 14B).

In sum, these results provide strong evidence that TNPO1 fulfills a dual function towards FUS: It not only mediates its nuclear import, but also keeps FUS soluble, by suppressing LLPS and subsequent solidification and aggregation of FUS *in vitro*.

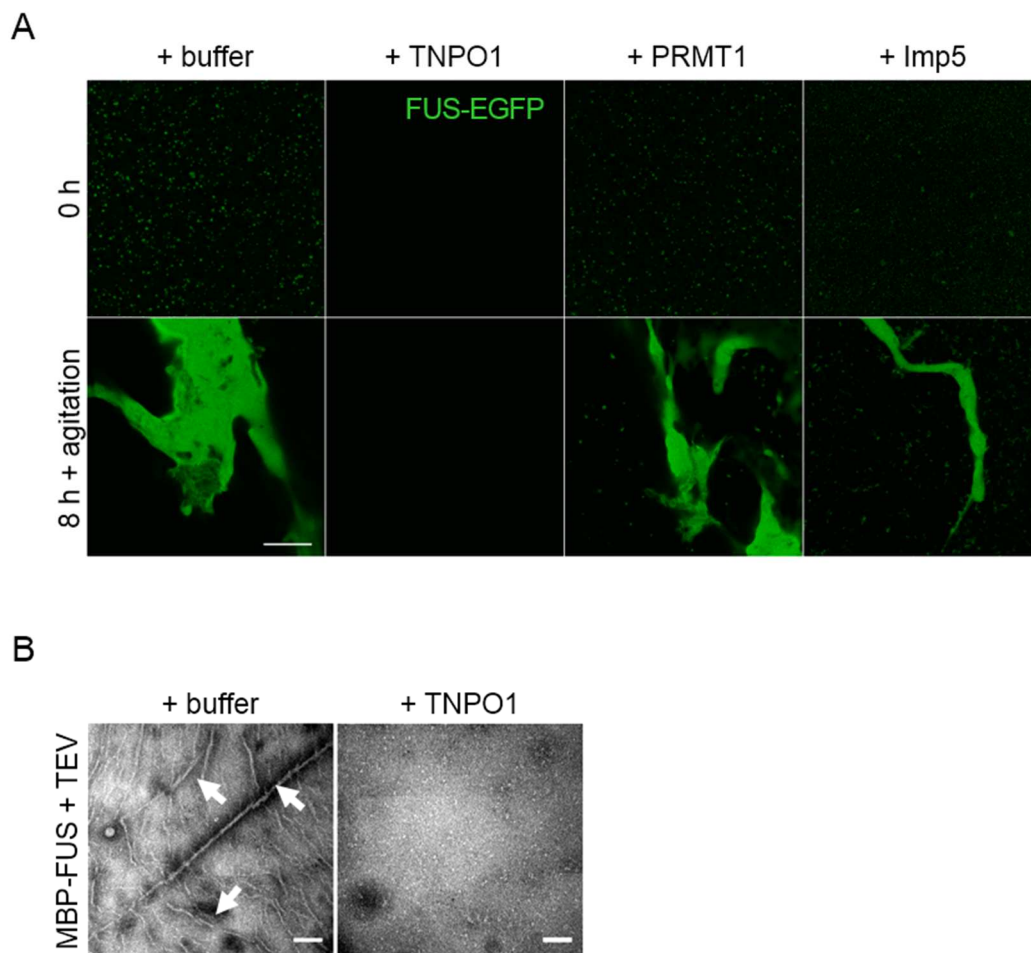


Figure 14: TNPO1 prevents solidification and fibrilization of FUS *in vitro*. **A)** *In vitro* liquid-to-solid phase transition of FUS-EGFP droplets (7 μ M) is suppressed by equimolar amounts TNPO1, but not by the control proteins PRMT1 and Imp5, respectively. Images were acquired by confocal fluorescence microscopy. Scale bar, 50 μ m. **B)** Fibril formation of FUS is suppressed in presence of equimolar amounts of TNPO1. MBP-FUS (7 μ M) was incubated with TEV protease for 90 min in presence or absence of equimolar amounts of TNPO1 and images acquired by TEM. Arrows denote fibrillary FUS aggregates. Scale bar, 200 nm.

2.4 TNPO1 exerts its chaperone function in cells independent of its nuclear import activity

As high RanGTP levels mediate dissociation of import complexes in the nucleus (Gorlich et al., 1996; Lee et al., 2006; Rexach and Blobel, 1995), it can be assumed that TNPO1 fulfills its chaperone activity towards FUS mainly in the cytoplasm, where RanGTP levels are low and therefore allow for the binding of TNPO1 to its cargoes. In order to test this hypothesis and to separate the chaperone activity of TNPO1 from its nuclear import activity, FUS was anchored in the cytoplasm by fusing it to a hormone-responsive domain of the glucocorticoid receptor (GCR) (GCR₂-tagRFP₂-FUS) (Love et al., 1998). Trapping of the GCR domain in the cytoplasm is maintained as long as no steroid hormones are present in the growth medium. In order to interfere with FUS-TNPO1 binding, a high affinity peptide inhibitor of TNPO1 (EGFP-M9M), that competes with regular TNPO1 cargoes (Cansizoglu et al., 2007), was co-expressed. Expression of the importin alpha (Imp α)-specific peptide inhibitor EGFP-bimax was used as a control. Bimax impairs Imp α -cargo interaction and consequently Imp α/β -dependent nuclear import (Bentmann et al., 2012; Dormann et al., 2010; Kosugi et al., 2008). Notably, expression levels of GCR₂-tagRFP₂-FUS in M9M-expressing cells were comparable or lower compared to cells co-expressing Bimax (data not shown). While Bimax-expressing cells show a diffuse cytosolic distribution of GCR₂-tagRFP₂-FUS, almost 50% of cells expressing the TNPO1-specific inhibitor M9M exhibit cytosolically anchored FUS localized to TIA1 positive SGs (Fig. 15A, see Fig. 15B for quantification), which were induced by transfection stress under both conditions. These results demonstrate that interference with FUS-TNPO1 binding promotes SG association of cytosolic FUS, suggesting that TNPO1 may chaperone cytoplasmic FUS and suppress its recruitment into SGs.

In order to directly assess the capability of TNPO1 to suppress SG partitioning of FUS, a variation of the semi-permeabilized cell assay was applied. Here, HeLa cells were treated with the proteasome inhibitor MG132 to evoke the formation of SGs (Ganassi et al., 2016), followed by selective permeabilization of the plasma membrane using digitonin. Subsequently, soluble proteins, including importins and other chaperones, were washed out from the cytoplasm (see scheme in Fig. 15C). Then,

in order to separate the nuclear import function of TNPO1 from its cytosolic chaperone activity, the nuclear pores were blocked using wheat germ agglutinin (WGA), thus preventing active nuclear transport through nuclear pore complexes (Yoneda et al., 1987). Afterwards, recombinant MBP-FUS-EGFP was added to the semi-permeabilized cells in presence or absence of TNPO1 and cells were washed to remove unbound proteins. In absence of TNPO1, recombinant FUS is bound to SGs, as indicated by co-staining with the SG marker protein G3BP1 (Fig. 15D). Notably, a 10-fold excess of TNPO1 was necessary to obtain efficient shielding of FUS in this assay. Equimolar amounts of TNPO1 are not sufficient, possibly due to a high abundance of other TNPO1 interactors in the preformed SGs that may capture most of TNPO1 added to the semi-permeabilized cells. Under these conditions, FUS shows significantly less association with SGs in presence of TNPO1 (Fig. 15D, see Fig. 15E for quantification).

Remarkably, these results demonstrate that TNPO1 suppresses SG association of FUS independent of its function as nuclear import receptor. Thus, in addition of its capability to suppress phase separation of FUS *in vitro*, TNPO1 also fulfills chaperone activity towards FUS in the cytoplasm, and hence reduces the likelihood of FUS to accumulate in SGs and undergo concentration-dependent aggregation in these structures.

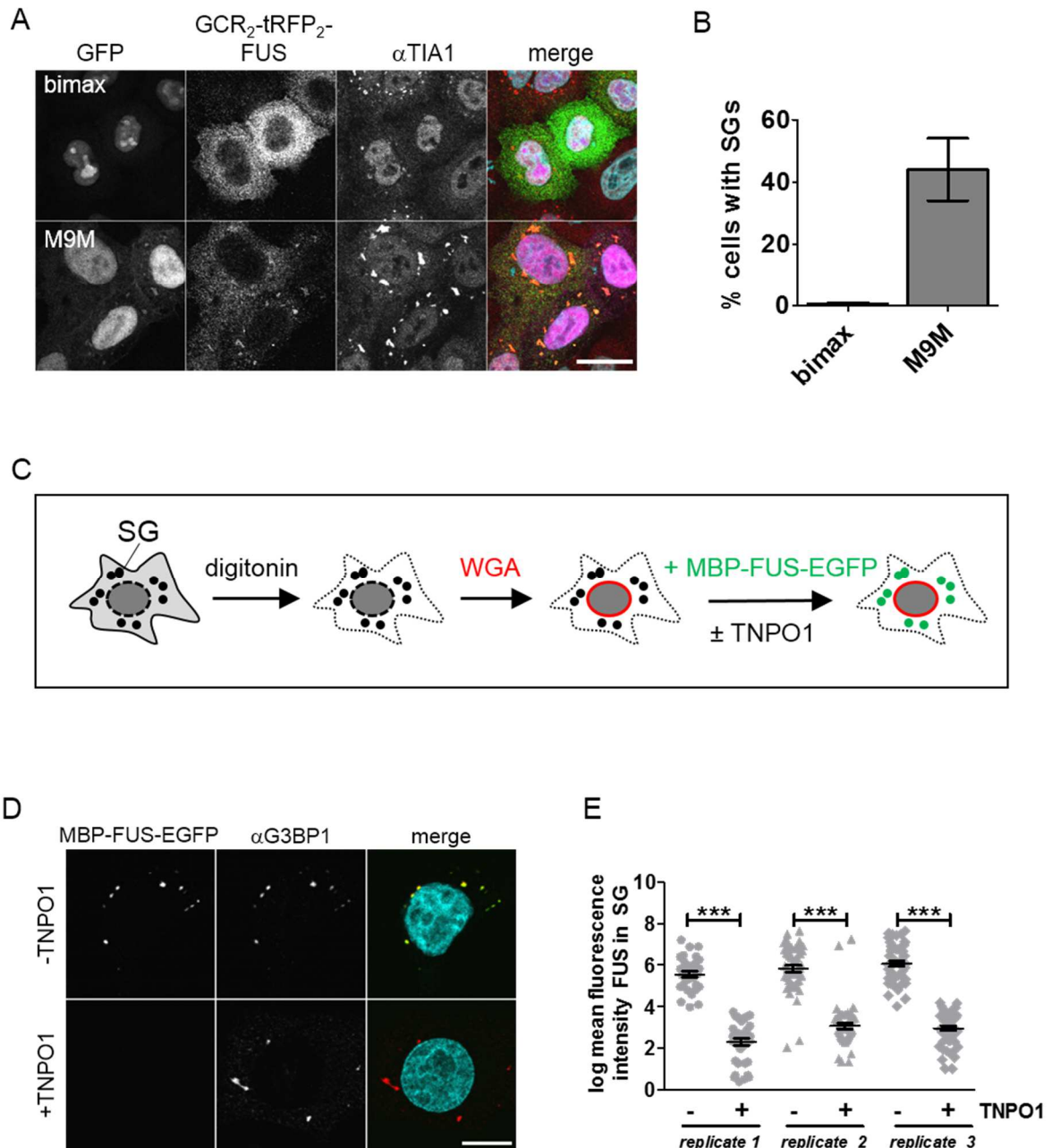


Figure 15: TNPO1 exerts chaperone activity in the cytoplasm and suppresses of SG association of FUS. A) Overexpression of the specific TNPO1 inhibitor EGFP-M9M causes a partial localization of cytosolically anchored FUS (GCR₂-tagRFP₂-FUS) with SGs, whereas overexpression of the importin α/β -specific inhibitor EGFP-bimax does not cause SG partitioning of GCR₂-tagRFP₂-FUS. For better visibility, the EGFP signal is depicted in magenta and the tRFP fluorescence is depicted in green in the overlay to the right. SGs were visualized by co-immunostaining with a TIA1-specific antibody (red) and nuclei were counterstained with DAPI (turquoise). Images were acquired by confocal fluorescence microscopy. Scale bar, 20 μ m. **B)** Quantification of cells exhibiting GCR₂-tagRFP₂-FUS localized to SGs. Values represent means \pm SEM (n=3; \geq 100 cells each). ***p < 0.001 by Fisher's exact test. **C)** Schematic representation of the modified semi-permeabilized cell assay allowing detection of SG partitioning of recombinant FUS. Following SG induction using MG132, the plasma membrane is selectively permeabilized by digitonine and all soluble proteins are washed out of the cytoplasm. In order to eliminate active nuclear import, nuclear pores are blocked by WGA prior to addition of recombinant MBP-FUS-EGFP in presence

or absence of TNPO1. **D)** SG recruitment of MBP-FUS-EGFP in semi-permeabilized cells is prevented by TNPO1. SGs visualized by G3BP1-immunostaining (red). Nuclei were counterstained with DAPI (turquoise). Images were acquired by confocal fluorescence microscopy. Scale bar, 10 μ m. **E)** Quantification of log-transformed mean fluorescence intensity MBP-FUS-EGFP in SGs from three replicates \pm SEM (\geq 10 cells, \geq 32 SGs each). *** $p < 0.001$ by Mann-Whitney test.

2.5 Mechanisms contributing to the chaperone activity of TNPO1

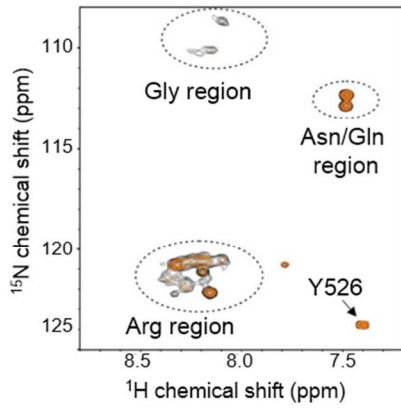
Based on our finding that the nuclear import receptor TNPO1 is able to suppress phase separation of FUS, we postulated two putative mechanisms how TNPO1 may interfere with phase separation of FUS. As FUS harbors multiple domains involved in RNA binding and specifically RGG/RG-rich motifs were recently reported to be essential for RNA-binding of FUS (Ozdilek et al., 2017), our first hypothesis was that TNPO1 may interfere with RNA-driven phase separation of FUS by competing with RNA-binding to RGG/RG motifs. Second, as arginines are crucial for phase separation of FUS (see section 2.2 and Fig. 11), we considered the possibility that TNPO1 suppresses arginine-driven phase separation of FUS by directly interacting with arginines.

In order to test the first hypothesis, the effect of TNPO1 on RNA-driven LLPS of the RGG3-PY domain was addressed by NMR spectroscopy. To this end, unlabeled (UG)₁₂ RNA was titrated to ¹⁵N-labeled RGG3-PY, causing an increase in turbidity and leading to progressive disappearance of ¹H-¹⁵N cross peaks (Fig. 16A). At the same time, the signal intensity in the corresponding 1D NMR spectrum decreases (Fig. 16B), indicating the formation of high-molecular weight RGG3-PY/RNA droplets, resulting in a broadening of NMR signals as a result of reduction in rotational tumbling time of the RGG3 region within droplets. Since NMR signals of unlabeled RNA were absent in the 1D NMR spectra (Fig. 16B), RNA is quantitatively bound in RGG3-PY droplets. Upon addition of equimolar amounts of TNPO1 to the RGG3-PY/RNA droplet sample, turbidity is lost and ¹H NMR signals of the RNA reappeared, indicating that RNA is displaced from RGG3-PY by TNPO1 binding and consequently droplets dissolved (Fig. 16B). Next, radioactive filter-binding experiments were conducted using RGG3-PY (Fig. 16C) or MBP-FUS (Fig. 16D) preincubated with radiolabeled *ASH1* E3-51 RNA, TNPO1 was subsequently titrated into the RGG3-PY- or MBP-FUS-RNA complexes in order to test whether TNPO1 displaces RNA from FUS. In a radioactive filter-binding assay, RNA-protein complexes are visualized on a nitrocellulose (NC) membrane, whereas free RNA is detected on a nylon membrane. Consistent with the NMR experiments, radioactive signal intensity on the nitrocellulose membrane (NC), decreases with increasing amounts of TNPO1, demonstrating that TNPO1 displaces RNA from RGG3-PY (Fig. 16C) and MBP-FUS (Fig. 16D and 16E). Thus, TNPO1 competes with RNA for the same binding sites and

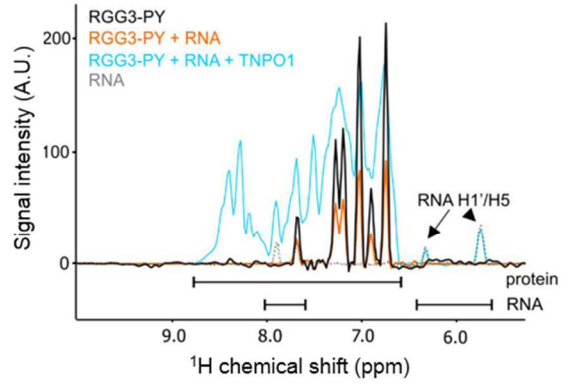
competes away RNA that is bound to the C-terminal RGG3-PY domain or full-length FUS. However, although phase separation of RGG3-PY is clearly promoted upon addition of RNA (Fig. 9D), we did not detect a significant alteration in phase separation of full-length FUS upon titration of *ASH1* E3-51 RNA (Fig. 16F). Concordantly, similar results were obtained for titration of *MAPT* RNA (Fig. 16G) and total RNA (data not shown). Together, these results indicate that, under our experimental conditions, phase separation of full-length FUS is not strongly affected by RNA. Consequently, the displacement of RNA from FUS by TNPO1, does not seem to be the major mechanism by which TNPO1 suppresses phase separation of FUS.

Previously published data have demonstrated that TNPO1 directly binds to a synthetic FUS-RGG3 peptide (Dormann et al., 2012) as well as to several arginine residues in the RGG3 motif of FUS (R472, R473, R476) (Gobl et al., 2016). This supports the second hypothesis that TNPO1 suppresses arginine-driven phase separation of FUS by direct interaction with arginines in the RGG3-PY domain. Our ITC data show a strong decrease in binding of TNPO1 to RGG3-PY at higher salt concentrations (Table 2), indicating that the interaction of TNPO1 with FUS-RGG3 is primarily charge-driven. This furthermore supports the idea that TNPO1 undergoes electrostatic interactions with positively charged arginines and thus may interfere with arginine-driven phase separation of FUS.

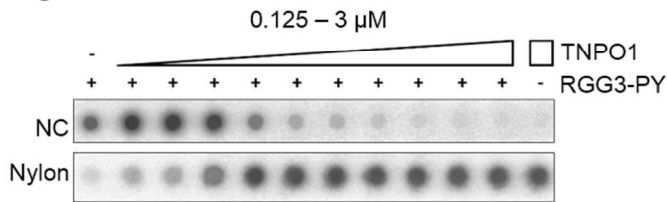
A



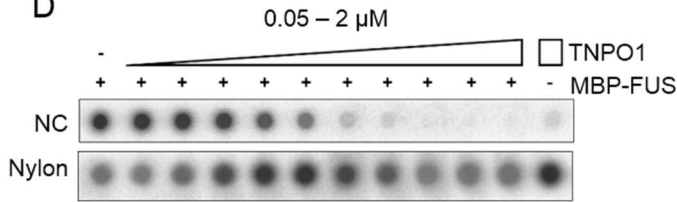
B



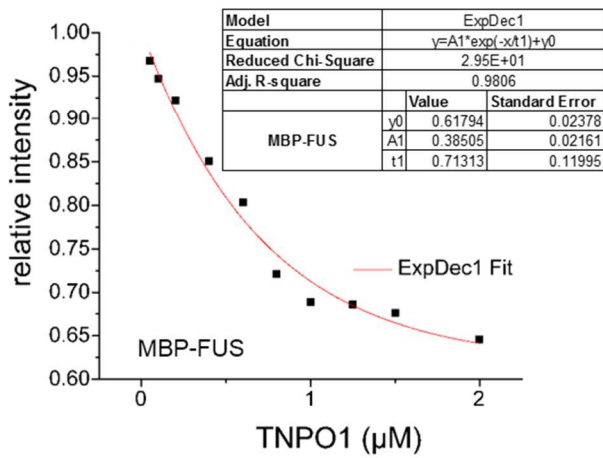
C



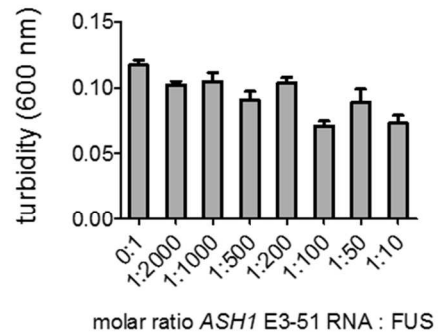
D



E



F



G

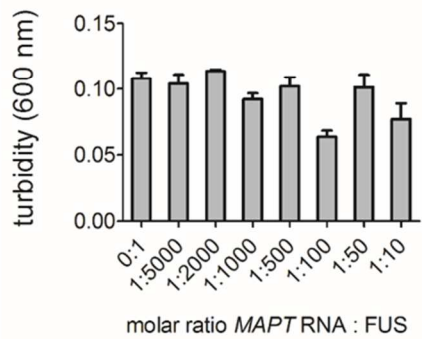


Figure 16: Different mechanisms may be involved in the chaperoning by TNPO1. **A)** NMR data visualizing RNA-driven phase separation of FUS RGG3-PY. ^1H - ^{15}N SOFAST HMQC spectrum of ^{15}N -labeled RGG3-PY in presence (orange) or absence (black) of 0.2 stoichiometric equivalents of (UG) $_{10}$ RNA. Spectra were recorded with an interscan delay of 1.0 s, spectral widths of 16/32 ppm, centered at 4.7/115.0 ppm in $^1\text{H}/^{15}\text{N}$, with 512 and 128 complex data points, respectively, and 8 scans per increment. **B)** NMR data confirming RNA displacement from FUS RGG3-PY by TNPO1. ^1H NMR spectra of ^{15}N -labeled RGG3-PY (black), supplemented with 0.2 stoichiometric equivalents of (UG) $_{10}$ RNA (orange), and with equimolar amounts of TNPO1 (light blue), respectively. The reference ^1H NMR spectrum of free RNA at the same concentration is depicted in grey (dotted line). Protein concentrations were 100 μM . Spectra were recorded with an interscan delay of 1.0 s, spectral widths of 20 ppm, centered at 4.7 ppm in ^1H , with 512 complex data points and 256 scans. **C)** Representative images of a filter-binding assay with FUS RGG3-PY, TNPO1, and radiolabeled *ASH1* E3-51 RNA. RNA-protein binding (nitrocellulose membrane: NC) and free RNA (nylon membrane) are visualized by phosphorimaging. Increasing amounts of TNPO1 displace bound RNA from FUS RGG3-PY (NC) and cause an increasing signal of liberated RNA (nylon). **D)** Representative images of a radioactive filter-binding experiment with MBP-FUS, TNPO1 and, radioactively labeled *ASH1* E3-51 RNA. Titration of TNPO1 results in reduction of RNA bound to MBP-FUS (NC) and concomitant increase in free RNA (nylon). **E)** Representative plot of relative signal intensities from radioactive filter-binding assay shown in D). The relative signal intensity was plotted over the titrated TNPO1 concentration. For curve fitting the exponential decay fitting algorithm (in Origin software) was applied. Summary of the decay factor and amplitude of three independent experiments are depicted in the table. **F)** and **G)** Turbidity assay to determine the influence of *in vitro* transcribed *ASH1* E3-51 RNA (F) and *MAPT* RNA (G) on TEV cleavage-induced phase separation of MBP-FUS (5 μM), demonstrating no promoting effect of RNA on LLPS of full-length FUS at the indicated RNA:FUS ratios. Values represent means \pm SEM (n=3).

Table 2: Thermodynamic parameters of ITC titrations to TNPO1

Protein	K_d (nM)	ΔH (kcal* mol^{-1})	ΔS (kcal* mol^{-1})
unmeRGG3-PY	3 ± 1	-26.5 ± 0.1	- 49.7
meRGG3-PY	126 ± 20	-25.3 ± 0.1	- 48.6
unmeRGG3-PY (1 M NaCl)	398 ± 31	-18.9 ± 0.4	-34.3
unmeRGG3-PY P525L	27 ± 2	-17.6 ± 0.1	-24.5
meRGG3-PY P525L	356 ± 27	-17.4 ± 0.2	-28.6
unmeRGG3-PY P525L (1M NaCl)	not detectable		

Errors represent the SD of the fit.

Stoichiometry associated with complex formation was set to 1.

2.6 Loss of arginine methylation promotes phase separation of FUS

Arginines in RGG/RG-rich motifs are common targets for PRMTs and therefore are frequently methylated (Guo et al., 2014; Thandapani et al., 2013; Wooderchak et al., 2008). As arginines in the RGG domains of FUS are usually asymmetrically dimethylated (Dormann et al., 2012; Guo et al., 2014; Ong et al., 2004; Rappsilber et al., 2003; Suarez-Calvet et al., 2016; Uhlmann et al., 2012) and we found that arginines and RGG/RG motifs have an essential contribution to phase separation of FUS (see section 2.2 and Fig. 11), we next addressed whether arginine methylation of RGG/RG motifs may alter phase separation of FUS. This question is of particular importance, since asymmetric dimethylation of arginines of FUS-RGG3 domain is lost in pathological inclusions of FTD-FUS patients and instead FUS is unmethylated and monomethylated (Dormann et al., 2012; Suarez-Calvet et al., 2016). In spite of that, it remains elusive whether and how loss of methylation of FUS contributes to pathology of FTD-FUS.

In order to address this question, we aimed to compare unmethylated and methylated MBP-FUS-EGFP, MBP-FUS or RGG3-PY in phase separation assays. As proteins are not post-translationally modified in bacteria, the purified proteins are originally unmethylated. In order to specifically obtain asymmetric dimethylated FUS, *in vitro* methylation of FUS proteins with PRMT1 as methylating enzyme was performed. To do so, recombinant His₆-PRMT1 was expressed in *E. coli* and purified via a HisTrap column. In order to remove bound nucleic acids, the bound protein was subjected to high salt washes (1M NaCl). Applying an imidazole gradient allowed to gradually elute contaminating proteins in a first peak followed by almost pure His₆-PRMT1 (second peak). Notably, fast buffer exchange of PRMT1 by a HiPrep Desalting column had to be performed (see scheme in Fig. 17A and 17B), as prompt use of PRMT1 in *in vitro* methylation reactions emerged to be crucial for efficient methyltransferase activity. Particularly, freezing or short term storage of recombinant PRMT1 was not possible, since PRMT1 precipitated and lost its enzymatic activity upon freeze-thawing or storage at 4°C. Similarly, buffer exchanges using overnight dialysis or spin concentrator tubes provoked precipitation and loss of activity (not shown). For *in vitro* methylation, FUS proteins were incubated with purified PRMT1 and SAM (+ SAM) as a methyl group donor. As a control, unmethylated FUS proteins were incubated with PRMT1 in absence of SAM (- SAM) (see scheme in Fig. 17C). Successful *in vitro* methylation was verified by Western blotting using antibodies specific for FUS-RGG3 carrying unmethylated arginines (UMA), monomethyl arginines (MMA), and asymmetric dimethylarginines (ADMA) (Dormann et al., 2012; Suarez-Calvet et al., 2016) (Fig. 17D). Incubation with PRMT1 and SAM caused a strong signal reduction for UMA-FUS and an appearance of an ADMA-FUS signal (Fig. 17D), confirming that

unmethylated proteins were efficiently converted to a primarily asymmetrically dimethylated form. In contrast, proteins remained unmethylated when incubated with PRMT1 only (- SAM) (Fig. 17D).

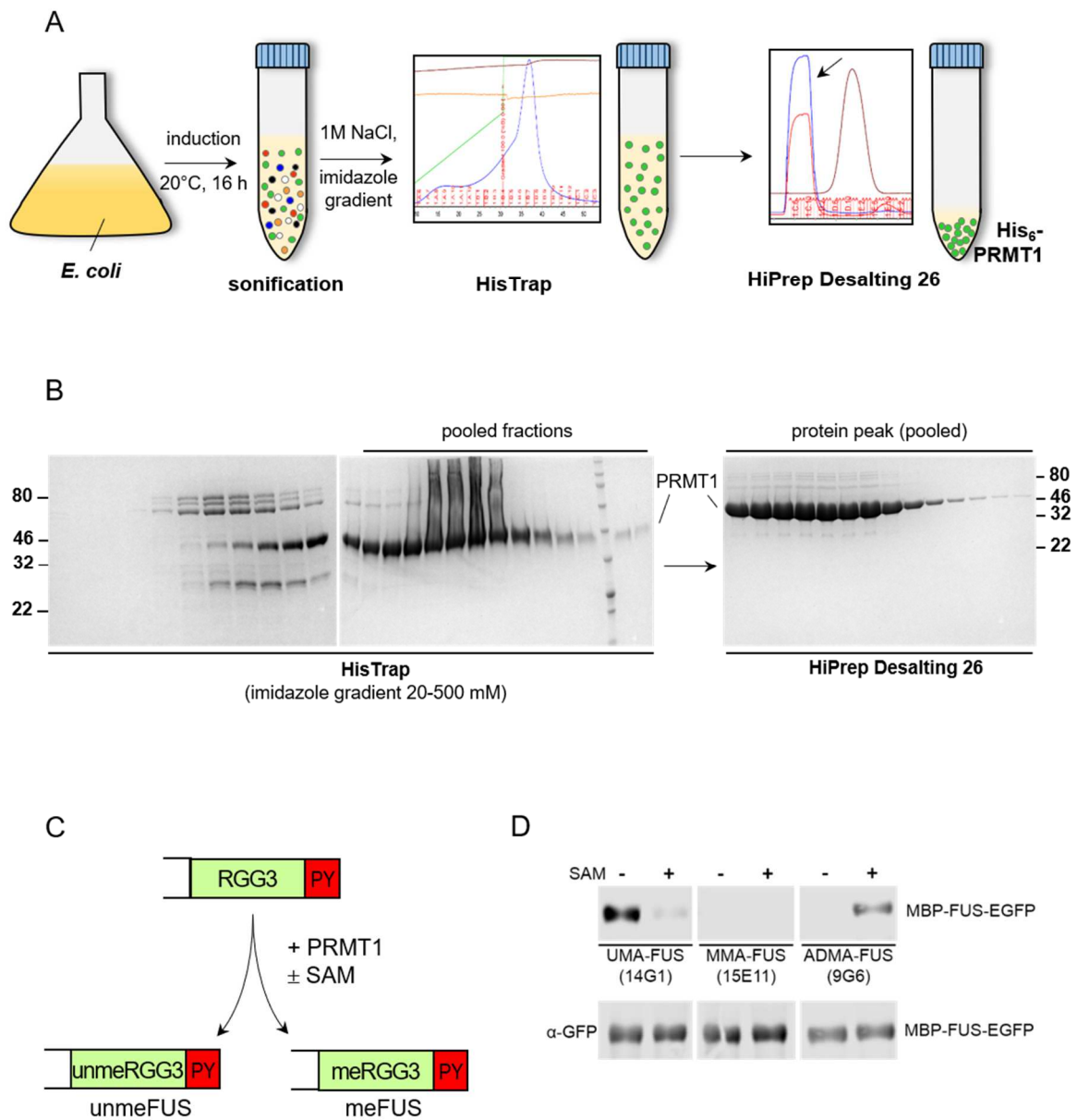


Figure 17: Purification of His₆-PRMT1 for *in vitro* methylation of FUS. A) Schematic of the workflow with representative ÄKTA chromatograms for purification of His₆-tagged protein arginine methyltransferase 1 (His₆-PRMT1). Following sonification, the cleared bacterial lysate was applied to a HisTrap column using a peristaltic pump and subjected to high salt washes (1M NaCl). Subsequently, imidazole gradient elution was performed via an ÄKTA system and the pooled elution fractions were desalted via a HiPrep Desalting column. The chromatogram of HiPrep Desalting provides a first peak containing the buffer exchanged protein (blue) followed by a salt peak. **B)** Exemplary SDS-PAGE gels visualizing the purification of His₆-PRMT1. Protein bands are visualized by Coomassie stain. Note that the lanes are not loaded equally. Indicated fractions yielded from gradient elution were pooled and further processed with a HiPrep Desalting column. All fractions of the protein peak were pooled and used for subsequent *in vitro* methylation. Molecular weight markers (in kDa) are indicated on the left. **C)** Schematic representation of *in vitro* methylation of FUS proteins. Purified proteins were incubated

with purified His₆-PRMT1 and the methyl group donor S-adenosylmethionine (+SAM overnight at room temperature). To obtain an unmethylated control, recombinant FUS was incubated with PRMT1 in absence of SAM (-SAM). **D**) Representative immunoblots for MBP-FUS-EGFP confirming successful *in vitro* methylation. Immunoblotting performed with monoclonal antibodies specific for FUS-RGG3 containing unmethylated arginines (UMA-FUS, 14G1), monomethylated arginines (MMA-FUS, 15E11) and asymmetrically dimethylated arginines (ADMA-FUS, 9G6), respectively, demonstrates a strong reduction of the UMA-FUS signal and a conversion to ADMA-FUS. Equal loading was confirmed by immunoblotting with an EGFP-specific antibody. Similar results were obtained for MBP-FUS and RGG3-PY *in vitro* methylation (data not shown).

First, we compared the propensity to undergo LLPS of unmethylated and methylated MBP-FUS-EGFP in a droplet assay. This revealed that unmethylated FUS forms liquid droplets at lower protein concentration than dimethylated FUS (Fig. 18A). In order to exclude that reduced phase separation of FUS is caused by the presence of SAM, addition of SAM alone did not alter LLPS of unmethylated FUS (data not shown). Similarly, in a sedimentation assay, unmethylated FUS shows a significantly higher degree of partitioning into the pellet fraction than methylated FUS (Fig. 18B, see Fig. 18C for quantification). Concordantly, in a turbidity assay where TEV-induced phase separation of unmethylated and methylated FUS was monitored over time, unmethylated FUS reaches higher turbidity compared to unmethylated FUS (Fig. 18D). In order to exclude that phase separation of methylated FUS is compromised by bound nucleic acids, since the protein samples used in Fig. 18 A-D were not completely nucleic acid-free, the droplet assay was repeated with a nucleic acid-free preparation of unmethylated and methylated FUS-EGFP (Fig. 18E). In line with the previously performed assays, RNA-free methylated FUS-EGFP also shows reduced droplet formation compared to unmethylated FUS-EGFP (Fig. 18E). Thus, irrespective of RNA-binding, loss of arginine methylation promotes LLPS of FUS.

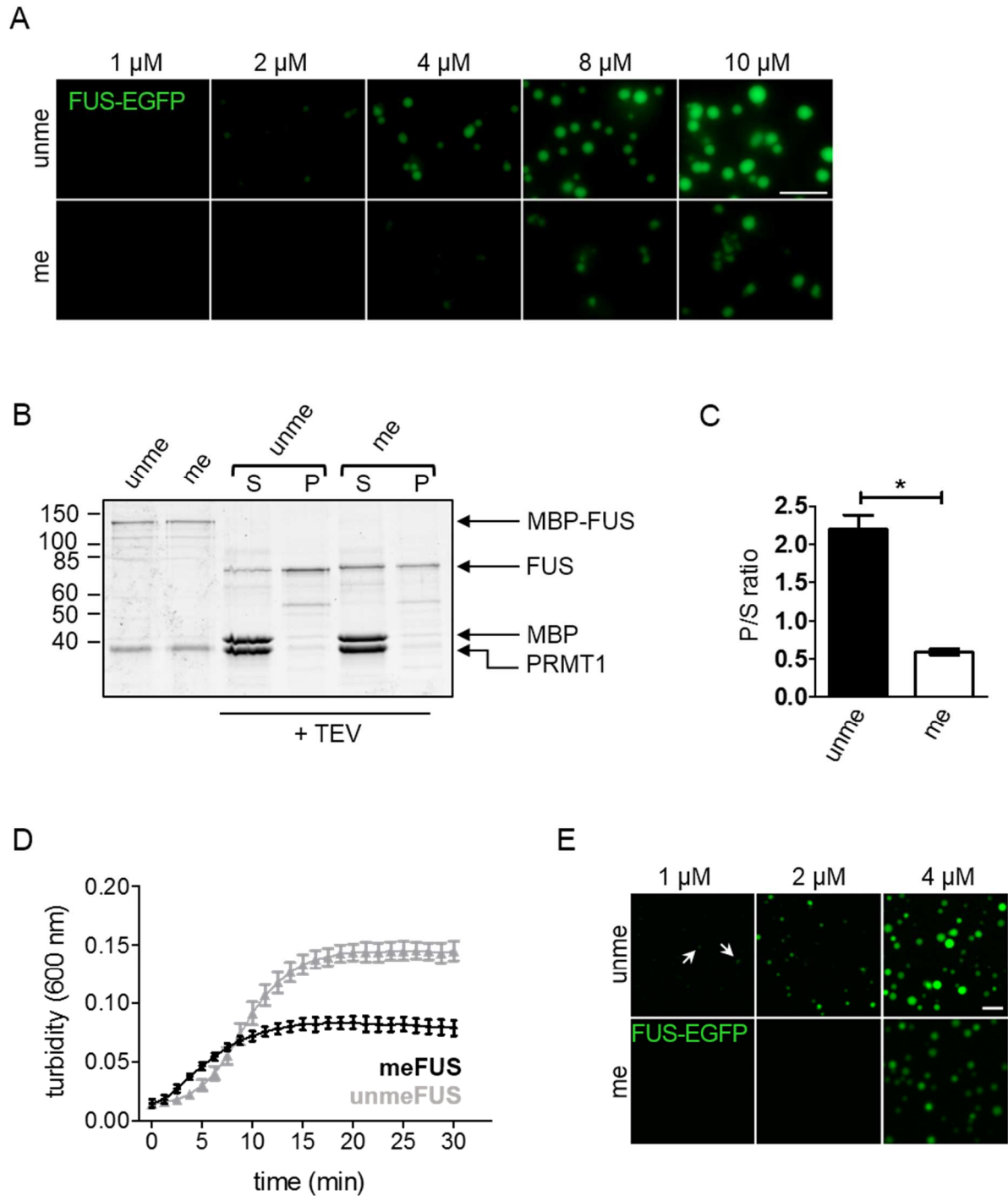


Figure 18: Arginine methylation reduces phase separation of FUS. **A)** Droplet formation of unmethylated (unme) FUS-EGFP is enhanced compared to methylated (me) FUS-EGFP after TEV protease-induced removal of the MBP-tag. Images were acquired by widefield fluorescence microscopy. Scale bar, 5 μ m. **B)** Phase separation of methylated (me) FUS is strongly reduced in comparison to unmethylated (unme) FUS. Sedimentation assay to compare precipitation of unmethylated (unme) and methylated (me) MBP-FUS upon TEV protease-cleavage. Equal volumes of supernatant (S) and pellet (P) fractions were visualized by SyproRuby stain. Molecular weight markers (in kDa) are indicated on the left. Note that PRMT1 (but not SAM) was present in both samples to assure comparability, as indicated in Fig. 17C. **C)** Quantification of FUS levels in supernatant (S) and pellet (P) fractions are depicted as P/S ratio. Values represent means \pm SEM (n=3). *p < 0.05 by paired t-test. **D)** Turbidity

measurements to monitor TEV protease-induced phase separation of unmethylated (unme) and methylated (me) MBP-FUS (7 μ M) in presence of 75 mM NaCl over time demonstrating reduced phase separation of methylated (me) FUS in comparison to unmethylated (unme) FUS. Values represent means \pm SEM (n=3). **E**) Droplet formation of unmethylated (unme) and methylated (me) FUS-EGFP from a nucleic-acid free preparation upon TEV protease cleavage. Arrows denote small droplets observed for unmethylated FUS-EGFP at a concentration of 1 μ M. Images were acquired by widefield fluorescence microscopy. Scale bar, 5 μ m.

2.7 Loss of arginine methylation alters droplet dynamics and promotes SG association of FUS

To address the effect of arginine methylation on phase separation of FUS in more detail, we examined the droplet dynamics of unmethylated FUS-EGFP compared to methylated FUS-EGFP and monitored fluorescence recovery after photobleaching (FRAP) in the bleached area. For these assays, in contrast to other droplet assays, the droplet buffer was supplemented with 150 mg/ml Ficoll 400 in order to obtain droplets of similar size and shape for unmethylated and methylated FUS. For droplet half-bleach, only droplets with a size of approximately 2 μ m were selected. In contrast to methylated FUS, unmethylated FUS displays incomplete and decelerated recovery of the bleached area (Fig. 19A and 19B). These results demonstrate reduced internal mobility within the dense droplet phase of unmethylated FUS. In accordance with the findings from the *in vitro* aging assays, droplets of both unmethylated and methylated FUS-EGFP show reduced mobility over time, indicating a progressive conversion from a liquid to a more solid state. To overcome this issue, no more than three droplets were analyzed per sample preparation and samples were prepared freshly.

In order to evaluate whether unmethylated and methylated FUS also show different dynamics in cells, we examined whether SG association in the semi-permeabilized cell assay is affected by arginine methylation of FUS. Therefore, unmethylated or methylated MBP-FUS-EGFP was added to stressed, WGA-blocked, semi-permeabilized HeLa cells (Fig. 19C, for schematic diagram see Fig. 15C). Significantly more unmethylated FUS binds to G3BP1-positive SGs (Fig. 19C, see quantification of log transformed fluorescent intensities in Fig. 19D), confirming a higher association of unmethylated FUS with SGs. These observations indicate that unmethylated FUS is more stably associated with SGs than methylated FUS. In conclusion, loss of arginine methylation of FUS, as detected in pathological inclusions of FTD-FUS patients (Dormann et al., 2012; Suarez-Calvet et al., 2016), promotes LLPS and SG association of FUS and reduces FUS droplet dynamics. This may contribute to altered SG dynamics and consequent solidification and aggregation of FUS in FTD-FUS patients.

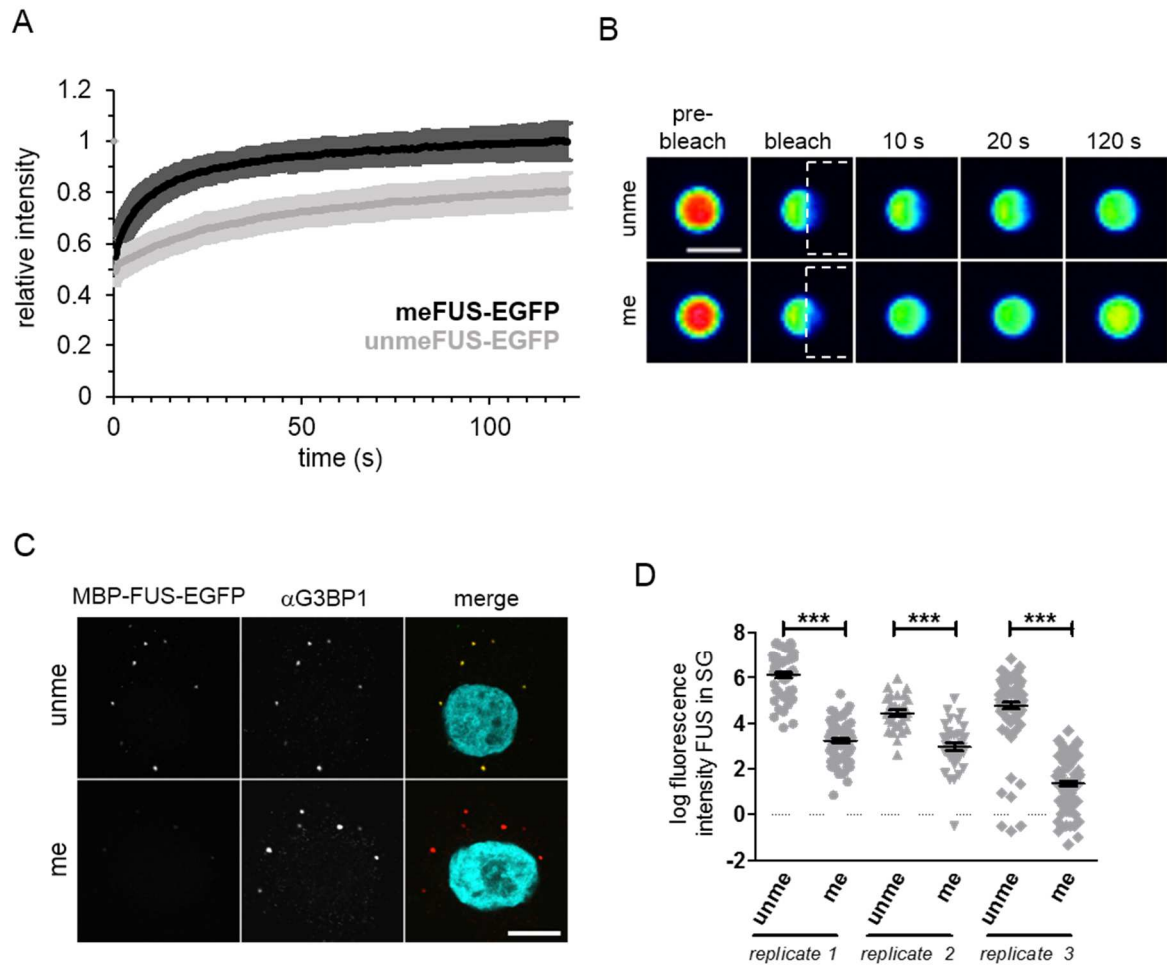


Figure 19: Arginine methylation alters droplet dynamics and reduces SG association of FUS. **A)** Droplets of unmethylated (unme) FUS-EGFP exhibit reduced droplet dynamics compared to methylated (me) FUS-EGFP. FRAP recovery curves following half-bleach of unmethylated (unme) and methylated (me) FUS-EGFP droplets (9 μ M). To obtain droplets of similar size and shape, droplet buffer (75 mM NaCl) was supplemented with 150 mg/ml Ficoll 400 in FRAP experiments. **B)** Representative heat map images of bleached droplets to visualize recovery over time. Boxes indicate bleached area. Scale bar, 2 μ m. Fluorescence in the bleached area recovers more quickly for meFUS-EGFP droplets, indicating higher droplet dynamics than for unmeFUS-EGFP. **C)** Semi-permeabilized cell assay demonstrating enhanced SG partitioning of unmethylated (unme) MBP-FUS-EGFP compared to methylated (me) MBP-FUS-EGFP. SGs were visualized by anti-G3BP1 immunostaining and nuclei were counterstained with DAPI (turquoise). Images were acquired by confocal fluorescence microscopy. Scale bar, 10 μ m. **D)** Quantification of the log-transformed mean fluorescence intensity of MBP-FUS-EGFP in SGs. (n = 3; ≥ 10 cells, ≥ 28 SGs each). ***p < 0.001 by Mann-Whitney test.

2.8 Arginine methylation stabilizes RNA binding of FUS-RGG3-PY

Titration of substoichiometric amounts of *in vitro* transcribed *MAPT* RNA to unmethylated and methylated RGG3-PY revealed that both proteins reach maximal turbidity at a molar RNA-to-protein ratio of 1:50. At this molar ratio, unmethylated RGG3-PY shows a significantly higher turbidity compared to methylated RGG3-PY (Fig. 20A). The different degrees of phase separation raise the question whether methylation of RGG3-PY alters RNA binding, consequently affecting phase separation. To address this question, we performed electrophoretic mobility shift assays (EMSAs) by titrating unmethylated or methylated RGG3-PY to radiolabeled *ASH1* E3-51 RNA (Fig. 20B). While a band shift is detectable upon titrating in methylated RGG3-PY, confirming RNA binding, no band shift is detectable by titrating in unmethylated RGG3-PY, indicating that RNA binding is altered by arginine methylation. As EMSA experiments indicate differences in RNA binding, we further investigated whether RNA binding affinities are altered by arginine methylation in RGG/RG motifs. Thus, we compared unmethylated and methylated RGG3-PY in filter-binding assays showing similar signal intensities for bound RNA (Fig. 20C). Determination of dissociation constants (K_d) using Hill fitting algorithm yields similar affinities and Hill coefficients (Fig. 20D, Table 3). Note, the obtained Hill coefficients indicate cooperative binding of RNA. At first glance, the result from the EMSAs and filter-binding assays appear contradictory, but in combination indicate higher complex stability for methylated RGG3-PY compared to unmethylated RGG3-PY. The contradictory results most likely arise from a different nature of the assays. Namely, the filter-binding assay has a relatively short incubation time and existing interactions between RNA and protein are promptly blotted on the membranes. In contrast, EMSAs have a longer incubation time and additional gel running time during which less stable complexes may dissociate again and may create a false appearance of a lack of RNA binding. In conclusion, our filter-binding assays demonstrate that the observed difference in LLPS of unmethylated and methylated RGG3-PY was not due to altered binding affinities. Importantly, the EMSA experiments indicate improved complex stability for methylated RGG3-PY which may have an effect on LLPS. Nevertheless, methylation-dependent differences in FUS-RNA complex stability may not be of particular importance for the phase separation behavior of full-length FUS proteins, as the presence of RNA has not a significant effect on the promotion of phase separation of full-length FUS (Fig. 16F and 16G).

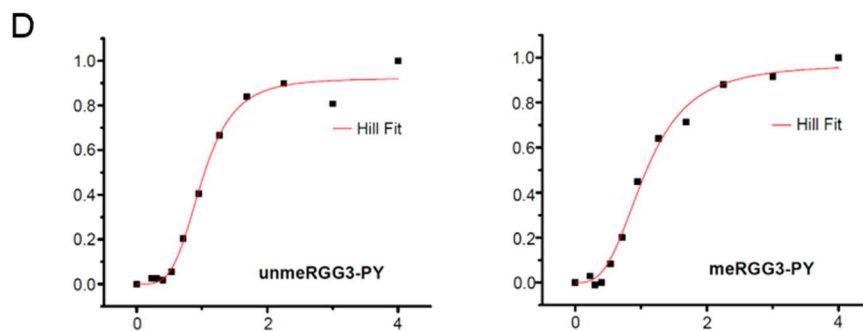
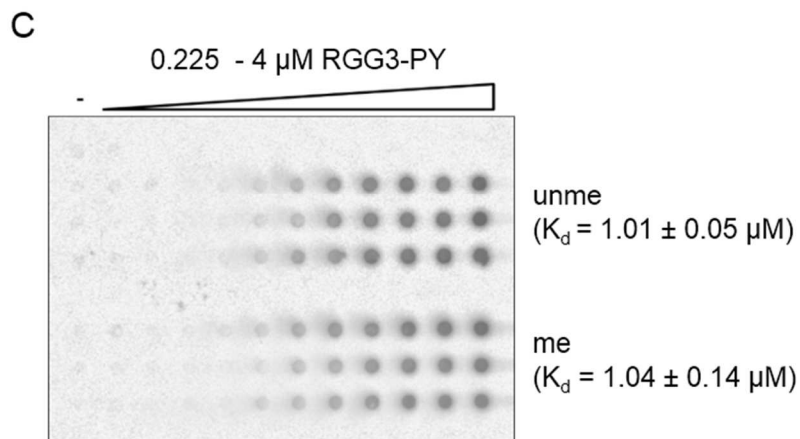
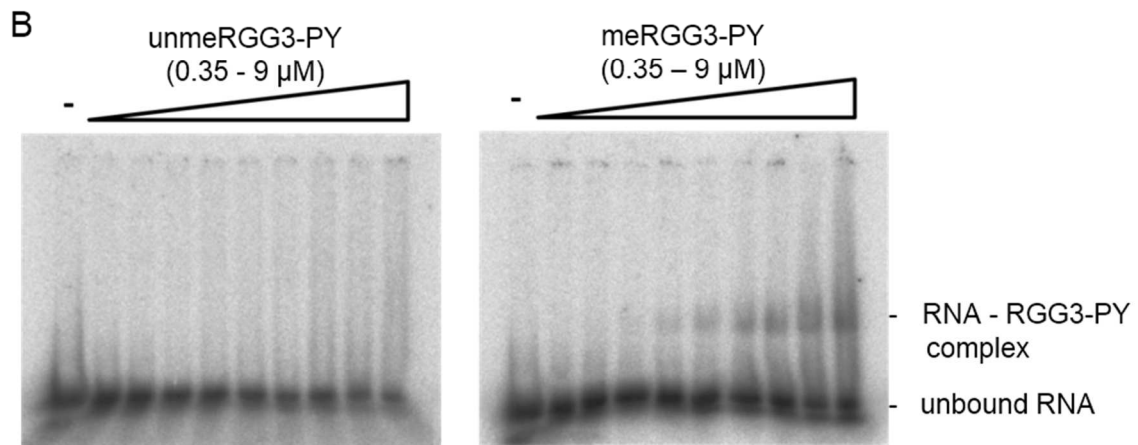
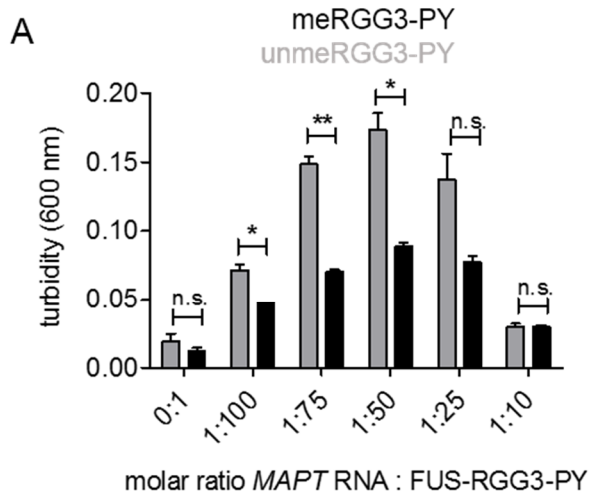


Figure 20: Arginine methylation stabilizes RNA binding of FUS RGG3-PY. **A)** Methylated (me) RGG3-PY exhibits strongly reduced phase separation compared to unmethylated (unme) RGG3-PY. Turbidity assay for quantitative analysis of phase separation of unmethylated (unme) or methylated (me) RGG3-PY (30 μ M) in presence of increasing amounts of *in vitro* transcribed *MAPT* RNA. Values represent means \pm SEM (n=3). *P < 0.05 and **p < 0.01 by paired t-test. **B)** Representative EMSAs with radiolabeled *ASH1* E3-51 RNA and increasing concentrations of unmethylated (unme) or methylated (me) RGG3-PY demonstrating a band shift only for meRGG3-PY, but not for unmeRGG3-PY. **C)** Unmethylated (unme) and methylated (me) RGG3-PY show similar binding affinities to RNA, indicating that RNA binding of RGG3-PY is not affected by arginine methylation. Representative images of nitrocellulose membranes from filter-binding assay with unmethylated (unme) and methylated (me) RGG3-PY and radiolabeled *ASH1* E3-51 RNA. **D)** Equilibrium dissociation constants (K_d) were determined using Hill fitting algorithm (n=6).

Table 3: Kinetic parameters of filter-binding assays (RGG3-PY with RNA)

	unmeRGG3-PY	meRGG3-PY
K_d (μM)	1.01 \pm 0.05	1.04 \pm 0.14
Hill coefficient	3.55 \pm 0.78	3.62 \pm 0.6
N	6	6

Values represent the mean \pm SD.

2.9 ALS-associated FUS-P525L mutant impairs chaperone activity of TNPO1

In contrast to FTD patients with FUS pathology, most ALS-FUS patients harbor a mutation in the C-terminal PY-NLS (Dormann and Haass, 2013; Mackenzie et al., 2010) that impair interaction with TNPO1 and thus severely impair nuclear import of FUS (Dormann et al., 2010; Niu et al., 2012; Zhang and Chook, 2012). There are more than 30 point-mutations identified in the PY-NLS of FUS that are associated with cases of ALS (Dormann and Haass, 2013). These mutations vary in the degree of cytosolic mislocalization that correlates with disease severity (Dormann et al., 2010). The P525L mutation severely impairs TNPO1 binding (Niu et al., 2012; Zhang and Chook, 2012) and in turn causes early disease onset and rapid progression of ALS (Chio et al., 2009; Kwiatkowski et al., 2009). Based on the results described above demonstrating that TNPO1 suppresses LLPS and SG partitioning of FUS (sections 2.3 and 2.4 and Figs. 12-15), we speculated that aberrant phase transition and SG association of mutant FUS may be promoted due to impaired binding and chaperoning of FUS by TNPO1.

To address this question, we purified recombinant RGG3-PY and MBP-FUS-EGFP with intact PY-NLS (WT) or carrying the P525L mutation. As arginines in the RGG3 domain of FUS are asymmetrically dimethylated both, under normal conditions as well as in ALS-FUS patients, and this additionally reduces binding affinity to TNPO1 (Dormann et al., 2012; Suarez-Calvet et al., 2016), WT and mutant FUS proteins were *in vitro* methylated to resemble the situation in healthy individuals and ALS-FUS patients (see Fig. 21A for protein purity). Immunoblotting using antibodies for UMA-FUS (14G1), MMA-FUS (15E11), and ADMA-FUS (9G6) confirms reduction of UMA-FUS and quantitative conversion to ADMA-FUS to a similar degree for both WT and mutant FUS (Fig. 21B). ITC measurements revealed that unmethylated RGG3-PY WT and P525L mutant show only slightly different binding affinities to TNPO1, but the dissociation constant (K_D) for TNPO1 interaction is drastically increased for the methylated RGG3-PY P525L mutant compared to the methylated RGG3-PY WT (Table 2). As the major binding epitopes for TNPO1 interaction are located in the RGG3-PY (Dormann et al., 2012; Zhang and Chook, 2012), similar affinities are expected for full-length FUS proteins. Subsequently, the phase separation behavior of WT and mutant in absence and presence of TNPO1 was explored. In the absence of TNPO1, both WT and mutant proteins undergo phase separation to a similar degree (Fig. 21C), indicating that LLPS of FUS is not directly affected by the P525L mutation. While LLPS of the WT protein is efficiently suppressed in the presence of TNPO1, the P525L mutant protein is completely insensitive to the chaperone activity of TNPO1 and still forms liquid droplets (Fig. 21C, see Fig. 21D for quantification), supporting of our hypothesis. In order to test whether chaperoning of the P525L mutant by TNPO1 can occur over time upon prolonged incubation of both proteins, WT and mutant FUS were subjected to prolonged incubation (8h) with TNPO1, revealing no difference to the early time point (microscopic examination immediately after mixing, 0h) (Fig. 21C and 21D).

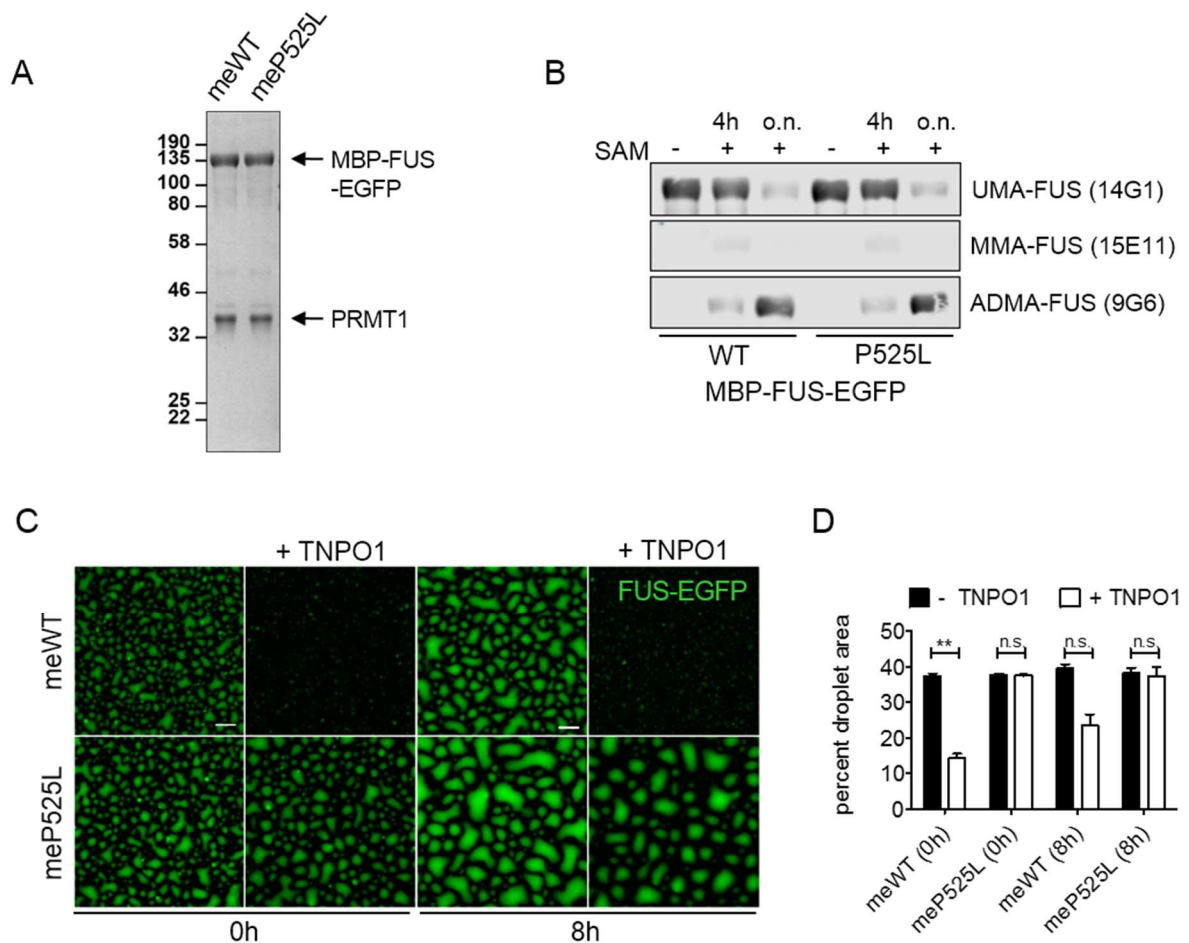


Figure 21: ALS-associated P525L mutation causes reduced chaperoning of FUS by TNPO1 *in vitro*. **A)** Coomassie-stained SDS-PAGE gels of purified, *in vitro* methylated WT and P525L mutant version of MBP-FUS-EGFP (~ 150 kDa), both samples contain recombinant PRMT1 (~ 40 kDa), as indicated in the scheme in Fig. 17C. Molecular weight markers (in kDa) are indicated on the left. **B)** Representative blot for MBP-FUS-EGFP WT and MBP-FUS-EGFP-P525L confirm similar degrees of methylation. Successful methylation was verified by immunoblotting with antibodies specific for FUS-RGG3 containing unmethylated arginines (UMA-FUS, 14G1), monomethylated arginines (MMA-FUS, 15E11) and asymmetrically dimethylated arginines (ADMA-FUS, 9G6), respectively. The blot demonstrates reduction of UMA-FUS signal and conversion to ADMA-FUS upon overnight incubation with PRMT1. Experiments depicted in Figures 21C-D and 22A-B were performed with samples from overnight (o.n.) *in vitro* methylation reaction. **C)** Droplets of the FUS-P525L mutant are less sensitive to the chaperone activity by TNPO1 compared to FUS WT droplets. TEV cleavage-induced droplet formation of methylated MBP-FUS-EGFP WT versus P525L (both at 11 μ M) in presence or absence of equimolar amounts of TNPO1. After 0 h and 8 h, images were acquired by confocal fluorescence microscopy. Scale bar, 15 μ m. **D)** Quantification of image area covered by FUS-EGFP droplets in percent. Values represent means \pm SEM (n=3). **p < 0.01 by paired t test.

In order to test whether chaperoning of the FUS-P525L mutant by TNPO1 is also impaired in cells, the ability of TNPO1 to reduce SG partitioning of WT and P525L mutant FUS was addressed in a semi-permeabilized cell assay (see scheme in Fig. 15C). In the absence of TNPO1, both WT and mutant FUS exhibit a similar degree of SG association (Fig. 22A). While SG association of the WT protein is significantly reduced in the presence of TNPO1, the P525L mutant protein show still a higher degree of SG association (Fig. 22A, see Fig. 22B for quantification), demonstrating that TNPO1 is unable to efficiently chaperone the mutant protein and prevent its accumulation in SGs. As nuclear import is abrogated in this assay due to blocked nuclear pores using WGA, better chaperoning of the WT protein is not a result of enhanced nuclear import.

To further examine the effect of the P525L mutation in the cellular context, cytosolically trapped GCR₂-tagRFP₂-FUS-WT or P525L were transiently expressed in HeLa cells, in order to assess whether chaperoning of the FUS-P525L mutant is also impaired in intact cells. The GCR-mediated cytosolic anchoring, which occurs in the absence of steroid hormones (Love et al., 1998), allows an investigation of the chaperoning activity of endogenous TNPO1 independent of its nuclear import activity. Notably, transient transfection of cytosolically anchored WT and mutant FUS yields comparable expression levels and both induced formation of TIA1-positive SGs (Fig. 22C). The WT protein exhibits diffuse cytosolic distribution with a low degree of SG partitioning. Contrary to that, the FUS-P525L mutant protein localizes to SGs in a significantly higher number of cells (Fig. 22C, see Fig. 22D for quantification).

In summary, the cellular assays and *in vitro* data demonstrate that besides impairing nuclear import of FUS, ALS-causing mutations localized in the NLS of FUS additionally abrogate the chaperone activity of TNPO1. These findings prove that ALS-associated FUS mutations, by disrupting proper interaction with TNPO1, promote aberrant phase transition and SG association of cytosolically mislocalized FUS. Thus, elevated phase separation and aggregation of FUS in stress granules could be a second detrimental consequence of ALS-associated FUS-NLS mutations and may contribute to the pathogenesis of ALS.

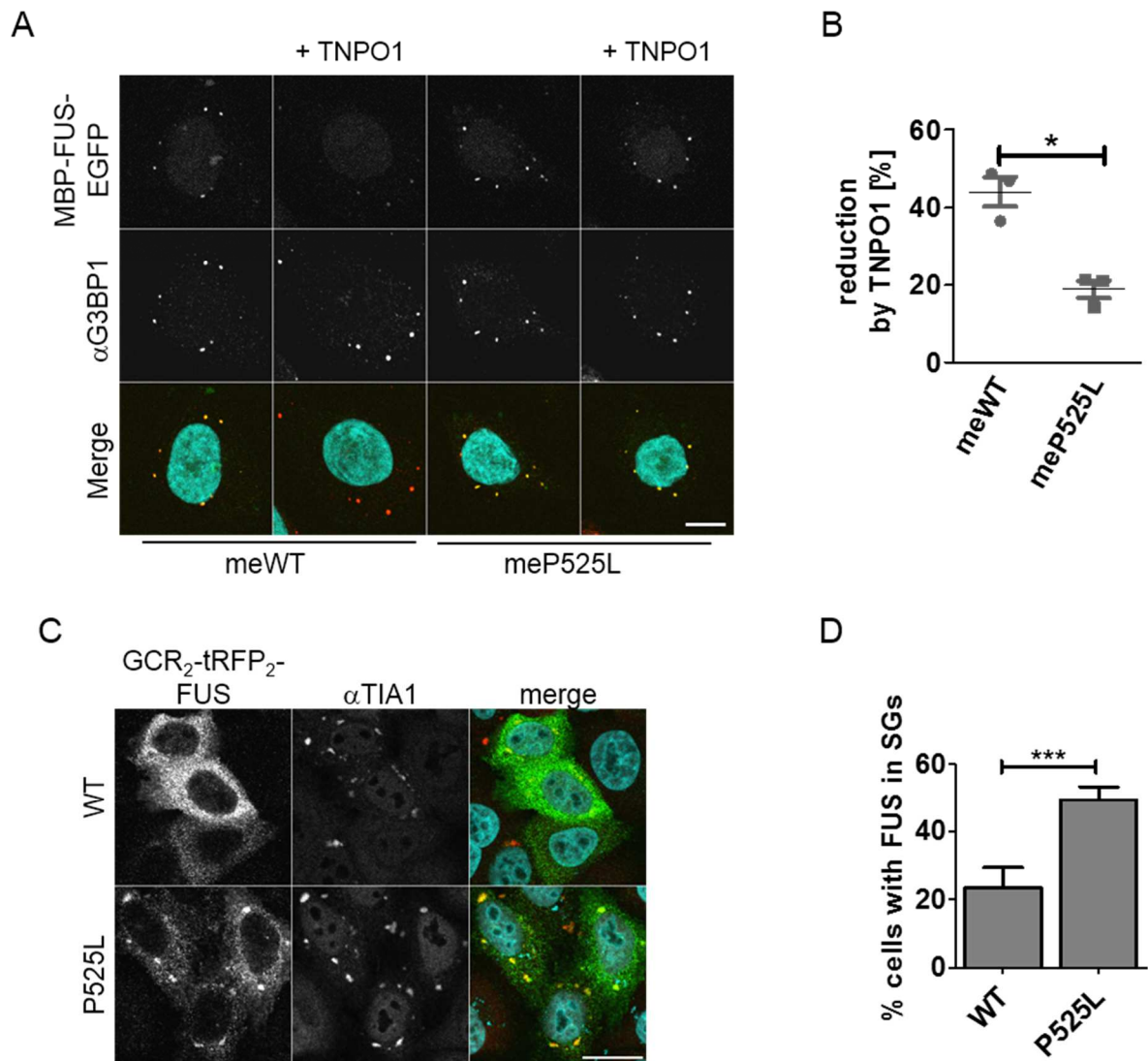


Figure 22: The P525L mutation renders FUS less sensitive to chaperone activity of TNPO1 in cellular assays. A) SG association of the P525L mutant is not strongly reduced in presence of TNPO1. Semi-permeabilized cell assay depicting SG partitioning of MBP-FUS-EGFP WT versus P525L in presence or absence of recombinant TNPO1. Nuclei were counterstained with DAPI (turquoise), SGs were stained with a G3BP1-specific antibody (red). Images were acquired by confocal fluorescence microscopy. Scale bar, 10 μ m. **B)** Mean reduction of SG association of FUS-EGFP WT and P525L normalized to respective condition with absence of TNPO1 (n=3; ≥ 10 cells, ≥ 37 SGs each). *p < 0.05 by paired t test. **C)** SG localization of the P525L mutant is higher compared to WT. SG recruitment of cytosolically anchored (GCR₂-tagRFP₂-tagged) FUS WT or P525L was assessed by co-immunostaining for tagRFP (displayed in green in the merge on the right for better visibility) and TIA1 (displayed in red). Nuclei were counterstained with DAPI (turquoise). Images were acquired by confocal fluorescence microscopy. Scale bar, 20 μ m. **D)** Quantification of the percentage of cells exhibiting GCR₂-tagRFP₂-FUS localized to SGs. Values represent means \pm SEM (n=3; ≥ 100 cells each). ***p < 0.01 by paired t test.

3 DISCUSSION

DECLARATION OF COPYRIGHT AND CONTRIBUTIONS

This section of my Ph.D. thesis was prepared in parallel to the paper 'Phase separation of FUS is suppressed by its nuclear import receptor and arginine methylation' published in *Cell* (Hofweber et al., 2018). Thus, the structure and text of this Ph.D. thesis and the paper will partially overlap. *Elsevier* holds the copyright (2018) for this article published in *Cell* and permits the usage of text and figures in this dissertation.

3.1 Arginines in the RGG/RG motif are crucial for phase separation of FUS

Previously published studies deemed the N-terminal SYGQ-rich domain to be the primary driver of phase separation and aggregation of FUS (Burke et al., 2015; Kato et al., 2012; Murakami et al., 2015; Patel et al., 2015; Sun et al., 2011). The data presented in this Ph.D. thesis and accompanying publications (Hofweber et al., 2018; Qamar et al., 2018; Wang et al., 2018b) reveal that, in addition to the SYGQ-rich domain, the C-terminal RGG3-PY domain and, in particular, arginine residues in the RGG/RG motifs of FUS have an essential contribution to phase separation of FUS (Fig. 9 and 11). The isolated RGG3-PY domain, similarly to SYGQ-rich alone (Burke et al., 2015; Murakami et al., 2015), requires much higher protein concentrations or presence of RNA to undergo phase separation compared to full-length FUS (Fig. 9C), which forms liquid droplets at physiological concentrations (Patel et al., 2015) upon proteolytic liberation from the solubility tag. Furthermore, deletion of the C-terminal RGG3-PY domain or the all-KGG mutant showed significantly reduced or no phase separation compared to full-length FUS (Fig. 11C-E). These data indicate that the C-terminal arginines in the RGG/RG motifs drive phase separation of FUS in conjunction with the N-terminal SYGQ-rich domain. These findings are in line with previous studies showing that a 40 amino-acid long, synthetic FUS peptide from the RGG3 domain (FUS471-510) undergoes phase separation in presence of a molecular crowder (PEG) or polyU RNA (Boeynaems et al., 2017) and that the RGG2-ZnF-RGG3 fragment of FUS forms fibrils in an RNA-dependent manner *in vitro* (Schwartz et al., 2013). The observation that RGG/RG motifs can drive phase separation are not exclusive to FUS, but have been demonstrated for multiple RBPs. Synthetic RGG boxes of hnRNP-A1, FMRP and arginine-rich dipeptide repeat (DPR) proteins, i.e. glycine-arginine (GR)_n and proline-arginine (PR)_n, produced by unconventional translation of the *C9orf72* repeat expansion, have also been reported to phase separate upon addition of a crowding agent (Boeynaems et al., 2017). Additionally, phase separation of human RNA helicase Ddx4 as well as the Ddx3 helicase LAF-1 and PGL-3, both found in P granules of *C. elegans*, is driven by their

RGG repeats (Elbaum-Garfinkle et al., 2015; Nott et al., 2016; Nott et al., 2015). The disordered domain of Ddx4 is highly enriched in FG/GF and RG/GR pairs, which are required for LLPS, indicating that aromatic phenylalanines and positively charged arginines are engaged in cation- π interactions driving droplet formation of Ddx4 (Nott et al., 2015). Similarly, to Ddx4, the RGG3-PY of FUS is also highly enriched in RGG and GR/RG repeat interspersed by YG/GY and FG/GF dipeptides. As droplet formation of the RGG3-PY domain can be promoted by the addition of RNA and lowering of the salt concentration, RNA-driven phase separation of RGG3-PY may be primarily driven by electrostatic interactions. The contribution of cation- π interactions between RGG3-PY molecules formed by RG(G)/GR and aromatic (F,Y) residues, as reported for Ddx4 (Nott et al., 2015), needs to be clarified. If this is the case, RNA may act as a scaffold to bring RGG3-PY molecules in close proximity.

Furthermore, it has been shown that the high density of tyrosine residues in the N-terminal SYGQ-rich domain of FUS is required to drive hydrogel formation of the SYGQ-rich domain (Kato et al., 2012). Furthermore, the SYGQ-rich domain requires higher concentrations to undergo phase separation compared to the full-length protein (Burke et al., 2015; Murakami et al., 2015). The full-length FUS protein is able to undergo phase separation at physiological conditions as soon as liberated from the MBP-tag. As full-length FUS does not require presence of RNA to phase separate and deletion of the RGG3-PY significantly reduces the phase separation propensity, it may be conjectured that the interplay between C-terminal arginines and N-terminal tyrosines in the SYGQ-rich domain have a crucial contribution to phase separation of FUS by forming tyrosine-arginine (cation- π) interactions that drive phase separation. Supporting this assumption, mixing of the N-terminal SYGQ-rich domain with the C-terminal arginine-containing RBDs was reported to cause enhanced co-phase separation. Moreover, substitutions of tyrosines (Y) in the SYGQ-rich domain with alanines (A) or serines (S) reduce the propensity of full-length FUS to undergo phase separation (Qamar et al., 2018; Wang et al., 2018b). Even though lysine substitutions in the all-KGG mutant maintain positive charge, this seems to be not sufficient to form cation- π interactions. In contrast to arginines, lysines form interactions involving the amine with reduced or negligible directionality towards aromatic residues (Wang et al., 2018b). In sum, the interplay between the prion-like SYGQ-rich domain and the C-terminal RGG-rich domains of FUS has an important contribution to LLPS of full-length by forming cation- π interactions between C-terminal arginines and N-terminal tyrosines.

3.2 Nuclear import receptors as chaperones

Our data reveal an unknown dual function of TNPO1 towards FUS, namely that it i) mediates not only nuclear import of FUS, ii) but it also acts as a chaperone that suppresses LLPS and solidification as well

as SG association of FUS. FUS is a highly abundant RBP (Patel et al., 2015; Wisniewski et al., 2014) with a concentration in the nucleus between 2 and 8 μM , which is within the concentration range where recombinant FUS undergoes LLPS and liquid-to-solid phase separation (Patel et al., 2015) (Fig. 11C and 12B). In order to regulate LLPS and prevent aberrant phase transitions in the cell, potent protein quality control (PQC) mechanisms have to be in place. Reported PQC mechanisms include ATP acting as a hydrotrope (Patel et al., 2017), high nuclear RNA concentrations (Maharana et al., 2018) and heat shock proteins (Ganassi et al., 2016; Mateju et al., 2017). Our data reveal that TNPO1 also has the ability to suppress phase transition of FUS *in vitro* and thus fulfills such a protein quality control function. Additionally, we have demonstrated that TNPO1 also exerts its chaperone function towards FUS in the cytoplasm and thus reduces association of FUS with SGs (Fig. 15) that may become aberrant and develop detrimental potential (Bentmann et al., 2013; Maziuk et al., 2017; Wolozin, 2012). It has been proposed that aggregation-prone RBPs like FUS are sequestered to SGs and become highly concentrated at these sites, thus promoting aberrant phase transition and aggregation (Alberti and Hyman, 2016; Dormann and Haass, 2011; Li et al., 2013). SGs are considered to play a pivotal role in pathogenesis as progenitors of pathological aggregates, as various SG marker proteins, such as TIA1 and G3BP1, have been identified in aggregates of ALS and FTD patients with FUS and TDP-43 pathology (Bentmann et al., 2013). Additionally, ALS-causing mutations in FUS and other RBPs, such as TIA1, hnRNP-A1/A2 and TDP-43, were recently reported to enhance SG association or impair SG dynamics (Dewey et al., 2011; Kim et al., 2013; Mackenzie et al., 2017; Martinez et al., 2016). These ALS-associated mutations increase the cytoplasmic protein concentration and/or enhance intermolecular interactions and thereby increase the propensity to undergo aberrant phase separation. Notably, our data demonstrate that TNPO1 reduces SG localization of FUS (Fig. 15) and disruption of FUS-TNPO1 interaction promotes SG partitioning in cells (Fig. 22A-D). Our cellular assays reveal that the chaperone activity of TNPO1 towards FUS is independent of its nuclear import activity, as nuclear import of FUS was disrupted in our assays either by cytosolic-anchoring of FUS or by blocking the nuclear pores with WGA. Taken together, our data indicate that the chaperone activity of importins towards phase separating RBPs may play an essential role in regulating SGs in the cytoplasm. This may not only be the case for SGs, but also apply for other FUS-containing cytoplasmic RNP granules, such as neuronal transport granules.

Supporting our finding, there are a number of studies showing that several other importins have been demonstrated to fulfill chaperone function and thereby prevent protein aggregation. In 2002, Jakel and colleagues demonstrated that, in addition to TNPO1, several other importin β -type importins suppress the aggregation of basic ribosomal proteins and histones. This indicates that also other importins may exert chaperone activity towards aggregation-prone RBPs with basic stretches.

Notably, they also showed that importins fulfill this chaperone function specifically towards their cognate import cargoes (Jakel et al., 2002). In line with that, we have shown that TNPO1, but not Imp5, suppresses phase separation of FUS. Further evidence for the importin-cargo specificity required to prevent phase transitions of aggregation-prone RBPs is provided by the data published by the groups of Shorter and Chook (Guo et al., 2018; Yoshizawa et al., 2018). Moreover, mere interaction with the RGG3 of FUS, is not sufficient to suppress phase separation of full-length FUS, as we show that other RGG3-binding proteins, i.e. PRMT1 and an α -RGG3 specific antibody, are unable to prevent droplet formation of FUS (Fig. 12B). As a side note, droplet size increases in presence of the α -RGG3 specific antibody whereas fluorescence intensity decreases. This may be caused by crosslinking of two FUS molecules by the antibody and incorporation of the antibody into the droplets. Overall, phase separation in general seems not to be promoted by the α -RGG3 specific antibody, as evidenced in the quantification of covered image area as well as turbidity and sedimentation assays (Fig. 12B-C and 13A-C). Similarly, Shorter and colleagues recently reported that importin α/β is able to inhibit and reverse fibril formation of TDP-43 and that TNPO1 prevents and reverses fibrilization of FUS and other PY-NLS-containing import cargoes such as TAF15, EWS, and hnRNPA-A1/A2 (Guo et al., 2018). In line with these findings, the Imp $\beta/7$ heterodimer was shown to prevent aggregation of the nucleolar RNA methyltransferase EMG1 by binding to its basic regions (Warda et al., 2016). Similar to heat shock proteins that act as chaperones for exposed hydrophobic patches, importins may have a general chaperone function preventing ionic aggregation of highly basic nucleic acid binding proteins, by shielding their basic nucleic acid-binding stretches (Jakel et al., 2002). As importins reach cellular concentrations of $\sim 1\text{-}2\ \mu\text{M}$ each, they are similarly abundant as HSPs (Jakel et al., 2002), they seem suitable to encounter the high abundance of RBPs associated with ALS cases, such as FUS, TDP-43, and hnRNP-A1/A2, by shielding their basic stretches. It has been proposed that although efficient nuclear import should be achievable by a common NLS in combination with a cognate import receptor, mammalian cells have ~ 15 different importins to encounter the polymorphism of basic nucleic-acid-binding stretches of cargoes and thereby execute their chaperone function. Notably, nuclear import of rpS7 can be mediated by Imp α/β and Imp 9, but its aggregation is chaperoned only by Imp9 (Jakel et al., 2002), indicating a complex network of importins mediate import and chaperone activity in response to particular cellular conditions. Interestingly, Lemke and co-workers showed that Importin β inhibits aggregation of FG-rich nucleoporins (Nups) (Milles et al., 2013). Furthermore, TNPO1 enables specific and fast nuclear import of its cargoes by disrupting weak transient interactions between FG-rich Nups when crossing the nuclear pore (Frey et al., 2006; Milles et al., 2015). Taken together, importins may furthermore have a chaperone function towards hydrophobic FG-Nups to

mediate passing of the nuclear pore complex, even though the chaperoning mechanism has to be determined.

3.3 Possible mechanisms underlying the chaperone activity of TNPO1

The findings presented in this thesis showing that TNPO1 is able to suppress and reverse phase separation of FUS raise the question of the underlying mechanism. According to the solved crystal structure of the FUS PY-NLS - TNPO1 complex, TNPO1 binds to three epitopes in the PY-NLS of FUS, namely the very C-terminal PY motif, a polarized arginine-rich α -helix and a hydrophobic motif (Zhang and Chook, 2012). Furthermore, there is also a fourth binding epitope of TNPO1 in the preceding RGG3 domain (Dormann et al., 2012) with direct binding to specific arginine residues (R472, R473, R476) (Gobl et al., 2016). As we show that arginines in the RGG/RG motifs drive phase separation of FUS (Fig. 9C and 11C-E), direct interaction of TNPO1 with arginine residues may mediate the chaperone activity of TNPO1 towards FUS by interfering with weak multivalent interactions of arginines, most likely cation- π interactions with tyrosines in the SYGQ-rich domain, and thereby suppress phase separation of FUS driven by arginines residues. Supporting the hypothesis of TNPO1 interfering with cation- π interactions, the study by Yoshizawa et al. demonstrated that TNPO1 additionally interacts with tyrosine motifs in the N-terminal SYGQ-rich domain (Yoshizawa et al., 2018) that are known to contribute to phase separation of FUS (Kato et al., 2012; Qamar et al., 2018; Wang et al., 2018b). Furthermore, recent NMR studies revealed that TNPO1 also forms weak interaction with the folded RRM and ZnF domains (Yoshizawa et al., 2018), suggesting that interactions of TNPO1 with these RNA binding domains may also be involved in the chaperoning mechanism.

TNPO1 interaction with multiple RNA-binding domains (RBDs) of FUS (RRM, ZnF and RGG/RG repeat motifs) may be the basis for the RNA displacement observed upon addition of TNPO1 to RNA-bound MBP-FUS and RGG3-PY, respectively (Fig. 16B-E). Since previous studies demonstrated a promoting effect of phase separation upon addition of RNA (Burke et al., 2015; Maharana et al., 2018; Schwartz et al., 2013), displacement of RNA from FUS by TNPO1 may also contribute to the chaperone activity of TNPO1. For the isolated RGG3-PY this seems to apply, as phase separation of RGG3-PY can be promoted by addition of RNA (Fig. 9C,D and 20A). Possible explanation for this may be that, first, electrostatic interactions with the negatively charged RNA-backbone drive phase separation, and/or second, RNA binding of isolated RGG3-PY brings more RGG3-PY molecules in close proximity and thereby RNA may act as a scaffold that allows the formation of more multivalent interactions between arginines in RGG/RG-rich motifs and aromatic residues driving phase separation (cation- π). As TNPO1

competes with RNA for FUS binding, RNA displacement eliminates RNA-driven phase separation of RGG3-PY.

In contrast to previously published data (Burke et al., 2015; Maharana et al., 2018; Schwartz et al., 2013), and to our results for the RGG3-PY domain, we did not observe a promotion of phase separation of full-length FUS by RNA in our turbidity assays. The absence of a promoting effect was most likely not due to the nature of the used RNAs, as we used different types of RNA (51 bp *ASH1* E3-51 RNA, 330 bp *MAPT* RNA or total RNA from HeLa cells) (Fig. 16F and 16G, data not shown), and of which *MAPT* RNA has been previously reported to interact with FUS (Orozco et al., 2012). High concentrations of RNA rather have a suppressive effect on phase separation of both full-length FUS and RGG3-PY (Fig. 16F, 16G and 20A), suggesting that high amounts of RNA may interfere with multivalent interactions within and between full-length FUS or RGG3-PY molecules, in particular cation- π interactions, driving phase separation. In regard of FUS being an RBP involved in many processes of RNA metabolism and the high concentrations of RNA in the nucleus, the observed suppressive effect of high RNA concentrations on phase separation of FUS *in vitro* may be a feasible strategy to prevent aberrant phase separation of FUS in addition to the chaperoning activity by TNPO1. This view is supported by a recent study demonstrating that high RNA/protein ratios prevent droplet formation of FUS *in vitro*. Furthermore, a reduction of nuclear RNA concentrations by microinjection of RNase A was shown to cause droplet formation and solidification of FUS in HeLa cells (Maharana et al., 2018). This may be of particular relevance in the nucleus where high RanGTP levels mediate dissociation of the TNPO-FUS import complex.

Even though RNA displacement from FUS by TNPO1 seems to be not involved in the chaperoning function of TNPO1 under our experimental conditions, it may nevertheless fulfill important functions in the cell. First, RNA displacement by TNPO1 may assure that FUS as well as other RBPs are imported in the nucleus in an RNA-free form and thus prevent mRNA reimport in the nucleus in order to fulfill their nuclear functions in RNA metabolism. Second, RNA displacement may permit the release of bound mRNAs from RBPs to allow local translation in the cytoplasm, as reported for Kap104p, the yeast homologue of TNPO1 (van den Bogaart et al., 2009). Such an RNA displacement mechanism mediated by TNPO1 may play a role in neuronal transport granules and thereby regulate local translation in axons and/or dendrites. Thus, further research is needed to follow up these potential functions of RNA displacement by TNPO1. In this regard, *in vitro* translation assays could be carried out to evaluate whether recombinant TNPO1 has a suppressive effect on translation. Furthermore, the presence of TNPO1 in neuronal RNP granules has to be validated and whether TNPO1 is responsive to neuronal stimulation.

3.4 Arginine methylations suppresses phase separation and SG association of FUS

We showed that RG/RGG motifs of FUS are essential for LLPS of FUS (Fig. 11). RGG motifs are the second most prevalent RNA-binding motif of RBPs and arginines in these domains have been shown to be extensively methylated (Araya et al., 2005; Belyanskaya et al., 2001; Du et al., 2011; Hung et al., 2009; Jobert et al., 2009; Ong et al., 2004; Pahlich et al., 2005; Rappsilber et al., 2003). As FUS is known to be asymmetrically dimethylated in RGG domains, but was shown to be hypomethylated in pathological inclusions of FTD-FUS patients (Dormann et al., 2012; Suarez-Calvet et al., 2016), we hypothesized that arginine methylation may be involved in phase separation of FUS. Indeed, we discovered that asymmetric dimethylation of RGG/RG motifs of FUS suppresses its propensity to undergo LLPS (Fig. 18) and methylated FUS exhibits higher droplet dynamics than unmethylated FUS (Fig. 19). Supporting these observations, Nott and colleagues reported that LLPS of the RGG domain of Ddx4 is significantly suppressed by asymmetric dimethylation of arginines and lowers phase transition temperature by 25 °C (Nott et al., 2015). Similarly, Fazwi and co-workers showed that arginine methylation of the hnRNP-A2 LC domain reduces its phase separation (Ryan et al., 2018). Concordantly, Qamar et al. reported in the same issue of *Cell* that asymmetrically dimethylated FUS purified from HeLa cells exhibits lower LLPS and a higher propensity for droplet fusion (Qamar et al., 2018). In contrast to phosphorylation, another common PTM in IDPs, methylation of arginines, does not alter the positive net charge, but alters hydrogen bonding and local hydrophobicity (Fuhrmann et al., 2015). Consequently, cation- π interactions between arginines and tyrosines driving the phase separation of FUS are mitigated. As RGG/RG motifs are highly prevalent in the human proteome and are frequently methylated further there is evidence by a number of recent studies that RGG/RG-rich motifs crucially contribute to phase separation (Boeynaems et al., 2017; Elbaum-Garfinkle et al., 2015; Hofweber et al., 2018; Nott et al., 2015; Saha et al., 2016), it is likely that arginine methylation also regulates phase separation of many other proteins.

Loss of arginine methylation is a pathological hallmark of aggregated FUS in FTD-FUS patients (Dormann et al., 2012; Suarez-Calvet et al., 2016), which may be also a major pathomechanism in other neurodegenerative diseases. Since we and others have demonstrated that LLPS of FUS is affected by arginine methylation (Hofweber et al., 2018; Qamar et al., 2018) (Fig. 18), it seems likely that the other members of the FET protein family, EWS and TAF15, that are co-aggregating with FUS in inclusions of FTD-FUS cases (Neumann et al., 2011), are also regulated by arginine methylation. Additionally, hnRNP-A1 and hnRNP-A2, that have been found in pathological aggregates of multisystem proteinopathy (MSP) and rare ALS cases (Kim et al., 2013; Mori et al., 2013b), undergo arginine methylation in RGG/RG motifs in their prion-like domain (Liu and Dreyfuss, 1995; Nichols et

al., 2000; Ong et al., 2004) that may affect LLPS. The first evidence for this assumption has been provided by Fawzi and colleagues by showing that arginine methylation within RGGs of hnRNP-A2 LC disrupts cation- π interactions with aromatic residues and consequently interferes with its phase separation (Ryan et al., 2018). Nevertheless, studies on the full-length hnRNP-A2, and other full-length RBPs in general, are required to unravel the actual role of methylation on its phase separation behavior. Notably, genetic screens in *Drosophila* have uncovered PRMT1 as a major modifier of DPR-toxicity (Boeynaems et al., 2016; Lee et al., 2016). This suggests that arginine-rich DPRs (i.e. PR, GR) may be also methylated *in vivo* and therefore arginine methylation may also play an important role in DPR toxicity.

Besides *in vitro* studies, arginine methylation has also been shown to be an essential determinant of phase separation in cells, by regulating RNP granule formation. PRMT1-overexpression causes hypermethylation of the SG-nucleating protein G3BP1 and suppresses SG nucleation (Tsai et al., 2016). Conversely, oxidative stress causes active demethylation of G3BP1 by JMJD6 and thereby promotes SG formation (Tsai et al., 2017). Therefore, arginine methylation may directly affect LLPS and RNP granule dynamics by interfering with cation- π interactions formed between arginines and aromatic residues. Furthermore, LLPS and RNP granule dynamics may be indirectly affected by methylation-dependent protein-protein as well as protein-RNA interactions. This may be of particular relevance for the recruitment or exclusion to/from preformed structures. Phase separation of FUS, and most likely other RBPs with similar domain structure, is driven by weak multivalent interactions between arginines within the RBDs and residues in the prion-like domains (Qamar et al., 2018; Wang et al., 2018b), which are enriched for amino acids that are potential targets for phosphorylation (Monahan et al., 2017). Thus, it seems likely that arginine methylation most likely acts together with other PTMs, such as phosphorylation. Eventually, combinations of different PTMs and binding partners control phase separation and RNP granule dynamics.

3.5 Distinct mechanisms driving phase separation and SG association of FUS in ALS-FUS and FTD-FUS

3.5.1 Pathomechanisms of FTD-FUS

Previous studies revealed that FUS in pathological aggregates of FTD-FUS cases is hypomethylated, i.e. unmethylated and monomethylated, whereas FUS in healthy individuals and ALS-FUS patients characteristically contains asymmetrically dimethylated arginines (Dormann et al., 2012; Suarez-Calvet et al., 2016). Since we show that loss of arginine methylation, as seen in FTD-FUS, enhances

phase separation and SG association of FUS, it can be speculated that this may favor aberrant phase separation and pathological aggregation of FUS and thus contribute to pathogenesis. Since unmethylated FUS is efficiently chaperoned by its nuclear import receptor TNPO1, it remains elusive why TNPO1 is not able to prevent aberrant phase transition and aggregation formation FUS in FTD-FUS patients. The pattern of arginine methylation does not impair chaperoning activity of TNPO1. Unmethylated and monomethylated FUS exhibit a higher binding affinity to TNPO1 (Dormann et al., 2012; Suarez-Calvet et al., 2016) (Table 2) and phase separation of both unmethylated (Guo et al., 2018; Yoshizawa et al., 2018) (Fig. 12 and 13) as well as asymmetrically dimethylated FUS (WT) (Fig. 21C and 21D) is efficiently suppressed by the chaperone function of TNPO1. Since TNPO1 is co-aggregating with FET proteins in FTD-FUS *post mortem* brains (Brelstaff et al., 2011; Davidson et al., 2013; Neumann et al., 2012; Troakes et al., 2013), irrespective of what may cause this, it is likely that TNPO1 may become functionally impaired and is not capable of exerting its cytosolic chaperone function towards its cargoes. Assuming TNPO1 is compromised in its functionality, nuclear import of TNPO1 cargoes (e.g. FUS, EWS, TAF15, hnRNPs) may also be disturbed, causing elevated levels of mislocalized RBPs and eventually a higher tendency to aggregate. So, there are two not mutually exclusive scenarios that could explain how aggregated TNPO1 is sequestered into detergent-insoluble aggregates.

A first hypothesis could be that, cellular stress causes the recruitment of TNPO1 to stress granules, as shown in several studies (Chang and Tarn, 2009; Jain et al., 2016b; Mahboubi et al., 2013). Then, altered SG dynamics or defective PQC mechanisms may cause a solidification and aggregation of TNPO1 (discussed in more detail below), resulting in functionally impaired TNPO1.

A possible hint towards a second hypothesis is provided by the study of Deng et al. (2014) that links the co-aggregation of TNPO1 and the FET proteins to DNA damage. Induction of DNA damage was shown to induce DNA-PK-dependent phosphorylation of FUS, causing cytosolic translocation and accumulation of FUS, EWS, TAF15, and TNPO1 (Deng et al., 2014). A possible explanation for the cytosolic translocation of TNPO1 may be that it also becomes phosphorylated upon DNA damage, but this has to be further investigated. Alternatively, phosphorylated FUS (or FET proteins) could show a higher affinity to TNPO1, thus sequestering TNPO1 into phosphorylated FET aggregates. Phosphorylated FUS may be also more prone to aggregation. Supporting this view, phospho-mimetic amino acid substitution (G/S/T-to-D) of the FUS LC domain was reported to enhance co-phase separation with the RBDs of FUS by the formation of electrostatic interactions with positively charged arginines, indicating that the introduction of negative charges by phosphorylation in the FUS LC domain enhances phase separation of full-length FUS (Wang et al., 2018b). As a side note, phase separation of the FUS LC domain alone is suppressed by phospho-mimetic substitution due to

electrostatic repulsion (Monahan et al., 2017; Wang et al., 2018b). Although phosphorylation of the FET proteins upon DNA damage may trigger a first accumulation in the cytoplasm (Deng et al., 2014), it is not clear whether this could affect the chaperone activity of TNPO1 and cause its aggregation. Furthermore, Deng et al. also showed that sections of *post mortem* brains from FTD-FUS patients have increased levels of the DNA DSBs marker p-H2AX. Even though phosphorylation seems to be transient, this may suggest that DNA-PK dependent phosphorylation of FUS triggered by DNA damage may contribute to the characteristic accumulations seen in FTD-FUS (Deng et al., 2014), although its validity has to be verified in regard of a recent publication reporting FUS phosphorylation upon a specific kind of DNA damage without altering nuclear FUS localization (Rhoads et al., 2018).

In order to assess which of the above mentioned hypotheses for the aggregation of TNPO1 in pathological FTD-FUS aggregates is more likely, the question whether TNPO1 or the FET proteins aggregate first has also to be addressed. Future research is needed to clarify whether TNPO1 gets aggregated and dysfunctional first (e.g. due to SG recruitment upon stress) and subsequently the FET protein become pathologically altered, or whether alternatively, the FET proteins aggregate first, e.g. due to loss of methylation, and subsequently trap TNPO1 into the granules/aggregates.

Since general methylation defects haven't been identified so far in FTD-FUS patients (Ravenscroft et al., 2013) and are expected to also affect other RGG-containing RBPs (e.g. EWS, TAF15, hnRNP-A1, hnRNP-A2, G3BP1), presumably causing even more detrimental effects, primary aggregation of the FET proteins due to general arginine methylation defects seems disputable, but may be specific for FET proteins.

In line with the "multiple hit theory" (see section 1.8.1), the SG hypothesis (or at least in combination with DNA damage) for TNPO1 aggregation appears more suitable to explain the pathogenesis in FTD-FUS. Recruitment of TNPO1 to SGs has been reported in multiple studies (Chang and Tarn, 2009; Jain et al., 2016b; Mahboubi et al., 2013). Abrogated nuclear import of the FET proteins due to impaired TNPO1 function could then lead to increasing cytosolic concentrations. Downregulation of arginine methylation of FUS, possibly by active demethylation or regulation of PRMT activity, could be a compensatory response to encounter reduced activity of TNPO1 by increasing the binding affinity and thus reestablish some degree of nuclear import. Fatally, this even worsens FUS aggregation in FTD-FUS patients, as it enhances phase separation and SG partitioning of FUS (Fig. 18, 19 and Fig. 23). Since p62 and ubiquitin are also present in pathological aggregates of FTD-FUS (and ALS-FUS) (Baumer et al., 2010; Neumann et al., 2009; Seelaar et al., 2010), PQC mechanisms may also be compromised (Pankiv et al., 2007) and further contribute to pathological aggregation. Nevertheless, it cannot be

excluded that DNA-damaged induced phosphorylation of FUS in combination with cellular stress may trigger initial SG formation followed by the above described cascade.

Still, the above postulated hits need to be validated in detail. Therefore, further components of FTD-FUS inclusions will have to be identified and TNPO1/FET protein ratios in the pathological aggregates have to be determined. Especially the relevance of DNA damage-induced FUS phosphorylation due to DNA damage or other stresses has to be examined. Furthermore, it is essential to address whether TNPO1 levels are altered in these patients or whether there are cell type-specific differences in TNPO1 levels. Moreover, it remains unclear how arginine methylation of FUS is regulated in cells and how the normal methylation pattern is lost in FTD-FUS patients. So far, no mutations or expression changes for PRMTs (PRMT1, PRMT3, PRMT8) have been identified in FTD-FUS cases (Ravenscroft et al., 2013), but the responsible PRMTs for arginine methylation of FUS (i.e. PRMT1 and PRMT8) have to be studied in further depth. Moreover, putative arginine demethylases, such as JMJD6 or JmJC enzymes (Tsai et al., 2016; Tsai et al., 2017; Walport et al., 2016) may be candidates for demethylation of FUS which need further testing.

3.5.2 Pathomechanisms of ALS-FUS

Patients suffering from ALS-FUS, in contrast to FTD-FUS, have a normal pattern of arginine methylation (Dormann et al., 2012; Suarez-Calvet et al., 2016), but typically carry a mutation in the PY-NLS of FUS that impair binding to TNPO1 (Niu et al., 2012; Zhang and Chook, 2012) and consequently interferes with nuclear import of FUS (Dormann et al., 2010; Niu et al., 2012; Vance et al., 2013; Zhang and Chook, 2012). Notably, there are also N-terminal FUS mutations associated with ALS cases not affecting the binding to TNPO1 (e.g. G156E and R244C), but promote LLPS (Patel et al., 2015) as well as aggregation (Nomura et al., 2014) by a different mechanism. Our data and an accompanying study (Guo et al., 2018) (Fig. 21 and 22) demonstrate that ALS-associated mutations affecting the PY-NLS of FUS, like P525L and 495X, render FUS less sensitive to the chaperone activity of TNPO1. Notably, ALS-linked FUS mutations causing mild cytosolic mislocalization of FUS (e.g. R521G) (Dormann et al., 2012) do not impair TNPO1 binding as much as P525L (Zhang and Chook, 2012) and are still efficiently chaperoned by TNPO1 (Guo et al., 2018). This indicates that the chaperone activity is only disrupted by mutations causing frame-shifts, truncations (495X) or severe point-mutations such as P525L. Even though our findings indicate that the ALS-linked P525L mutation does not promote phase separation *per se* (Fig. 21C), it provides multiple hits towards pathogenesis of ALS-FUS, by impairing nuclear import causing cytosolic mislocalization and accumulation under stress as well as abolished chaperoning by TNPO1 (Fig. 21-23). Notably, hypomethylation of FUS, which promotes detrimental

aggregation in FTD-FUS, may be a potential treatment approach for ALS-FUS as it restores binding of ALS-associated FUS mutations to TNPO1 and thus reestablishes the chaperone activity and rescues cytosolic mislocalization (Dormann et al., 2012; Tradewell et al., 2012).

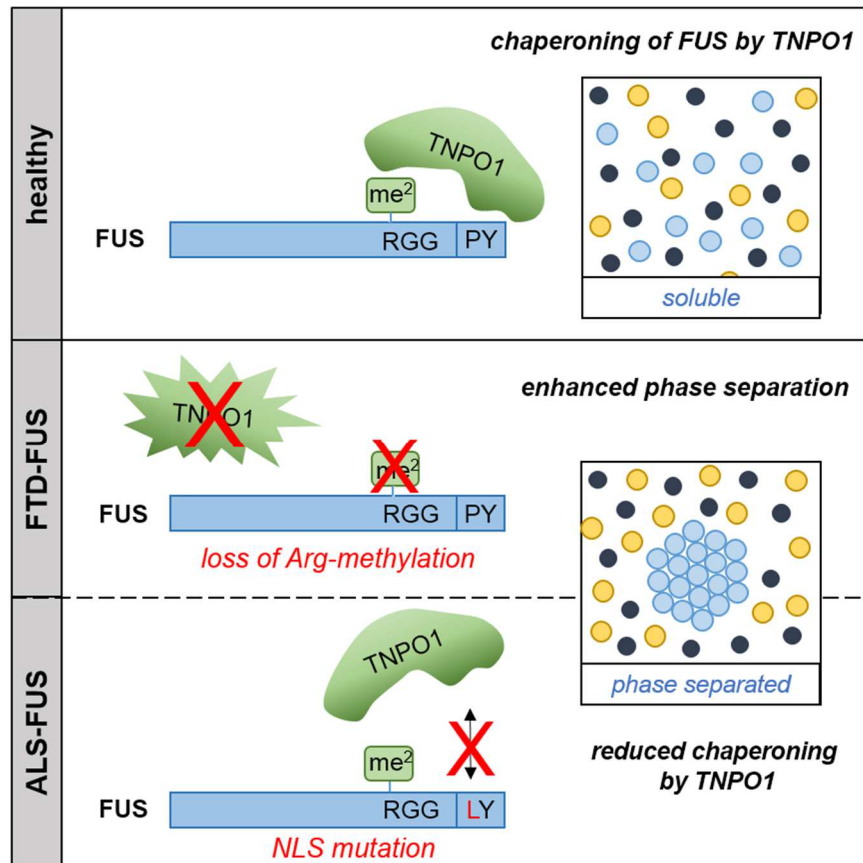


Figure 23: Distinct pathomechanisms drive phase separation of FUS in FTD and ALS. In healthy individuals, FUS is kept soluble by the cytoplasmic chaperone activity of TNPO1 (top panel). Loss of arginine methylation, as seen in FTD-FUS patients, enhances the phase separation of FUS. Furthermore, TNPO1 is aggregating in FTD-FUS patients and its chaperone function towards FUS is disturbed (middle panel). ALS-associated mutations in the FUS-NLS impair the interaction with TNPO1 causing reduced chaperoning by TNPO1 (bottom panel).

3.6 Conclusion and Outlook

In sum, we report two novel mechanisms to regulate liquid-liquid phase separation of aggregation-prone RBPs, namely suppression of LLPS by specific binding proteins and post-translational modifications (PTMs), in the case of FUS by the import receptor TNPO1 and arginine methylation (Fig. 23). Both are not only involved in nuclear import of FUS, but furthermore suppress phase separation and SG association of FUS. When these control mechanisms are disrupted, they may lead to

neurodegeneration. Therefore, such LLPS-regulating binding partners and PTMs of aggregation-prone RBPs need to be identified and subsequently verified whether these are affected in ALS/FTD cases and whether they have potential for therapeutic targeting.

Aberrant phase separation is not exclusive to FUS, but seems to be a common mechanism in neurodegeneration. Notably, for the hexanucleotide repeat expansion in the *C9orf72* gene as most common genetic cause of ALS-FTD (DeJesus-Hernandez et al., 2011; Renton et al., 2011), a similar pathomechanism has been suggested recently. One of the three proposed mechanisms how the GGGGCC repeat expansions contribute to pathology is the synthesis of dipeptide repeat (DPR) proteins that arise from unconventional RAN translation (Ash et al., 2013; Gendron et al., 2013; Mori et al., 2013a; Mori et al., 2013b; Zu et al., 2013). The most toxic forms of these DPR proteins, arginine-containing poly-GR and poly-PR, have been demonstrated to not only undergo liquid-liquid phase separation in the presence of RNA or crowding agent but also to interact with LC-containing RBPs that are components of membrane-less organelles, such as SGs and nucleoli (Boeynaems et al., 2017; Lee et al., 2016; Lin et al., 2016). Poly-GR and poly-PR promote droplet formation of LC-containing proteins *in vitro* and furthermore reduce dynamics of stress granule and nuclear speckles in living cells (Lee et al., 2016). Furthermore, the microtubule-associated protein Tau is aggregating in Alzheimer's disease (AD) and other neurodegenerative diseases (Goedert and Spillantini, 2011; Maziuk et al., 2017). Tau has been shown to accelerate SG formation (Vanderweyde et al., 2016), to undergo phase separation *in vitro* and form droplet-like condensates in neurons (Ambadipudi et al., 2017; Hernandez-Vega et al., 2017; Wegmann et al., 2018). Hyperphosphorylation of Tau, as found in AD and FTD patients (Braak and Braak, 1995; Gong et al., 2005; Kopke et al., 1993), enhances phase separation and aggregation of FUS (Ambadipudi et al., 2017; Wegmann et al., 2018). Further studies demonstrated that a number of ALS/FTD-associated mutations in the LC domains of hnRNP-A1/A2, TIA1 and FUS impair SG dynamics (Kim et al., 2013; Mackenzie et al., 2017; Martinez et al., 2016; Patel et al., 2015).

Besides disturbed phase transition, defective nuclear import seems to be another common theme in the pathogenesis of ALS and FTD, as nuclear import defects were not only shown for cases with FUS pathology, but also linked to DPR toxicity (Boeynaems et al., 2016; Freibaum et al., 2015; Jovicic et al., 2015; Zhang et al., 2015) and TDP-43 pathology (Chou et al., 2018; Nishimura et al., 2010). Furthermore, polyglutamine repeats (polyQ) in the huntingtin (Htt) protein were shown to cause co-aggregation of Ran GTPase-activating protein 1 (RanGAP1) and to impair nuclear export of mRNAs (Gasset-Rosa et al., 2017). Similarly, aggregation of RanGAP1 and NUP62 in *post mortem* brains from patients with Huntington's disease (HD) and defective nucleocytoplasmic transport in human HD iPSC-derived neurons have been shown (Grima et al., 2017). In general, defects in nucleocytoplasmic

transport seem to be characteristic for aged neurons (Mertens et al., 2015). Defective nuclear transport factors found in neurodegenerative diseases or the aging brain may have several detrimental downstream consequences: First, nuclear export of factors required in the cytoplasm, such as mRNA, may be disturbed. Second, disturbed nuclear import of aggregation-prone RBPs may elevate their cytosolic concentrations. Third, the cytosolic chaperone function of nuclear import receptor to suppress detrimental aggregation may be also disturbed.

To put it in a nutshell, both aberrant phase transition and defective nuclear import seem to play key roles in the pathology of ALS/FTD.

4 EXPERIMENTAL PROCEDURES

DECLARATION OF COPYRIGHT AND CONTRIBUTIONS

This section of my Ph.D. thesis was prepared in parallel to the paper 'Phase separation of FUS is suppressed by its nuclear import receptor and arginine methylation' published in *Cell* (Hofweber et al., 2018). Thus, the structure and text of this Ph.D. thesis and the paper will partially overlap. *Elsevier* holds the copyright (2018) for this article published in *Cell* and permits the usage of text and figures in this dissertation.

4.1 Cloning of cDNA constructs

pMal-*Tev*-Flag-FUS-*Tev*-His₆ was created by cloning PCR amplified N-terminal Flag-tagged and C-terminal *Tev*-His₆ tagged FUS cDNA into the Sall-HindIII sites of pMal-*Tev* using primers Sall_flag_F and HindIII_His₆-*Tev*-FUS_R. pMal-*Tev* was created by cloning annealed double stranded oligonucleotides *Tev*_F and *Tev*_R (coding for the *Tev* cleavage site) into the EcoRI-Sall sites of pMal-c.

To generate pMal-*Tev*-FUS-EGFP-*Tev*-His₆, FUS cDNA was PCR amplified from pMal-*Tev*-Flag-FUS-*Tev*-His₆ using primers Sall_FUS_F and BamHI_FUS_R, thus introducing a C-terminal BamHI restriction site. EGFP-His₆ with low-complexity linker was cut from synthetic pEX-A2-linker-EGFP-His₆ (IDT) using BamHI and HindIII sites. In a triple ligation, FUS and EGFP-His₆ fragments were cloned into the pMal-*Tev* backbone derived from pMal-*Tev*-flag-FUS-*Tev*-His₆.

pMal-*Tev*-FUS (P525L)-EGFP-*Tev*-His₆ was generated by site directed mutagenesis of pMal-*Tev*-FUS-EGFP-*Tev*-His₆ using primers FUS wt-EGFP mut P525L_F and FUS wt-EGFP mut P525L_R.

To generate pMal-C2-*Tev*, the C-terminus of MBP including parts of the MCS was PCR-amplified (MBP_NcoI_F; MBPLinker-*Tev*_EcoRI) introducing a *Tev*-cleavage site in the reverse primer and replacing the factor Xa cleavage site in the original pMal-C2 (NEB) vector.

pMal-C2-*Tev*-Flag-FUS ΔRGG3-PY-*Tev*-His₆ was generated by cloning PCR amplified N-terminal Flag-tagged and C-terminal *Tev*-His₆ tagged FUS cDNA encoding amino acids 1-453 into the Sall-HindIII sites of pMal-C2-*Tev* using primers Sall_flag_F and HindIII_FUS453X-*Tev*-His₆_R.

To generate pMal-C2-*Tev*-Flag-FUS-all-KGG-*Tev*-His₆, FUS cDNA was PCR amplified from a synthetic plasmid with all RGGs mutated to KGGs using primers XhoI_FUS_F and HindIII_*Tev*-His₆-FUS_R and cloned into the pMal-C2-*TEV* backbone derived from pMal-C2-*Tev*-Flag-FUS Δ RGG3-PY-*Tev*-His₆.

petM11-His₆-ZZ-*Tev*-FUS-KGG3-PY was generated by cloning FUS cDNA encoding amino acids 454-526 from a synthetic plasmid with all RGGs mutated to KGGs using primers FUS 454_NcoI_F and BamHI_FUS_R and cloned into the petM11-His₆-ZZ backbone derived from petM11-His₆-ZZ-*Tev*-FUS-RGG3-PY.

To generate pETM11-His₆-ZZ-*Tev*-TNPO1, the human TNPO1 cDNA sequence was codon optimized for protein production in bacterial cells and flanked by NcoI and BamHI restriction sites (Genscript). The coding region was cloned into a modified pETM11 bacterial expression vector, which includes an N-terminal His₆, protein A (ZZ) tag and a TEV protease cleavage site.

To generate GCR₂-tagRFP₂-FUS, the EGFP₂-sequence in a modified EGFP-C1 vector containing a GCR₂-EGFP₂-cassette (Hutten et al., 2008) was replaced sequentially with two cDNAs coding for tagRFP (primer: TagRFP_AgeI/TagRFP_EcoRV and TagRFP_Spe/ TagRFP_AgeI_R). FUS wt or P525L was inserted via EcoRV/BamHI sites replacing the NLS sequence (primer: FUS_EcoRV_f with either FUS_BamHI_R or FusP525L_BamHIr).

The pRSV-EGFP-M9M construct was generated by replacing the CMV-promoter in pEGFP-M9M (Dormann et al., 2010) by a RSV promoter sequence (gift from M. Kiebler) via *Asel*/*NheI*.

For detailed list of bacterial expression constructs as well as primer sequences see appendix.

4.2 Recombinant protein expression and purification

All bacterial cultures were grown at 37°C under constant shaking (140-160 rpm) in standard lysogeny broth (LB) medium. Before induction of protein expression, cultures were cooled down to the temperature indicated for the respective protein.

For expression of recombinant MBP-FUS-His₆ (WT, Δ RGG3-PY, and all-KGG) and MBP-FUS-EGFP-His₆ (WT and P525L), the respective bacterial expression vectors were transformed into *E. coli* BL21-DE3-R IPL and BL21-DE3-Rosetta-LysS, respectively, and grown in standard lysogeny broth (LB) medium. At an OD (600 nm) of ~ 0.8, cells were induced with 0.1 mM IPTG for 22 h at 12°C. Cells were lysed in resuspension buffer (50 mM Na₂HPO₄/NaH₂PO₄, pH 8.0, 300 mM NaCl, 10 μ M ZnCl₂, 40 mM imidazole,

4 mM β ME) + 10 % glycerol and tandem-affinity purification using HisTrap FF columns (GE Healthcare) and amylose resin (NEB) was performed. The protein was washed with resuspension buffer and eluted in resuspension buffer including 250 mM imidazole and 20 mM maltose, respectively.

For expression of recombinant His₆-TEV, *E. coli* BL21-Ros-LysS were transformed with the expression plasmid and grown in standard LB medium. Induction of expression was induced at OD (600 nm) of ~0.6 with 1 mM IPTG overnight at 20°C. Cells were lysed in lysis buffer (50 mM Tris pH 8.0, 200 mM NaCl, 20 mM imidazole, 10% glycerol, 4 mM β -mercaptoethanol, 1 μ g/ml each of aprotinin, leupeptin and pepstatin) by addition of lysozyme and sonification. The lysate was incubated in the presence of RNase A (0.1mg/ml final concentration) for 30 min at RT. His₆-TEV was purified using Ni-NTA beads and washed using lysis buffer containing 1 M NaCl. His₆-TEV was eluted in lysis buffer (pH 8.5) containing 800 mM imidazole and dialyzed against storage buffer (20 mM Tris-HCl pH 7.4; 150 mM NaCl; 20% glycerol, 2 mM DTT).

For expression of the RGG3-PY domain, pETM11-His₆-ZZ-FUS-RGG3-PY (WT and KGG3-PY) were transformed into *E. coli* BL21-DE3 Rosetta and were expressed at 37 °C for 4 h. Cells in resuspension buffer were lysed by boiling for 20 min at 90 °C, as boiling lysis allows removal of folded proteins from cell lysates, while intrinsically disordered proteins stay soluble (Livernois et al., 2009). His₆-Z-tagged proteins were bound to nickel-nitrilotriacetic (Ni-NTA) resin (Qiagen), incubated with Benzonase® Nuclease (Sigma) overnight at 4°C in Benzonase buffer (50 mM Na₂HPO₄/NaH₂PO₄, pH 8.0, 50 mM NaCl, 2 mM MgCl₂) and subjected to high salt washes with resuspension buffer containing 2 M NaCl and then eluted in resuspension buffer + 250 mM imidazole. In order to proteolytically remove the His₆-Z-tag, His₆-TEV protease (2.5 mg) was added to eluted His₆-Z-RGG3-PY proteins and dialyzed against TEV cleavage buffer (20 mM Na₂HPO₄/NaH₂PO₄, pH 8.1, 150 mM NaCl, 5% glycerol, 4 mM β ME) overnight at 4 °C. His₆-TEV and His₆-Z-tag were removed by incubation with Ni-NTA resin (Qiagen), while untagged RGG3-PY remains in the supernatant.

For ITC or NMR experiments, pETM11-His₆-Z-FUS-RGG3-PY (WT or P525L) were transformed into *E. coli* BL21-DE3 Star strain. For the unlabeled protein, cells were grown for 1 day at 37°C in standard lysogeny broth (LB) medium. At an OD (600 nm) of ~ 0.8, cells were induced with 0.1 mM IPTG for 22 h at 12°C. To obtain ¹⁵N labeled protein, cells were grown for 1 day at 37°C in minimal medium (100 mM KH₂PO₄, 50 mM K₂HPO₄, 60 mM Na₂HPO₄, 14 mM K₂SO₄, 5 mM MgCl₂; pH 7.2 adjusted with HCl and NaOH with 0.1 dilution of trace element solution (41 mM CaCl₂, 22 mM FeSO₄, 6 mM MnCl₂, 3 mM CoCl₂, 1 mM ZnSO₄, 0.1 mM CuCl₂, 0.2 mM (NH₄)₆Mo₇O₂₄, 17 mM EDTA) supplemented with 6 g of ¹²C₆H₁₂O₆ and 1 g of ¹⁵NH₄Cl (Sigma). At an OD (600 nm) of ~ 0.8, cells were induced with 0.5 mM IPTG for 16 h at 20°C. Cell pellets were harvested and sonicated in denaturing buffer containing 50

mM Tris-HCl pH 7.5, 150 mM NaCl, 20 mM imidazole, 2 mM Tris(2-carboxyethyl)phosphine (TCEP), 20% glycerol and 6 M urea. His₆-ZZ proteins were purified using Ni-NTA agarose (Qiagen) and eluted in 50 mM Tris-HCl pH 7.5, 150 mM NaCl, 200 mM imidazole, 2 mM TCEP and subjected to TEV treatment. Untagged proteins were then isolated performing a second affinity purification using NiNTA beads. A final exclusion chromatography purification step was performed in the buffer of interest on a gel filtration column (Superdex peptide, GE Healthcare).

For expression of recombinant His₆-TNPO1, the bacterial expression vector pETM11-His₆-ZZ-Tev-TNPO1 was transformed into *E. coli* BL21-DE3 Star cells. Expression cultures of 1 l volume were grown for 2 days in minimal medium (100 mM KH₂PO₄, 50 mM K₂HPO₄, 60 mM Na₂HPO₄, 14 mM K₂SO₄, 5 mM MgCl₂; pH 7.2 adjusted with HCl and NaOH with 0.1 dilution of trace element solution (41 mM CaCl₂, 22 mM FeSO₄, 6 mM MnCl₂, 3 mM CoCl₂, 1 mM ZnSO₄, 0.1 mM CuCl₂, 0.2 mM (NH₄)₆Mo₇O₂₄, 17 mM EDTA) supplemented with 6 g of glucose and 3 g of NH₄Cl. Cells were diluted to an OD (600 nm) of 0.8 and induced with 0.5 mM IPTG followed by protein expression for 4 h at room temperature. His₆-TNPO1 was purified using Ni-NTA agarose (Qiagen) and eluted in 50 mM Tris-HCl pH 7.5, 150 mM NaCl, 200 mM imidazole, 2 mM TCEP. A final size exclusion chromatography step was performed in 50 mM Tris-HCl pH 7.5, 150 mM NaCl, 20 mM imidazole, 2 mM TCEP, 20% glycerol on a gel filtration column (HiLoad 16/600 Superdex 200 pg, GE Healthcare). Note, that for ITC/NMR experiments, the His-tag was removed by TEV cleavage.

For expression of recombinant His₆-PRMT1, the pET28b-PRMT1 vector was transformed into *E. coli* BL21-DE3 Star and 1 l expression culture was grown in LB medium. Cells were induced at an OD (600 nm) of 0.8 with 0.5 mM IPTG followed by protein expression for 16 h at 20°C. Cell pellets were harvested and sonicated in 50 mM Tris-HCl pH 7.5, 150 mM NaCl, 20 mM imidazole, 2 mM TCEP, 20% glycerol. His₆-PRMT1 was purified using 5 mL HisTrap HP column (GE Healthcare), washed with lysis buffer supplemented with 1 M NaCl, and eluted with a gradient of 20-500 mM imidazole in 50 mM Tris-HCl pH 7.5, 1 M NaCl, 2 mM TCEP. Subsequently, elution fractions were pool and concentrated to ≤ 15 ml and applied to a HiPrep Desalting Column 26 (GE healthcare) to *in vitro methylation* (IVM) buffer. Alternatively, elution fractions of HisTrap column were further purified by size exclusion chromatography as described for TNPO1 above.

Protein concentrations were determined from their absorbance at 280 nm using ϵ predicted by the ProtParam tool. For all assay that involved addition of RNA, 260/280 nm ratios of purified proteins were between 0.6 and 0.8.

4.3 *In vitro* methylation

FUS proteins and PRMT1 were dialyzed against *in vitro* methylation (IVM) buffer containing 20 mM Na₂HPO₄/NaH₂PO₄, pH 8.1, 150 mM NaCl, 5% glycerol, 1 mM EDTA, 1 mM DTT or 50 mM Na₂HPO₄/NaH₂PO₄, pH 8.0, 150 mM NaCl, 2 mM TCEP for ITC and NMR experiments. FUS proteins were *in vitro* methylated by incubating with PRMT1 and 1 mM S-adenosyl-L-methionine (SAM) overnight at room temperature. PRMT1 was used at a molar ratio of 2:1 for MBP-FUS, 1.5:1 for RGG3-PY or KGG3-PY (used in droplet and turbidity assays) and 0.2:1 for RGG-PY proteins used in ITC or NMR experiments. For RGG3-PY proteins, PRMT1 was removed by boiling the samples for 10 min at 90°C.

4.4 *In vitro* transcription

MAPT RNA and *ASH1* E3-51 RNA were produced by *in vitro* transcription (MEGAscript Kit; Ambion) using linearized pGM3 mTaul9-28560 or primers P45 and P132, respectively.

For electrophoretic mobility shift assays (EMSAs) and filter-binding assays the *ASH1* E3-51 RNA was radioactively labeled using [³²P]ATP and T4 polynucleotide kinase (NEB). The RNA was separated from free nucleotides using NucAway spin columns (Ambion).

4.5 *In vitro* phase separation assays

4.5.1 Droplet assay for microscopy

Purified RGG3-PY or KGG3-PY and His₆-TNPO1 were buffer exchanged to droplet buffer (20 mM Na₂HPO₄/NaH₂PO₄, pH 7.5, 75 mM NaCl, 2.5% glycerol, 1 mM DTT) and concentrated in Amicon® Ultra Centrifugal Filter Devices (Millipore). For droplet formation of C-terminal RGG3-PY proteins, proteins were diluted to indicated concentrations and supplemented with *in vitro* transcribed *MAPT* RNA (a known FUS target RNA, Orozco et al., 2012) at a molar ratio of 1:50, as this ratio was found to maximally promote phase separation. His₆-TNPO1, His₆-Importin 5, α-FUS-RGG3, or His₆-PRMT1, respectively, were used at equimolar concentrations to FUS.

Purified full-length MBP-FUS-EGFP (WT or P525L) or MBP-FUS were diluted in droplet buffer including 150 mM NaCl, if not otherwise stated in the figure legend. Full-length FUS was only supplemented with RNA when explicitly mentioned in the figure legend (Fig. 16F and 16G). Phase separation was

induced by addition of acTEV protease (Invitrogen) at 25°C. With the exception of Figure 18A and 18E, where widefield fluorescence microscopy was applied, imaging of EGFP-tagged FUS was performed by confocal microscopy. Non-fluorescent FUS-droplets were imaged by phase contrast microscopy.

Note that phase separation properties, i.e. critical concentration for droplet formation, differ slightly between different protein preparations.

4.5.2 *In vitro* aging assay

To induce aging of FUS-EGFP droplets, TEV-cleaved samples were subjected to 700 rpm on an orbital shaker at RT for 8h and additionally mixed by pipetting up and down every hour. Samples were imaged in 384-well plates by confocal microscopy.

4.5.3 Turbidity assay

Phase separation of RGG3-PY and MBP-FUS in the absence or presence of equimolar amounts of His₆-TNPO1, His₆-Importin 5, α -FUS-RGG3, or His₆-PRMT1, respectively, was induced as described above for the droplet assay. Turbidity measurements were conducted at 600 nm in 384-well plates with 20 μ l samples using a BioTek Power Wave HT plate reader. All experiments were performed in triplicate.

4.5.4 Sedimentation assay

For sedimentation analysis of full-length FUS, the MBP-tag of 1 μ M purified MBP-FUS protein in the absence or presence of equimolar amounts of His₆-TNPO1, His₆-Importin 5, α -FUS-RGG3, or His₆-PRMT1, respectively, was cleaved using 0.1 mg/ml His₆-TEV in 50 μ l reaction buffer (50 mM Tris pH 8, 0.5 mM EDTA, 1 mM DTT) for 60 min at 30 °C, followed by centrifugation at room temperature for 15 min at 16,000-20,000 g. Equal volumes of supernatant and pellet fraction were analyzed by SDS-PAGE and either SyproRuby stain (Fig. 11D, 18B) or Western Blot with a FUS-specific antibody (4H11) (Fig. 13B).

4.6 Cell culture and transfection

HeLa Kyoto cells for transient transfection experiments and HeLa-P4 cells (Charneau et al., 1994) for semi-permeabilized cell assays were grown in DMEM high glucose GlutaMAX (Invitrogen) supplemented with 10% dialyzed FBS, or 10% standard FBS and 10 µg/ml gentamicin, respectively. Cells were maintained in a humidified incubator at 37°C with 5% CO₂. Transient transfections were performed using Turbofect following manual instructions. Note, that for transfection of GCR₂-tagRFP₂-FUS constructs low DNA amounts (20% GCR₂-tagRFP₂-FUS, 80% plasmid coding for EGFP/EGFP-bimax/EGFP-M9M) to minimize aggregation of FUS due to overexpression.

4.7 Semi-permeabilized cell assay

HeLa P4 cells were grown on poly-L-lysine coated 12 mm coverslips, permeabilized with 0.003-0.005% digitonin in KPB (20 mM potassium phosphate pH 7.4, 250 mM sucrose, 5 mM Mg(OAc)₂, 200 mM KOAc, 1 mM EGTA, 2 mM DTT and 1 µg/ml each aprotinin, pepstatin and leupeptin). After several washes to remove soluble proteins (4 x 4 min in KPB on ice), nuclear pores were blocked by 15 min incubation with 200 µg/ml wheat germ agglutinin (WGA) on ice. Cells were then incubated for 30 min at room temperature with 125 nM MBP-FUS-EGFP in the absence or presence of 1.25 µM His₆-TNPO1 in KPB. Note that a 10-fold excess of TNPO1 was required for efficient shielding of FUS, possibly due to other RBPs present in SGs that bind to TNPO1. Subsequently, cells were washed (3 x 5 min in KPB on ice) to remove unbound MBP-FUS-EGFP. SGs were visualized by immunostaining of G3BP1. Note that G3BP1 immunostaining also served as a control for proper permeabilization, as non/poorly-permeabilized cells still show diffuse cytoplasmic G3BP1 staining. Cells were imaged by confocal microscopy using identical settings for reactions within the same experiment.

4.8 Filter-binding assay

The indicated protein concentrations were incubated with 0.5 nM of *in vitro* transcribed, radiolabeled *ASH1* E3-51 RNA in a total volume of 80 µL in filter-binding buffer (20 mM Na phosphate, 50 mM NaCl, 2 mM DTT, pH 7.5). Samples were applied to nitrocellulose and nylon membranes, using a Dot Blot Aparatus (BioRad), and washed twice with 80 µl filter-binding buffer. Membranes were air-dried and analyzed by phosphorimaging using a Fujifilm FLA-3000 scanner.

4.9 Electrophoretic mobility shift assay (EMSA)

Experiments were conducted according to (Niedner et al., 2013). Increasing protein concentrations (0.35 - 9 μ M) were mixed with 5 nM of radiolabeled *ASH1* E3-51 RNA in droplet buffer (20 mM $\text{Na}_2\text{HPO}_4/\text{NaH}_2\text{PO}_4$, pH 7.5, 75 mM NaCl, 1 mM DTT) with 4% glycerol in a final volume of 20 μ l. The samples were incubated for 25 min at room temperature and afterwards resolved on a 6% native TBE-PAGE gel in 1x TBE running buffer. Gels were incubated in fixation solution [10% (v/v) acetic acid, 30% (v/v) methanol] for 15 min and vacuum dried and subsequently analyzed with radiograph films.

4.10 Immunostaining or Immunocytochemistry

Cells grown on coverslips were either fixed ~20 h after transfection or after the semi-permeabilized cell assay in 3.7% formaldehyde/PBS buffer for 7-10 min at RT and permeabilized in 0.5% TX-100/ PBS for 5 min at room temperature. Cells were blocked for 10 min in blocking buffer (1% donkey serum in PBS/ 0.1% Tween-20) and incubated with primary antibodies in blocking buffer for 1-2h at RT or overnight at 4°C. Secondary antibodies were diluted in blocking buffer and incubated for 1h at room temperature. Washing steps after antibody incubation were performed with PBS/0.1% Tween-20. DNA was stained with DAPI at 0.5 μ g/ml in PBS and cells mounted in ProLong™ Diamond Antifade. Imaging was performed by confocal microscopy.

For detailed list of used antibodies see appendix.

4.11 Microscopy

4.11.1 Phase contrast and wide-field fluorescence microscopy

For imaging of FUS droplets, samples were placed in sealed sample chambers formed by a hole punched into a double-sided sticky tape, taped onto a glass slide and sealed with a coverslip.

For imaging of RGG3-PY and FUS droplets by phase contrast microscopy, a 63x/1.40 Oil/Ph3 objective was used; FUS-EGFP droplets in Fig. 18A and Fig. 18E were imaged by fluorescence microscopy using a 63x/1.40 Oil objective, both on an Axio Observer.Z1 wide-field fluorescence microscope and an AxioCam 506 (Zeiss, Oberkochen, Germany).

4.11.2 Confocal microscopy

Confocal microscopy was performed at the Bioimaging core facility of the Biomedical Center with an inverted Leica SP8 microscope, equipped with lasers for 405, 488, 552 and 638 nm excitation. Images were acquired using two-fold frame averaging with a 63x1.4 oil objective, and an image pixel size of 71 nm or 59 nm for droplets and cells, respectively. The following fluorescence settings were used for detection: DAPI: 419-442 nm, GFP: 498-533 nm, RFP/Alexa 555: 562-598 nm, Alexa 647: 650-700 nm. If applicable, recording was performed sequentially to avoid bleed-through using a conventional photomultiplier tube.

4.11.3 Fluorescence Recovery after Photobleaching (FRAP)

In contrast to all other experiments in this study, droplet buffer including 75 mM NaCl was supplemented with 150 mg/ml Ficoll 400 in order to obtain droplets of similar size and shape for FRAP experiments. Experiments were performed on an inverted microscope (Axio Observer.Z1; Carl Zeiss, Oberkochen, Germany) equipped with a confocal spinning disk unit (CSU-X1; Yokogawa, Tokyo, Japan) and a Zeiss 100x/1.46 Oil Ph3 oil immersion lens. Images were acquired in the streaming mode using the 488 nm SD laser line and fixed exposure times of 50 ms and an EM-CCD camera (EvolveDelta; Photomoetrics) at bin 1x1. For localized photobleaching (“half-bleach”), a laser scanning device (UGA-42 Geo; Rapp OptoElectronic, Hamburg, Germany) was used. The “Geo” module allowed for simultaneous laser illumination within hardware-defined shapes of different sizes. Here, a square-like shape with an illumination size of $\sim 4 \mu\text{m}$ in the sample was selected. For each experiment, half of the observed structure was bleached to approximately 50% of the initial intensity using a 473 nm diode laser (DL-473/75; Rapp OptoElectronic, Hamburg, Germany).

4.11.4 Transmission electron microscopy (TEM)

Carbon coated copper grids (carbon film coated 400 mesh copper grids, Science Services) were glow discharged for 2 min in a Harrick plasma cleaner (PDC-32G-2) to facilitate protein adsorption. MBP-FUS (7 μM) +/- TNPO1 (7 μM) was incubated with TEV protease for 90 min and subsequently diluted to 2 μM and deposited on the grid surface. The grid was washed twice in a drop of double distilled water, blotted shortly using filter paper. Fixing the grid by inverse forceps, 3 μl of 1% uranyl acetate were added to the grid for 30 s. After blotting, the grid was air dried for at least 30 min. Mosaics of

three by three images were obtained at a magnification of 60.000 using a JEOL JEM 1400-plus electron microscope at 120 kV (TEM Center software, JEOL). The Sight X Viewer (JEOL) and ImageJ (NIH) Software packages were applied for mosaic stitching.

4.12 Nuclear magnetic resonance (NMR)

All proteins / RNA samples were prepared in 20 mM $\text{Na}_2\text{HPO}_4/\text{NaH}_2\text{PO}_4$ pH 7.5, 75 mM NaCl, 2.5% glycerol, 1 mM DTT and 10% $^2\text{H}_2\text{O}$ added for the lock signal. NMR experiments were performed at 25°C on Bruker 700 MHz spectrometer. Spectra were processed using Topspin 3.5 and Mnova 11.

4.13 Isothermal Calorimetry (ITC)

All protein samples were prepared either in 50 mM Tris-HCl (pH 7.5), 150 mM NaCl and 2 mM Tris(2-carboxyethyl)phosphine (TCEP) or in 50 mM Tris-HCl (pH 7.5), 1 M NaCl and 2 mM TCEP. ITC measurements were carried out on a MicroCal VP-ITC instrument (Microcal, Northampton, USA) with 36 rounds of 8 μl injections at 25 °C. Integration of peaks corresponding to each injection, subtraction of the contribution of protein dilution and correction for the baseline were performed using the Origin-based 7.0 software provided by the manufacturer. Curve fitting was done with a standard one-site model and gives the equilibrium binding constant (K_a), and enthalpy of the complex formation (ΔH).

4.14 Quantification and analysis

4.14.1 Statistics

Statistical analyses were performed in GraphPad Prism 5. For 2-grouped analyses, for which control and treatment groups were handled in parallel, a paired t-test was applied. If measurements were not normally distributed, a non-parametric test (Mann-Whitney) was chosen. 1-way ANOVAs were applied to multi-group comparisons. Here, a Bonferroni post-test was applied when significance between all groups was analyzed, whereas a Dunnett's multiple comparison test was applied when the significance of all values to a single condition was analyzed.

4.14.2 Image analysis

Confocal images were acquired using LAS X (Leica), all other images were acquired in ZEN2 (Zeiss). For illustration of FRAP of FUS-EGFP droplets, images were displayed as heat map and processed using the interpolation function in ZEN2. All other images were processed using Image J/Fiji software applying linear enhancement for brightness and contrast. For quantitative measurements, equal exposure times and processing conditions for respective channels were applied to all samples within one experiment. For better visibility, in some figures the individual channels were displayed in artificial colors as indicated in the figure legends.

4.14.3 Droplet quantification

Confocal images were imported in the public-domain software Image J/Fiji (Schindelin et al., 2012) and a Median filter with radius 2 was applied. Huang auto threshold method providing best coverage of the droplet area was applied. Structures touching the edge of the image section and/or smaller than $0.5 \mu\text{m}^2$ were excluded from particle analysis. If required, a watershed analysis was performed.

4.14.4 Quantification of MBP-FUS-EGFP in SGs

For quantitative measurements, equal exposure times and processing conditions for respective channels were applied to all samples within one experiment. In Image J/Fiji, ROIs corresponding to SGs were identified using the wand tool by G3BP1 staining and mean fluorescence intensity in the EGFP channel was determined. For each condition, at least 10 cells and at least 28 SGs were analyzed. For display of fluorescence intensity of FUS in SGs, measured fluorescence values were log transformed to achieve a more balanced spread. Statistical analyses were performed in GraphPad Prism 5.

4.14.5 Quantification of filter-binding assays

Membranes from filter-binding assays were scanned by a FujiFilm FLA-3000 imaging machine. Quantification of signal intensities was carried out using the Dot Blot Analyzer macro within the Image J software. For binding experiments, the raw intensities of the individual dots on the nitrocellulose

membrane were normalized against the raw intensity measured for the highest FUS concentration. For outcompetition experiments, a ratio of the intensity on the nitrocellulose membrane versus the intensity on nitrocellulose and nylon membrane was determined. The obtained relative intensities were plotted against the protein concentration and fitted using the non-linear curve-fitting tool in Origin software.

4.14.6 FRAP analysis

Intensities of bleached areas were corrected both for bleaching due to imaging over time and background noise. The corresponding calculations were performed with the Fiji/ImageJ macro “TimeSeries Analyzer” by calculating the fluorescence intensity over time ($I(t)$) as follows:

$$I(t) = [ROI1(t) - ROI3(t)] / [ROI2(t) - ROI3(t)]$$

with ROI1 giving the averaged gray values of the bleached area, and ROI2 corresponds to the averaged gray values of the total droplet. ROI3 corresponded to the averaged background values. Obtained values were further normalized to the initial fluorescence by dividing $I(t)$ by the mean gray value of the initial 4 time steps before bleaching $\langle I(1-4) \rangle$.

4.14.7 Densitometry measurements

To determine the solubility of FUS by sedimentation analysis of TEV-cleaved MBP-FUS, densitometry measurements of band intensities after Sypro-Ruby staining or FUS immunoblotting of supernatant and pellet fractions, respectively, were performed using standard plugins in the Image J software. The ratio of signal intensity of the FUS bands in the supernatant and pellet was determined. The lower the S/P ratio the higher the degree of phase separation.

For detailed list of used software and algorithms see appendix.

5 APPENDIX

Antibodies

Table 4: Summary of used antibodies.

Name	Source	Host species
FUS (4H11)	Santa Cruz (RRID:AB_2105208)	mouse, monoclonal
UMA-FUS (14G1)	D. Dormann; (Suarez-Calvet et al., 2016)	rat, monoclonal
MMA-FUS (15E11)	D. Dormann; (Suarez-Calvet et al., 2016)	rat, monoclonal
ADMA-FUS (9G6)	D. Dormann; (Dormann et al., 2012)	rat, monoclonal
G3BP1	Proteintech (RRID:AB_2232034)	rabbit, polyclonal
GFP (K3-184-2)	A. Noegel; (Noegel et al., 2004)	mouse
RFP	Thermo (RRID:AB_2315269)	rabbit, polyclonal
TIA1	Santa Cruz (AB_2201433)	goat, polyclonal
Alexa 555 Donkey anti-rabbit	Thermo (RRID:AB_162543)	donkey, polyclonal
Alexa 647 Donkey anti-rabbit	Thermo (RRID:AB_2536183)	donkey, polyclonal
Alexa 647 Donkey anti-goat	Thermo (RRID:AB_2535864)	donkey, polyclonal
IRDye 680RD Donkey anti-Mouse IgG	LI-COR (RRID:AB_10953628)	donkey, polyclonal
IRDye 680RD Goat anti-Rat IgG	LI-COR (RRID:AB_10956590)	goat, polyclonal
IRDye 800VW Donkey anti-Mouse IgG	LI-COR (RRID:AB_621847)	donkey, polyclonal

Bacterial strains

Table 5: Summary of used bacterial strains.

Name	Source
BL21-Codon Plus (DE3)-RIPL	Agilent Technologies
BL21-DE3-Rosetta-LysS	D. Niessing
BL21-DE3 Rosetta	C. Haass
BL21-DE3	Agilent Technologies

Cell lines

Table 6: Summary of used cell lines.

Name	Source
HeLa P4	R. Kehlenbach, (Charneau et al., 1994)
HeLa Kyoto	I. Poser and A. Hyman

Recombinant DNA

Table 7: Summary of used recombinant DNA.

Name	Source	encoded protein
pMal- <i>Tev</i> -Flag-FUS- <i>Tev</i> -His ₆	M. Ruepp; this Ph.D. thesis; (Hofweber et al., 2018)	MBP-FUS-His ₆ WT
pMal- <i>Tev</i> -FUS (WT)-EGFP- <i>Tev</i> -His ₆	this Ph.D. thesis; (Hofweber et al., 2018)	MBP-FUS-EGFP-His ₆ WT
pMal- <i>Tev</i> -FUS (P525L)-EGFP- <i>Tev</i> -His ₆	this Ph.D. thesis; (Hofweber et al., 2018)	MBP-FUS-EGFP-His ₆ P525L
pMal-C2- <i>Tev</i> -Flag-FUS-ΔRGG3-PY- <i>Tev</i> -His ₆	this Ph.D. thesis; (Hofweber et al., 2018)	MBP-FUS-His ₆ ΔRGG3-PY
pMal-C2- <i>Tev</i> -Flag-FUS-all-KGG- <i>Tev</i> -His ₆	this Ph.D. thesis; (Hofweber et al., 2018)	MBP-FUS-His ₆ all-KGG
pEX-A2-linker-EGFP-His ₆	this Ph.D. thesis	
petM11-His ₆ -ZZ- <i>Tev</i> -FUS-RGG3-PY WT	D. Dormann; (Dormann et al., 2012)	His ₆ -Z-FUS RGG3-PY WT
petM11-His ₆ -ZZ- <i>Tev</i> -FUS-RGG3-PY P525L	D. Dormann; (Dormann et al., 2012)	His ₆ -Z-FUS RGG3-PY P525L
petM11-His ₆ -ZZ- <i>Tev</i> -FUS-KGG3-PY	this Ph.D. thesis; (Hofweber et al., 2018)	His ₆ -Z-FUS KGG3-PY
petM11-His ₆ -ZZ- <i>Tev</i> -TNPO1	T. Madl; (Suarez-Calvet et al., 2016)	
pET28b-PRMT1	E. Wahle; (Zhang and Cheng, 2003)	His ₆ -PRMT1
His ₆ -TEV in a pET-24d(+) vector	A. Geerlof	
pEGFP-bimax	D. Dormann; (Dormann et al., 2010)	EGFP-bimax
pRSV-EGFP-M9M	S. Hutten; this Ph.D. thesis; (Hofweber et al., 2018)	EGFP-M9M
GCR ₂ -tagRFP ₂ -FUS WT	S. Hutten; this Ph.D. thesis; (Hofweber et al., 2018)	GCR ₂ -tagRFP ₂ -FUS WT
GCR ₂ -tagRFP ₂ -FUS P525L	S. Hutten; this Ph.D. thesis; (Hofweber et al., 2018)	GCR ₂ -tagRFP ₂ -FUS P525L
pGM3 mTauI9-28560	D. Edbauer; (Orozco et al., 2012)	

PCR primers and oligonucleotides

Table 8: Summary of used PCR primers and oligonucleotides.

Name	Sequence
Sall_flag_F	AAAAGTCGACATGGACTACAAGGACGACGATG
HindIII_Tev-His ₆ -FUS_R	GTGCCAAGCTTTCAGTGATGATGATGATGATGGCTTTGGAAA TACAGATTTTCATACGGCCTCTCCCTGCGATCC
Tev_F	AATTCGGCGGCGAAAATCTGTATTTCCAAAGCG
Tev_R	TCGACGCTTTGGAAATACAGATTTTCGCCGCCG
Sall_FUS_F	AAAAGTCGACATGGCCTCAAACGATTATA
BamHI_FUS_R	TTTTGGATCCATACGGCCTCTCCCT
FUS wt-EGFP mut P525L_F	AGGGAGAGGCTGTATGGATCCGGCGCACCTGGCTCA
FUS wt-EGFP mut P525L_R	TGAGCCAGGTGCGCCGGATCCATACAGCCTCTCCCT
HindIII_FUS453X-Tev-His ₆ _R	TTTTAAGCTTTCAGTGATGATGATGATGATGGCTTTGGAAATA CAGATTTTCGCCATCTGGTTTAGGGGCCTTACA
XhoI_FUS_F	AAAACCTCGAGATGGCCTCAAACGATTATACCCAAC
FUS 454_NcoI_F	GATACCATGGGCCAGGAGGGGGACCAGGTGG
P45	AATTTAATACGACTCACTATAG
P132	ATTGTTTCGTGATAATGTCTCTTATTAGTTGAAAGAGATTGAG TTATCCATCTATAGTGAGTCGTATTAAT
TagRFP_AgeI	TTTTTACCGGTCGCCACCATGGTGTCTAAGGGCGA
TagRFP_EcoRV_R	TTTTTGATATCCATTAAGTTTGTGCCCCAGTTT
TagRFP_SpeI	TTTTTACTAGTCATGGTGTCTAAGGGCGA
TagRFP_AgeI_R	TTTTTACCGGTCCATTAAGTTTGTGCCCCAGTTT
FUS_EcoRV_F	AATTCGATATCCCATGGCCTCAAACGATTATACCCAACAAG
FUS_BamHI_R	CGGGATCCTTAATACGGCCTCTCCCTGCGATCC
FusP525L_BamHlr	TTTTTGGATCCTTAATACAGCCTCTC
MBP_NcoI_F	CGCCACCATGAA AACG
MBPLinker_Tev_EcoRI	GAATTCTGAAATGCCTTGGAAATACAGATTTTCCCGAGGTTG TTGTTATTGTATTGTT
(UG) ₁₀ RNA	UGUGUGUGUG UGUGUGUGUG

Recombinant proteins

Table 9: Summary of used recombinant proteins.

Name	Source
AcTEV Protease	Thermo
GST-Precision	Geyer
Benzonase Nuclease	Sigma
Importin 5	D. Görlich; (Jakel et al., 2002)

Chemicals and reagents

Table 10: Summary of used chemicals and reagents.

Name	Source
S-(5'-Adenosyl)-L-methionine <i>p</i> -toluenesulfonate	Sigma
TEM grids, carbon film coated, approx. 5-6 nm, 400 Mesh, Cu	Science Services
4% Uranyl Acetate Solution	Science Services
[γ 32P]ATP	Hartmann Analytic
DMEM, high glucose, GutaMAX™ supplement	Thermo
Fetal Bovine Serum, qualified, heat inactivated, E.U.-approved, South America Origin	Thermo
Fetal Bovine Serum, dialyzed, US origin	Thermo
Gentamicin (10 mg/mL)	Thermo
TurboFect™ Transfection Reagent	Thermo
Aprotinin	Roth
Leupeptin hemisulfate	Roth
Pepstatin A	Roth
Lectin from <i>Triticum vulgare</i> (Wheat germ agglutinin, WGA)	Sigma
Digitonin	Calbiochem
ProLong™ Diamond Antifade Mountant	Thermo
DAPI	Sigma
Poly-L-Lysine	Sigma
Sypro-Ruby Protein Gel Stain	Sigma

Software and Algorithms

Table 11: Summary of used software and algorithms.

Name	Source
ImageJ (Fiji)	NIH; (Schindelin et al., 2012)
Image Studio Lite	Li-COR
Zen2 blue edition (lite)	Zeiss
LAS X	Leica
GraphPad Prism5	GraphPad Software, Ink
PONDR® VL-XT	Molecular Kinetics, Inc., Washington State University; WSU Research Foundation
TEM Center Software	JEOL
Sight X Viewer Software	JEOL
Origin	OriginLab
TopSpin3.1	Bruker

6 REFERENCES

- Agashe, V.R., and Hartl, F.U. (2000). Roles of molecular chaperones in cytoplasmic protein folding. *Semin Cell Dev Biol* *11*, 15-25.
- Alberti, S., Halfmann, R., King, O., Kapila, A., and Lindquist, S. (2009). A systematic survey identifies prions and illuminates sequence features of prionogenic proteins. *Cell* *137*, 146-158.
- Alberti, S., and Hyman, A.A. (2016). Are aberrant phase transitions a driver of cellular aging? *Bioessays* *38*, 959-968.
- Alberti, S., Mateju, D., Mediani, L., and Carra, S. (2017). Granulostasis: Protein Quality Control of RNP Granules. *Front Mol Neurosci* *10*, 84.
- Altmeyer, M., Neelsen, K.J., Teloni, F., Pozdnyakova, I., Pellegrino, S., Grofte, M., Rask, M.B., Streicher, W., Jungmichel, S., Nielsen, M.L., *et al.* (2015). Liquid demixing of intrinsically disordered proteins is seeded by poly(ADP-ribose). *Nat Commun* *6*, 8088.
- Ambadipudi, S., Biernat, J., Riedel, D., Mandelkow, E., and Zweckstetter, M. (2017). Liquid-liquid phase separation of the microtubule-binding repeats of the Alzheimer-related protein Tau. *Nat Commun* *8*, 275.
- Anderson, P., and Kedersha, N. (2006). RNA granules. *J Cell Biol* *172*, 803-808.
- Anderson, P., and Kedersha, N. (2008). Stress granules: the Tao of RNA triage. *Trends Biochem Sci* *33*, 141-150.
- Antonyamy, S., Bonday, Z., Campbell, R.M., Doyle, B., Druzina, Z., Gheyi, T., Han, B., Jungheim, L.N., Qian, Y., Rauch, C., *et al.* (2012). Crystal structure of the human PRMT5:MEP50 complex. *Proc Natl Acad Sci U S A* *109*, 17960-17965.
- Anzilotti, C., Pratesi, F., Tommasi, C., and Migliorini, P. (2010). Peptidylarginine deiminase 4 and citrullination in health and disease. *Autoimmun Rev* *9*, 158-160.
- Aoki, K., Ishii, Y., Matsumoto, K., and Tsujimoto, M. (2002). Methylation of *Xenopus* CIRP2 regulates its arginine- and glycine-rich region-mediated nucleocytoplasmic distribution. *Nucleic Acids Res* *30*, 5182-5192.
- Apicco, D.J., Ash, P.E.A., Maziuk, B., LeBlang, C., Medalla, M., Al Abdullatif, A., Ferragud, A., Botelho, E., Ballance, H.I., Dhawan, U., *et al.* (2018). Reducing the RNA binding protein TIA1 protects against tau-mediated neurodegeneration in vivo. *Nat Neurosci* *21*, 72-80.
- Arai, T., Hasegawa, M., Akiyama, H., Ikeda, K., Nonaka, T., Mori, H., Mann, D., Tsuchiya, K., Yoshida, M., Hashizume, Y., *et al.* (2006). TDP-43 is a component of ubiquitin-positive tau-negative inclusions in frontotemporal lobar degeneration and amyotrophic lateral sclerosis. *Biochem Biophys Res Commun* *351*, 602-611.
- Araya, N., Hiraga, H., Kako, K., Arao, Y., Kato, S., and Fukamizu, A. (2005). Transcriptional down-regulation through nuclear exclusion of EWS methylated by PRMT1. *Biochem Biophys Res Commun* *329*, 653-660.
- Ash, P.E., Bieniek, K.F., Gendron, T.F., Caulfield, T., Lin, W.L., DeJesus-Hernandez, M., van Blitterswijk, M.M., Jansen-West, K., Paul, J.W., 3rd, Rademakers, R., *et al.* (2013). Unconventional translation of C9ORF72 GGGGCC expansion generates insoluble polypeptides specific to c9FTD/ALS. *Neuron* *77*, 639-646.

Baechtold, H., Kuroda, M., Sok, J., Ron, D., Lopez, B.S., and Akhmedov, A.T. (1999). Human 75-kDa DNA-pairing protein is identical to the pro-oncoprotein TLS/FUS and is able to promote D-loop formation. *J Biol Chem* 274, 34337-34342.

Banani, S.F., Lee, H.O., Hyman, A.A., and Rosen, M.K. (2017). Biomolecular condensates: organizers of cellular biochemistry. *Nat Rev Mol Cell Biol* 18, 285-298.

Baron, D.M., Kaushansky, L.J., Ward, C.L., Sama, R.R., Chian, R.J., Boggio, K.J., Quaresma, A.J., Nickerson, J.A., and Bosco, D.A. (2013). Amyotrophic lateral sclerosis-linked FUS/TLS alters stress granule assembly and dynamics. *Mol Neurodegener* 8, 30.

Baumer, D., Hilton, D., Paine, S.M., Turner, M.R., Lowe, J., Talbot, K., and Ansorge, O. (2010). Juvenile ALS with basophilic inclusions is a FUS proteinopathy with FUS mutations. *Neurology* 75, 611-618.

Bedford, M.T., and Clarke, S.G. (2009). Protein arginine methylation in mammals: who, what, and why. *Mol Cell* 33, 1-13.

Belly, A., Moreau-Gachelin, F., Sadoul, R., and Goldberg, Y. (2005). Delocalization of the multifunctional RNA splicing factor TLS/FUS in hippocampal neurones: exclusion from the nucleus and accumulation in dendritic granules and spine heads. *Neurosci Lett* 379, 152-157.

Belyanskaya, L.L., Gehrig, P.M., and Gehring, H. (2001). Exposure on cell surface and extensive arginine methylation of ewing sarcoma (EWS) protein. *J Biol Chem* 276, 18681-18687.

Bentmann, E., Haass, C., and Dormann, D. (2013). Stress granules in neurodegeneration--lessons learnt from TAR DNA binding protein of 43 kDa and fused in sarcoma. *FEBS J* 280, 4348-4370.

Bentmann, E., Neumann, M., Tahirovic, S., Rodde, R., Dormann, D., and Haass, C. (2012). Requirements for stress granule recruitment of fused in sarcoma (FUS) and TAR DNA-binding protein of 43 kDa (TDP-43). *J Biol Chem* 287, 23079-23094.

Bertolotti, A., Lutz, Y., Heard, D., Chambon, P., and Tora, L. (1996). hTAF(II)68, a novel RNA/ssDNA-binding protein with homology to the pro-oncoproteins TLS/FUS and EWS is associated with both TFIID and RNA polymerase II. *EMBO J* 15, 5022-5031.

Blanc, R.S., and Richard, S. (2017). Arginine Methylation: The Coming of Age. *Mol Cell* 65, 8-24.

Boeynaems, S., Bogaert, E., Kovacs, D., Konijnenberg, A., Timmerman, E., Volkov, A., Guharoy, M., De Decker, M., Jaspers, T., Ryan, V.H., *et al.* (2017). Phase Separation of C9orf72 Dipeptide Repeats Perturbs Stress Granule Dynamics. *Mol Cell* 65, 1044-1055 e1045.

Boeynaems, S., Bogaert, E., Michiels, E., Gijssels, I., Sieben, A., Jovicic, A., De Baets, G., Scheveneels, W., Steyaert, J., Cuijt, I., *et al.* (2016). Drosophila screen connects nuclear transport genes to DPR pathology in c9ALS/FTD. *Sci Rep* 6, 20877.

Bosco, D.A., Lemay, N., Ko, H.K., Zhou, H., Burke, C., Kwiatkowski, T.J., Jr., Sapp, P., McKenna-Yasek, D., Brown, R.H., Jr., and Hayward, L.J. (2010). Mutant FUS proteins that cause amyotrophic lateral sclerosis incorporate into stress granules. *Hum Mol Genet* 19, 4160-4175.

Bowden, H.A., and Dormann, D. (2016). Altered mRNP granule dynamics in FTLD pathogenesis. *J Neurochem* 138 Suppl 1, 112-133.

Braak, H., and Braak, E. (1995). Staging of Alzheimer's disease-related neurofibrillary changes. *Neurobiol Aging* 16, 271-278; discussion 278-284.

Brangwynne, C.P., Eckmann, C.R., Courson, D.S., Rybarska, A., Hoege, C., Gharakhani, J., Julicher, F., and Hyman, A.A. (2009). Germline P granules are liquid droplets that localize by controlled dissolution/condensation. *Science* 324, 1729-1732.

- Brangwynne, C.P., Mitchison, T.J., and Hyman, A.A. (2011). Active liquid-like behavior of nucleoli determines their size and shape in *Xenopus laevis* oocytes. *Proc Natl Acad Sci U S A* *108*, 4334-4339.
- Brangwynne, Clifford P., Tompa, P., and Pappu, Rohit V. (2015). Polymer physics of intracellular phase transitions. *Nature Physics* *11*, 899-904.
- Brelstaff, J., Lashley, T., Holton, J.L., Lees, A.J., Rossor, M.N., Bandopadhyay, R., and Revesz, T. (2011). Transportin1: a marker of FTL-D-FUS. *Acta Neuropathol* *122*, 591-600.
- Buchan, J.R., Kolaitis, R.M., Taylor, J.P., and Parker, R. (2013). Eukaryotic stress granules are cleared by autophagy and Cdc48/VCP function. *Cell* *153*, 1461-1474.
- Buchan, J.R., Muhlrad, D., and Parker, R. (2008). P bodies promote stress granule assembly in *Saccharomyces cerevisiae*. *J Cell Biol* *183*, 441-455.
- Buchan, J.R., and Parker, R. (2009). Eukaryotic stress granules: the ins and outs of translation. *Mol Cell* *36*, 932-941.
- Burke, K.A., Janke, A.M., Rhine, C.L., and Fawzi, N.L. (2015). Residue-by-Residue View of In Vitro FUS Granules that Bind the C-Terminal Domain of RNA Polymerase II. *Mol Cell* *60*, 231-241.
- Cansizoglu, A.E., Lee, B.J., Zhang, Z.C., Fontoura, B.M., and Chook, Y.M. (2007). Structure-based design of a pathway-specific nuclear import inhibitor. *Nat Struct Mol Biol* *14*, 452-454.
- Chang, B., Chen, Y., Zhao, Y., and Bruick, R.K. (2007). JMJD6 is a histone arginine demethylase. *Science* *318*, 444-447.
- Chang, W.L., and Tarn, W.Y. (2009). A role for transportin in deposition of TTP to cytoplasmic RNA granules and mRNA decay. *Nucleic Acids Res* *37*, 6600-6612.
- Charneau, P., Mirambeau, G., Roux, P., Paulous, S., Buc, H., and Clavel, F. (1994). HIV-1 reverse transcription. A termination step at the center of the genome. *J Mol Biol* *241*, 651-662.
- Chio, A., Restagno, G., Brunetti, M., Ossola, I., Calvo, A., Mora, G., Sabatelli, M., Monsurro, M.R., Battistini, S., Mandrioli, J., *et al.* (2009). Two Italian kindreds with familial amyotrophic lateral sclerosis due to FUS mutation. *Neurobiol Aging* *30*, 1272-1275.
- Chou, C.C., Zhang, Y., Umoh, M.E., Vaughan, S.W., Lorenzini, I., Liu, F., Sayegh, M., Donlin-Asp, P.G., Chen, Y.H., Duong, D.M., *et al.* (2018). TDP-43 pathology disrupts nuclear pore complexes and nucleocytoplasmic transport in ALS/FTD. *Nat Neurosci* *21*, 228-239.
- Colombrita, C., Onesto, E., Megiorni, F., Pizzuti, A., Baralle, F.E., Buratti, E., Silani, V., and Ratti, A. (2012). TDP-43 and FUS RNA-binding proteins bind distinct sets of cytoplasmic messenger RNAs and differently regulate their post-transcriptional fate in motoneuron-like cells. *J Biol Chem* *287*, 15635-15647.
- Colombrita, C., Zennaro, E., Fallini, C., Weber, M., Sommacal, A., Buratti, E., Silani, V., and Ratti, A. (2009). TDP-43 is recruited to stress granules in conditions of oxidative insult. *J Neurochem* *111*, 1051-1061.
- Conicella, A.E., Zerze, G.H., Mittal, J., and Fawzi, N.L. (2016). ALS Mutations Disrupt Phase Separation Mediated by alpha-Helical Structure in the TDP-43 Low-Complexity C-Terminal Domain. *Structure* *24*, 1537-1549.
- Cote, J., Boisvert, F.M., Boulanger, M.C., Bedford, M.T., and Richard, S. (2003). Sam68 RNA binding protein is an in vivo substrate for protein arginine N-methyltransferase 1. *Mol Biol Cell* *14*, 274-287.

- Crozat, A., Aman, P., Mandahl, N., and Ron, D. (1993). Fusion of CHOP to a novel RNA-binding protein in human myxoid liposarcoma. *Nature* *363*, 640-644.
- Cui, W., Yoneda, R., Ueda, N., and Kurokawa, R. (2018). Arginine methylation of translocated in liposarcoma (TLS) inhibits its binding to long noncoding RNA, abrogating TLS-mediated repression of CBP/p300 activity. *J Biol Chem*.
- Cushman, M., Johnson, B.S., King, O.D., Gitler, A.D., and Shorter, J. (2010). Prion-like disorders: blurring the divide between transmissibility and infectivity. *J Cell Sci* *123*, 1191-1201.
- Da Cruz, S., and Cleveland, D.W. (2011). Understanding the role of TDP-43 and FUS/TLS in ALS and beyond. *Curr Opin Neurobiol* *21*, 904-919.
- Davidson, Y.S., Robinson, A.C., Hu, Q., Mishra, M., Baborie, A., Jaros, E., Perry, R.H., Cairns, N.J., Richardson, A., Gerhard, A., *et al.* (2013). Nuclear carrier and RNA-binding proteins in frontotemporal lobar degeneration associated with fused in sarcoma (FUS) pathological changes. *Neuropathol Appl Neurobiol* *39*, 157-165.
- Debler, E.W., Jain, K., Warmack, R.A., Feng, Y., Clarke, S.G., Blobel, G., and Stavropoulos, P. (2016). A glutamate/aspartate switch controls product specificity in a protein arginine methyltransferase. *Proc Natl Acad Sci U S A* *113*, 2068-2073.
- DeJesus-Hernandez, M., Mackenzie, I.R., Boeve, B.F., Boxer, A.L., Baker, M., Rutherford, N.J., Nicholson, A.M., Finch, N.A., Flynn, H., Adamson, J., *et al.* (2011). Expanded GGGGCC hexanucleotide repeat in noncoding region of C9ORF72 causes chromosome 9p-linked FTD and ALS. *Neuron* *72*, 245-256.
- Deng, Q., Holler, C.J., Taylor, G., Hudson, K.F., Watkins, W., Gearing, M., Ito, D., Murray, M.E., Dickson, D.W., Seyfried, N.T., *et al.* (2014). FUS is phosphorylated by DNA-PK and accumulates in the cytoplasm after DNA damage. *J Neurosci* *34*, 7802-7813.
- Desantis, M.E., and Shorter, J. (2012). The elusive middle domain of Hsp104 and ClpB: location and function. *Biochim Biophys Acta* *1823*, 29-39.
- Devoy, A., Kalmar, B., Stewart, M., Park, H., Burke, B., Noy, S.J., Redhead, Y., Humphrey, J., Lo, K., Jaeger, J., *et al.* (2017). Humanized mutant FUS drives progressive motor neuron degeneration without aggregation in 'FUSDelta14' knockin mice. *Brain* *140*, 2797-2805.
- Dewey, C.M., Cenik, B., Sephton, C.F., Dries, D.R., Mayer, P., 3rd, Good, S.K., Johnson, B.A., Herz, J., and Yu, G. (2011). TDP-43 is directed to stress granules by sorbitol, a novel physiological osmotic and oxidative stressor. *Mol Cell Biol* *31*, 1098-1108.
- Dingwall, C., and Laskey, R.A. (1990). Nucleoplasm: the archetypal molecular chaperone. *Semin Cell Biol* *1*, 11-17.
- Dini Modigliani, S., Morlando, M., Errichelli, L., Sabatelli, M., and Bozzoni, I. (2014). An ALS-associated mutation in the FUS 3'-UTR disrupts a microRNA-FUS regulatory circuitry. *Nat Commun* *5*, 4335.
- Dormann, D., and Haass, C. (2011). TDP-43 and FUS: a nuclear affair. *Trends Neurosci* *34*, 339-348.
- Dormann, D., and Haass, C. (2013). Fused in sarcoma (FUS): an oncogene goes awry in neurodegeneration. *Mol Cell Neurosci* *56*, 475-486.
- Dormann, D., Madl, T., Valori, C.F., Bentmann, E., Tahirovic, S., Abou-Ajram, C., Kremmer, E., Ansorge, O., Mackenzie, I.R., Neumann, M., *et al.* (2012). Arginine methylation next to the PY-NLS modulates Transportin binding and nuclear import of FUS. *EMBO J* *31*, 4258-4275.

Dormann, D., Rodde, R., Edbauer, D., Bentmann, E., Fischer, I., Hruscha, A., Than, M.E., Mackenzie, I.R., Capell, A., Schmid, B., *et al.* (2010). ALS-associated fused in sarcoma (FUS) mutations disrupt Transportin-mediated nuclear import. *EMBO J* 29, 2841-2857.

Du, K., Arai, S., Kawamura, T., Matsushita, A., and Kurokawa, R. (2011). TLS and PRMT1 synergistically coactivate transcription at the survivin promoter through TLS arginine methylation. *Biochem Biophys Res Commun* 404, 991-996.

Ederle, H., and Dormann, D. (2017). TDP-43 and FUS en route from the nucleus to the cytoplasm. *FEBS Lett* 591, 1489-1507.

Elbaum-Garfinkle, S., Kim, Y., Szczepaniak, K., Chen, C.C., Eckmann, C.R., Myong, S., and Brangwynne, C.P. (2015). The disordered P granule protein LAF-1 drives phase separation into droplets with tunable viscosity and dynamics. *Proc Natl Acad Sci U S A* 112, 7189-7194.

Erickson, S.L., and Lykke-Andersen, J. (2011). Cytoplasmic mRNP granules at a glance. *J Cell Sci* 124, 293-297.

Feng, Y., Maity, R., Whitelegge, J.P., Hadjikyriacou, A., Li, Z., Zurita-Lopez, C., Al-Hadid, Q., Clark, A.T., Bedford, M.T., Masson, J.Y., *et al.* (2013). Mammalian protein arginine methyltransferase 7 (PRMT7) specifically targets RXR sites in lysine- and arginine-rich regions. *J Biol Chem* 288, 37010-37025.

Freibaum, B.D., Lu, Y., Lopez-Gonzalez, R., Kim, N.C., Almeida, S., Lee, K.H., Badders, N., Valentine, M., Miller, B.L., Wong, P.C., *et al.* (2015). GGGGCC repeat expansion in C9orf72 compromises nucleocytoplasmic transport. *Nature* 525, 129-133.

Frey, S., Richter, R.P., and Gorlich, D. (2006). FG-rich repeats of nuclear pore proteins form a three-dimensional meshwork with hydrogel-like properties. *Science* 314, 815-817.

Fuentealba, R.A., Udan, M., Bell, S., Wegorzewska, I., Shao, J., Diamond, M.I., Weihl, C.C., and Baloh, R.H. (2010). Interaction with polyglutamine aggregates reveals a Q/N-rich domain in TDP-43. *J Biol Chem* 285, 26304-26314.

Fuhrmann, J., Clancy, K.W., and Thompson, P.R. (2015). Chemical biology of protein arginine modifications in epigenetic regulation. *Chem Rev* 115, 5413-5461.

Fujii, R., Okabe, S., Urushido, T., Inoue, K., Yoshimura, A., Tachibana, T., Nishikawa, T., Hicks, G.G., and Takumi, T. (2005). The RNA binding protein TLS is translocated to dendritic spines by mGluR5 activation and regulates spine morphology. *Curr Biol* 15, 587-593.

Fujii, R., and Takumi, T. (2005). TLS facilitates transport of mRNA encoding an actin-stabilizing protein to dendritic spines. *J Cell Sci* 118, 5755-5765.

Fujita, K., Ito, H., Nakano, S., Kinoshita, Y., Wate, R., and Kusaka, H. (2008). Immunohistochemical identification of messenger RNA-related proteins in basophilic inclusions of adult-onset atypical motor neuron disease. *Acta Neuropathol* 116, 439-445.

Ganassi, M., Mateju, D., Bigi, I., Mediani, L., Poser, I., Lee, H.O., Seguin, S.J., Morelli, F.F., Vinet, J., Leo, G., *et al.* (2016). A Surveillance Function of the HSPB8-BAG3-HSP70 Chaperone Complex Ensures Stress Granule Integrity and Dynamism. *Mol Cell* 63, 796-810.

Gasset-Rosa, F., Chillon-Marin, C., Goginashvili, A., Atwal, R.S., Artates, J.W., Tabet, R., Wheeler, V.C., Bang, A.G., Cleveland, D.W., and Lagier-Tourenne, C. (2017). Polyglutamine-Expanded Huntingtin Exacerbates Age-Related Disruption of Nuclear Integrity and Nucleocytoplasmic Transport. *Neuron* 94, 48-57 e44.

Gendron, T.F., Bieniek, K.F., Zhang, Y.J., Jansen-West, K., Ash, P.E., Caulfield, T., Daugherty, L., Dunmore, J.H., Castanedes-Casey, M., Chew, J., *et al.* (2013). Antisense transcripts of the expanded

C9ORF72 hexanucleotide repeat form nuclear RNA foci and undergo repeat-associated non-ATG translation in c9FTD/ALS. *Acta Neuropathol* 126, 829-844.

Gerbino, V., Carri, M.T., Cozzolino, M., and Achsel, T. (2013). Mislocalised FUS mutants stall spliceosomal snRNPs in the cytoplasm. *Neurobiol Dis* 55, 120-128.

Gilks, N., Kedersha, N., Ayodele, M., Shen, L., Stoecklin, G., Dember, L.M., and Anderson, P. (2004). Stress granule assembly is mediated by prion-like aggregation of TIA-1. *Mol Biol Cell* 15, 5383-5398.

Gitler, A.D., and Tsuiji, H. (2016). There has been an awakening: Emerging mechanisms of C9orf72 mutations in FTD/ALS. *Brain Res* 1647, 19-29.

Gobl, C., Resch, M., Strickland, M., Hartmuller, C., Viertler, M., Tjandra, N., and Madl, T. (2016). Increasing the Chemical-Shift Dispersion of Unstructured Proteins with a Covalent Lanthanide Shift Reagent. *Angew Chem Int Ed Engl* 55, 14847-14851.

Goedert, M., and Spillantini, M.G. (2011). Pathogenesis of the tauopathies. *J Mol Neurosci* 45, 425-431.

Gong, C.X., Liu, F., Grundke-Iqbal, I., and Iqbal, K. (2005). Post-translational modifications of tau protein in Alzheimer's disease. *J Neural Transm (Vienna)* 112, 813-838.

Gorlich, D., Pante, N., Kutay, U., Aebi, U., and Bischoff, F.R. (1996). Identification of different roles for RanGDP and RanGTP in nuclear protein import. *EMBO J* 15, 5584-5594.

Gorno-Tempini, M.L., Hillis, A.E., Weintraub, S., Kertesz, A., Mendez, M., Cappa, S.F., Ogar, J.M., Rohrer, J.D., Black, S., Boeve, B.F., *et al.* (2011). Classification of primary progressive aphasia and its variants. *Neurology* 76, 1006-1014.

Gregory, R.I., Yan, K.P., Amuthan, G., Chendrimada, T., Doratotaj, B., Cooch, N., and Shiekhattar, R. (2004). The Microprocessor complex mediates the genesis of microRNAs. *Nature* 432, 235-240.

Grima, J.C., Daigle, J.G., Arbez, N., Cunningham, K.C., Zhang, K., Ochaba, J., Geater, C., Morozko, E., Stocksdales, J., Glatzer, J.C., *et al.* (2017). Mutant Huntingtin Disrupts the Nuclear Pore Complex. *Neuron* 94, 93-107 e106.

Guo, A., Gu, H., Zhou, J., Mulhern, D., Wang, Y., Lee, K.A., Yang, V., Aguiar, M., Kornhauser, J., Jia, X., *et al.* (2014). Immunoaffinity enrichment and mass spectrometry analysis of protein methylation. *Mol Cell Proteomics* 13, 372-387.

Guo, L., Kim, H.J., Wang, H., Monaghan, J., Freyermuth, F., Sung, J.C., O'Donovan, K., Fare, C.M., Diaz, Z., Singh, N., *et al.* (2018). Nuclear-Import Receptors Reverse Aberrant Phase Transitions of RNA-Binding Proteins with Prion-like Domains. *Cell* 173, 677-692.e620.

Haeusler, A.R., Donnelly, C.J., Periz, G., Simko, E.A., Shaw, P.G., Kim, M.S., Maragakis, N.J., Troncoso, J.C., Pandey, A., Sattler, R., *et al.* (2014). C9orf72 nucleotide repeat structures initiate molecular cascades of disease. *Nature* 507, 195-200.

Han, T.W., Kato, M., Xie, S., Wu, L.C., Mirzaei, H., Pei, J., Chen, M., Xie, Y., Allen, J., Xiao, G., *et al.* (2012). Cell-free formation of RNA granules: bound RNAs identify features and components of cellular assemblies. *Cell* 149, 768-779.

Hasegawa, M., Arai, T., Nonaka, T., Kametani, F., Yoshida, M., Hashizume, Y., Beach, T.G., Buratti, E., Baralle, F., Morita, M., *et al.* (2008). Phosphorylated TDP-43 in frontotemporal lobar degeneration and amyotrophic lateral sclerosis. *Ann Neurol* 64, 60-70.

Hernandez-Vega, A., Braun, M., Scharrel, L., Jahnel, M., Wegmann, S., Hyman, B.T., Alberti, S., Diez, S., and Hyman, A.A. (2017). Local Nucleation of Microtubule Bundles through Tubulin Concentration into a Condensed Tau Phase. *Cell Rep* 20, 2304-2312.

Hicks, G.G., Singh, N., Nashabi, A., Mai, S., Bozek, G., Klewes, L., Arapovic, D., White, E.K., Koury, M.J., Oltz, E.M., *et al.* (2000). Fus deficiency in mice results in defective B-lymphocyte development and activation, high levels of chromosomal instability and perinatal death. *Nat Genet* 24, 175-179.

Hock, E.M., and Polymenidou, M. (2016). Prion-like propagation as a pathogenic principle in frontotemporal dementia. *J Neurochem* 138 Suppl 1, 163-183.

Hoell, J.I., Larsson, E., Runge, S., Nusbaum, J.D., Duggimpudi, S., Farazi, T.A., Hafner, M., Borkhardt, A., Sander, C., and Tuschl, T. (2011). RNA targets of wild-type and mutant FET family proteins. *Nat Struct Mol Biol* 18, 1428-1431.

Hofmann, S., Cherkasova, V., Bankhead, P., Bukau, B., and Stoecklin, G. (2012). Translation suppression promotes stress granule formation and cell survival in response to cold shock. *Mol Biol Cell* 23, 3786-3800.

Hofweber, M., Hutten, S., Bourgeois, B., Spreitzer, E., Niedner-Boblentz, A., Schifferer, M., Ruepp, M.-D., Simons, M., Niessing, D., Madl, T., *et al.* (2018). Phase Separation of FUS Is Suppressed by Its Nuclear Import Receptor and Arginine Methylation. *Cell* 173, 706-719.e713.

Hubstenberger, A., Noble, S.L., Cameron, C., and Evans, T.C. (2013). Translation repressors, an RNA helicase, and developmental cues control RNP phase transitions during early development. *Dev Cell* 27, 161-173.

Hung, C.J., Lee, Y.J., Chen, D.H., and Li, C. (2009). Proteomic analysis of methylarginine-containing proteins in HeLa cells by two-dimensional gel electrophoresis and immunoblotting with a methylarginine-specific antibody. *Protein J* 28, 139-147.

Hung, M.L., Hautbergue, G.M., Snijders, A.P., Dickman, M.J., and Wilson, S.A. (2010). Arginine methylation of REF/ALY promotes efficient handover of mRNA to TAP/NXF1. *Nucleic Acids Res* 38, 3351-3361.

Igaz, L.M., Kwong, L.K., Xu, Y., Truax, A.C., Uryu, K., Neumann, M., Clark, C.M., Elman, L.B., Miller, B.L., Grossman, M., *et al.* (2008). Enrichment of C-terminal fragments in TAR DNA-binding protein-43 cytoplasmic inclusions in brain but not in spinal cord of frontotemporal lobar degeneration and amyotrophic lateral sclerosis. *Am J Pathol* 173, 182-194.

Jackrel, M.E., DeSantis, M.E., Martinez, B.A., Castellano, L.M., Stewart, R.M., Caldwell, K.A., Caldwell, G.A., and Shorter, J. (2014). Potentiated Hsp104 variants antagonize diverse proteotoxic misfolding events. *Cell* 156, 170-182.

Jackrel, M.E., and Shorter, J. (2015). Engineering enhanced protein disaggregases for neurodegenerative disease. *Prion* 9, 90-109.

Jackrel, M.E., and Shorter, J. (2017). Protein-Remodeling Factors As Potential Therapeutics for Neurodegenerative Disease. *Front Neurosci* 11, 99.

Jain, A., and Vale, R.D. (2017). RNA phase transitions in repeat expansion disorders. *Nature* 546, 243-247.

Jain, K., Warmack, R.A., Debler, E.W., Hadjikyriacou, A., Stavropoulos, P., and Clarke, S.G. (2016a). Protein Arginine Methyltransferase Product Specificity Is Mediated by Distinct Active-site Architectures. *J Biol Chem* 291, 18299-18308.

- Jain, S., Wheeler, J.R., Walters, R.W., Agrawal, A., Barsic, A., and Parker, R. (2016b). ATPase-Modulated Stress Granules Contain a Diverse Proteome and Substructure. *Cell* *164*, 487-498.
- Jakel, S., Mingot, J.M., Schwarzmaier, P., Hartmann, E., and Gorlich, D. (2002). Importins fulfil a dual function as nuclear import receptors and cytoplasmic chaperones for exposed basic domains. *EMBO J* *21*, 377-386.
- Jamison, J.T., Kayali, F., Rudolph, J., Marshall, M., Kimball, S.R., and DeGracia, D.J. (2008). Persistent redistribution of poly-adenylated mRNAs correlates with translation arrest and cell death following global brain ischemia and reperfusion. *Neuroscience* *154*, 504-520.
- Jobert, L., Argentini, M., and Tora, L. (2009). PRMT1 mediated methylation of TAF15 is required for its positive gene regulatory function. *Exp Cell Res* *315*, 1273-1286.
- Johnson, J.O., Mandrioli, J., Benatar, M., Abramzon, Y., Van Deerlin, V.M., Trojanowski, J.Q., Gibbs, J.R., Brunetti, M., Gronka, S., Wu, J., *et al.* (2010). Exome sequencing reveals VCP mutations as a cause of familial ALS. *Neuron* *68*, 857-864.
- Jovicic, A., Mertens, J., Boeynaems, S., Bogaert, E., Chai, N., Yamada, S.B., Paul, J.W., 3rd, Sun, S., Herdy, J.R., Bieri, G., *et al.* (2015). Modifiers of C9orf72 dipeptide repeat toxicity connect nucleocytoplasmic transport defects to FTD/ALS. *Nat Neurosci* *18*, 1226-1229.
- Jovicic, A., Paul, J.W., 3rd, and Gitler, A.D. (2016). Nuclear transport dysfunction: a common theme in amyotrophic lateral sclerosis and frontotemporal dementia. *J Neurochem* *138 Suppl 1*, 134-144.
- Ju, J.S., Fuentealba, R.A., Miller, S.E., Jackson, E., Piwnica-Worms, D., Baloh, R.H., and Weihl, C.C. (2009). Valosin-containing protein (VCP) is required for autophagy and is disrupted in VCP disease. *J Cell Biol* *187*, 875-888.
- Ju, J.S., Miller, S.E., Hanson, P.I., and Weihl, C.C. (2008). Impaired protein aggregate handling and clearance underlie the pathogenesis of p97/VCP-associated disease. *J Biol Chem* *283*, 30289-30299.
- Kato, M., Han, T.W., Xie, S., Shi, K., Du, X., Wu, L.C., Mirzaei, H., Goldsmith, E.J., Longgood, J., Pei, J., *et al.* (2012). Cell-free formation of RNA granules: low complexity sequence domains form dynamic fibers within hydrogels. *Cell* *149*, 753-767.
- Kato, M., and McKnight, S.L. (2017). A Solid-State Conceptualization of Information Transfer from Gene to Message to Protein. *Annu Rev Biochem*.
- Kawaguchi, Y., Kovacs, J.J., McLaurin, A., Vance, J.M., Ito, A., and Yao, T.P. (2003). The deacetylase HDAC6 regulates aggresome formation and cell viability in response to misfolded protein stress. *Cell* *115*, 727-738.
- Kayali, F., Montie, H.L., Rafols, J.A., and DeGracia, D.J. (2005). Prolonged translation arrest in reperfused hippocampal cornu Ammonis 1 is mediated by stress granules. *Neuroscience* *134*, 1223-1245.
- Kedersha, N., Stoecklin, G., Ayodele, M., Yacono, P., Lykke-Andersen, J., Fritzler, M.J., Scheuner, D., Kaufman, R.J., Golan, D.E., and Anderson, P. (2005). Stress granules and processing bodies are dynamically linked sites of mRNP remodeling. *J Cell Biol* *169*, 871-884.
- Kiernan, M.C., Vucic, S., Cheah, B.C., Turner, M.R., Eisen, A., Hardiman, O., Burrell, J.R., and Zoing, M.C. (2011). Amyotrophic lateral sclerosis. *The Lancet* *377*, 942-955.
- Kim, H.J., Kim, N.C., Wang, Y.D., Scarborough, E.A., Moore, J., Diaz, Z., MacLea, K.S., Freibaum, B., Li, S., Molliex, A., *et al.* (2013). Mutations in prion-like domains in hnRNPA2B1 and hnRNPA1 cause multisystem proteinopathy and ALS. *Nature* *495*, 467-473.

- King, O.D., Gitler, A.D., and Shorter, J. (2012). The tip of the iceberg: RNA-binding proteins with prion-like domains in neurodegenerative disease. *Brain Res* 1462, 61-80.
- Kinoshita, Y., Ito, H., Hirano, A., Fujita, K., Wate, R., Nakamura, M., Kaneko, S., Nakano, S., and Kusaka, H. (2009). Nuclear contour irregularity and abnormal transporter protein distribution in anterior horn cells in amyotrophic lateral sclerosis. *J Neuropathol Exp Neurol* 68, 1184-1192.
- Kopke, E., Tung, Y.C., Shaikh, S., Alonso, A.C., Iqbal, K., and Grundke-Iqbal, I. (1993). Microtubule-associated protein tau. Abnormal phosphorylation of a non-paired helical filament pool in Alzheimer disease. *J Biol Chem* 268, 24374-24384.
- Korolchuk, V.I., Menzies, F.M., and Rubinsztein, D.C. (2010). Mechanisms of cross-talk between the ubiquitin-proteasome and autophagy-lysosome systems. *FEBS Lett* 584, 1393-1398.
- Kosugi, S., Hasebe, M., Entani, T., Takayama, S., Tomita, M., and Yanagawa, H. (2008). Design of peptide inhibitors for the importin alpha/beta nuclear import pathway by activity-based profiling. *Chem Biol* 15, 940-949.
- Kroschwald, S., Maharana, S., Mateju, D., Malinowska, L., Nuske, E., Poser, I., Richter, D., and Alberti, S. (2015). Promiscuous interactions and protein disaggregases determine the material state of stress-inducible RNP granules. *Elife* 4, e06807.
- Kuroda, M., Sok, J., Webb, L., Baechtold, H., Urano, F., Yin, Y., Chung, P., de Rooij, D.G., Akhmedov, A., Ashley, T., *et al.* (2000). Male sterility and enhanced radiation sensitivity in TLS(-/-) mice. *EMBO J* 19, 453-462.
- Kwiatkowski, T.J., Jr., Bosco, D.A., Leclerc, A.L., Tamrazian, E., Vanderburg, C.R., Russ, C., Davis, A., Gilchrist, J., Kasarskis, E.J., Munsat, T., *et al.* (2009). Mutations in the FUS/TLS gene on chromosome 16 cause familial amyotrophic lateral sclerosis. *Science* 323, 1205-1208.
- Kwon, I., Xiang, S., Kato, M., Wu, L., Theodoropoulos, P., Wang, T., Kim, J., Yun, J., Xie, Y., and McKnight, S.L. (2014). Poly-dipeptides encoded by the C9orf72 repeats bind nucleoli, impede RNA biogenesis, and kill cells. *Science* 345, 1139-1145.
- Kwon, S., Zhang, Y., and Matthias, P. (2007). The deacetylase HDAC6 is a novel critical component of stress granules involved in the stress response. *Genes Dev* 21, 3381-3394.
- Lagier-Tourenne, C., Polymenidou, M., and Cleveland, D.W. (2010). TDP-43 and FUS/TLS: emerging roles in RNA processing and neurodegeneration. *Hum Mol Genet* 19, R46-64.
- Lagier-Tourenne, C., Polymenidou, M., Hutt, K.R., Vu, A.Q., Baughn, M., Huelga, S.C., Clutario, K.M., Ling, S.C., Liang, T.Y., Mazur, C., *et al.* (2012). Divergent roles of ALS-linked proteins FUS/TLS and TDP-43 intersect in processing long pre-mRNAs. *Nat Neurosci* 15, 1488-1497.
- Larsen, S.C., Sylvestersen, K.B., Mund, A., Lyon, D., Mullari, M., Madsen, M.V., Daniel, J.A., Jensen, L.J., and Nielsen, M.L. (2016). Proteome-wide analysis of arginine monomethylation reveals widespread occurrence in human cells. *Sci Signal* 9, rs9.
- Lee, B.J., Cansizoglu, A.E., Suel, K.E., Louis, T.H., Zhang, Z., and Chook, Y.M. (2006). Rules for nuclear localization sequence recognition by karyopherin beta 2. *Cell* 126, 543-558.
- Lee, K.H., Zhang, P., Kim, H.J., Mitrea, D.M., Sarkar, M., Freibaum, B.D., Cika, J., Coughlin, M., Messing, J., Molliex, A., *et al.* (2016). C9orf72 Dipeptide Repeats Impair the Assembly, Dynamics, and Function of Membrane-Less Organelles. *Cell* 167, 774-788 e717.
- Lee, Y.B., Chen, H.J., Peres, J.N., Gomez-Deza, J., Attig, J., Stalekar, M., Troakes, C., Nishimura, A.L., Scotter, E.L., Vance, C., *et al.* (2013). Hexanucleotide repeats in ALS/FTD form length-dependent RNA foci, sequester RNA binding proteins, and are neurotoxic. *Cell Rep* 5, 1178-1186.

- Li, H.Y., Yeh, P.A., Chiu, H.C., Tang, C.Y., and Tu, B.P. (2011). Hyperphosphorylation as a defense mechanism to reduce TDP-43 aggregation. *PLoS One* 6, e23075.
- Li, P., Banjade, S., Cheng, H.C., Kim, S., Chen, B., Guo, L., Llaguno, M., Hollingsworth, J.V., King, D.S., Banani, S.F., *et al.* (2012). Phase transitions in the assembly of multivalent signalling proteins. *Nature* 483, 336-340.
- Li, Y.R., King, O.D., Shorter, J., and Gitler, A.D. (2013). Stress granules as crucibles of ALS pathogenesis. *J Cell Biol* 201, 361-372.
- Lin, Y., Mori, E., Kato, M., Xiang, S., Wu, L., Kwon, I., and McKnight, S.L. (2016). Toxic PR Poly-Dipeptides Encoded by the C9orf72 Repeat Expansion Target LC Domain Polymers. *Cell* 167, 789-802 e712.
- Ling, S.C., Polymenidou, M., and Cleveland, D.W. (2013). Converging mechanisms in ALS and FTD: disrupted RNA and protein homeostasis. *Neuron* 79, 416-438.
- Liu-Yesucevitz, L., Bilgutay, A., Zhang, Y.J., Vanderweyde, T., Citro, A., Mehta, T., Zaarur, N., McKee, A., Bowser, R., Sherman, M., *et al.* (2010). Tar DNA binding protein-43 (TDP-43) associates with stress granules: analysis of cultured cells and pathological brain tissue. *PLoS One* 5, e13250.
- Liu, Q., and Dreyfuss, G. (1995). In vivo and in vitro arginine methylation of RNA-binding proteins. *Mol Cell Biol* 15, 2800-2808.
- Livernois, A.M., Hnatchuk, D.J., Findlater, E.E., and Graether, S.P. (2009). Obtaining highly purified intrinsically disordered protein by boiling lysis and single step ion exchange. *Anal Biochem* 392, 70-76.
- Lomen-Hoerth, C., Anderson, T., and Miller, B. (2002). The overlap of amyotrophic lateral sclerosis and frontotemporal dementia. *Neurology* 59, 1077-1079.
- Love, D.C., Sweitzer, T.D., and Hanover, J.A. (1998). Reconstitution of HIV-1 rev nuclear export: independent requirements for nuclear import and export. *Proc Natl Acad Sci U S A* 95, 10608-10613.
- Lu, L., Wang, S., Zheng, L., Li, X., Suswam, E.A., Zhang, X., Wheeler, C.G., Nabors, L.B., Filippova, N., and King, P.H. (2009). Amyotrophic lateral sclerosis-linked mutant SOD1 sequesters Hu antigen R (HuR) and TIA-1-related protein (TIAR): implications for impaired post-transcriptional regulation of vascular endothelial growth factor. *J Biol Chem* 284, 33989-33998.
- Mackenzie, I.R., Arzberger, T., Kremmer, E., Troost, D., Lorenzl, S., Mori, K., Weng, S.M., Haass, C., Kretzschmar, H.A., Edbauer, D., *et al.* (2013). Dipeptide repeat protein pathology in C9ORF72 mutation cases: clinico-pathological correlations. *Acta Neuropathol* 126, 859-879.
- Mackenzie, I.R., and Neumann, M. (2016). Molecular neuropathology of frontotemporal dementia: insights into disease mechanisms from postmortem studies. *J Neurochem* 138 Suppl 1, 54-70.
- Mackenzie, I.R., Nicholson, A.M., Sarkar, M., Messing, J., Purice, M.D., Pottier, C., Annu, K., Baker, M., Perkerson, R.B., Kurti, A., *et al.* (2017). TIA1 Mutations in Amyotrophic Lateral Sclerosis and Frontotemporal Dementia Promote Phase Separation and Alter Stress Granule Dynamics. *Neuron* 95, 808-816 e809.
- Mackenzie, I.R.A., Rademakers, R., and Neumann, M. (2010). TDP-43 and FUS in amyotrophic lateral sclerosis and frontotemporal dementia. *The Lancet Neurology* 9, 995-1007.
- Maharana, S., Wang, J., Papadopoulos, D.K., Richter, D., Pozniakovskiy, A., Poser, I., Bickle, M., Rizk, S., Guillen-Boixet, J., Franzmann, T.M., *et al.* (2018). RNA buffers the phase separation behavior of prion-like RNA binding proteins. *Science* 360, 918-921.
- Mahboubi, H., Seganathy, E., Kong, D., and Stochaj, U. (2013). Identification of Novel Stress Granule Components That Are Involved in Nuclear Transport. *PLoS One* 8, e68356.

- Malinowska, L., Kroschwald, S., and Alberti, S. (2013). Protein disorder, prion propensities, and self-organizing macromolecular collectives. *Biochim Biophys Acta* 1834, 918-931.
- March, Z.M., King, O.D., and Shorter, J. (2016). Prion-like domains as epigenetic regulators, scaffolds for subcellular organization, and drivers of neurodegenerative disease. *Brain Res* 1647, 9-18.
- Martinez, F.J., Pratt, G.A., Van Nostrand, E.L., Batra, R., Huelga, S.C., Kapeli, K., Freese, P., Chun, S.J., Ling, K., Gelboin-Burkhart, C., *et al.* (2016). Protein-RNA Networks Regulated by Normal and ALS-Associated Mutant HNRNPA2B1 in the Nervous System. *Neuron* 92, 780-795.
- Mastrocola, A.S., Kim, S.H., Trinh, A.T., Rodenkirch, L.A., and Tibbetts, R.S. (2013). The RNA-binding protein fused in sarcoma (FUS) functions downstream of poly(ADP-ribose) polymerase (PARP) in response to DNA damage. *J Biol Chem* 288, 24731-24741.
- Mateju, D., Franzmann, T.M., Patel, A., Kopach, A., Boczek, E.E., Maharana, S., Lee, H.O., Carra, S., Hyman, A.A., and Alberti, S. (2017). An aberrant phase transition of stress granules triggered by misfolded protein and prevented by chaperone function. *EMBO J* 36, 1669-1687.
- Matus, S., Bosco, D.A., and Hetz, C. (2014). Autophagy meets fused in sarcoma-positive stress granules. *Neurobiol Aging* 35, 2832-2835.
- Maziuk, B., Ballance, H.I., and Wolozin, B. (2017). Dysregulation of RNA Binding Protein Aggregation in Neurodegenerative Disorders. *Front Mol Neurosci* 10, 89.
- McGurk, L., Lee, V.M., Trojanowski, J.Q., Van Deerlin, V.M., Lee, E.B., and Bonini, N.M. (2014). Poly-A binding protein-1 localization to a subset of TDP-43 inclusions in amyotrophic lateral sclerosis occurs more frequently in patients harboring an expansion in C9orf72. *J Neuropathol Exp Neurol* 73, 837-845.
- Mertens, J., Paquola, A.C.M., Ku, M., Hatch, E., Bohnke, L., Ladjevardi, S., McGrath, S., Campbell, B., Lee, H., Herdy, J.R., *et al.* (2015). Directly Reprogrammed Human Neurons Retain Aging-Associated Transcriptomic Signatures and Reveal Age-Related Nucleocytoplasmic Defects. *Cell Stem Cell* 17, 705-718.
- Milles, S., Huy Bui, K., Koehler, C., Eltsov, M., Beck, M., and Lemke, E.A. (2013). Facilitated aggregation of FG nucleoporins under molecular crowding conditions. *EMBO Rep* 14, 178-183.
- Milles, S., Mercadante, D., Aramburu, I.V., Jensen, M.R., Banterle, N., Koehler, C., Tyagi, S., Clarke, J., Shammas, S.L., Blackledge, M., *et al.* (2015). Plasticity of an ultrafast interaction between nucleoporins and nuclear transport receptors. *Cell* 163, 734-745.
- Molliex, A., Temirov, J., Lee, J., Coughlin, M., Kanagaraj, A.P., Kim, H.J., Mittag, T., and Taylor, J.P. (2015). Phase separation by low complexity domains promotes stress granule assembly and drives pathological fibrillization. *Cell* 163, 123-133.
- Monahan, Z., Ryan, V.H., Janke, A.M., Burke, K.A., Rhoads, S.N., Zerze, G.H., O'Meally, R., Dignon, G.L., Conicella, A.E., Zheng, W., *et al.* (2017). Phosphorylation of the FUS low-complexity domain disrupts phase separation, aggregation, and toxicity. *EMBO J* 36, 2951-2967.
- Moreno, J.A., Radford, H., Peretti, D., Steinert, J.R., Verity, N., Martin, M.G., Halliday, M., Morgan, J., Dinsdale, D., Ortore, C.A., *et al.* (2012). Sustained translational repression by eIF2alpha-P mediates prion neurodegeneration. *Nature* 485, 507-511.
- Mori, K., Arzberger, T., Grasser, F.A., Gijssels, I., May, S., Rentzsch, K., Weng, S.M., Schludi, M.H., van der Zee, J., Cruts, M., *et al.* (2013a). Bidirectional transcripts of the expanded C9orf72 hexanucleotide repeat are translated into aggregating dipeptide repeat proteins. *Acta Neuropathol* 126, 881-893.
- Mori, K., Lammich, S., Mackenzie, I.R., Forne, I., Zilow, S., Kretzschmar, H., Edbauer, D., Janssens, J., Kleinberger, G., Cruts, M., *et al.* (2013b). hnRNP A3 binds to GGGGCC repeats and is a constituent of

p62-positive/TDP43-negative inclusions in the hippocampus of patients with C9orf72 mutations. *Acta Neuropathol* 125, 413-423.

Morlando, M., Dini Modigliani, S., Torrelli, G., Rosa, A., Di Carlo, V., Caffarelli, E., and Bozzoni, I. (2012). FUS stimulates microRNA biogenesis by facilitating co-transcriptional Drosha recruitment. *EMBO J* 31, 4502-4510.

Munoz, D.G., Neumann, M., Kusaka, H., Yokota, O., Ishihara, K., Terada, S., Kuroda, S., and Mackenzie, I.R. (2009). FUS pathology in basophilic inclusion body disease. *Acta Neuropathol* 118, 617-627.

Murakami, T., Qamar, S., Lin, J.Q., Schierle, G.S., Rees, E., Miyashita, A., Costa, A.R., Dodd, R.B., Chan, F.T., Michel, C.H., *et al.* (2015). ALS/FTD Mutation-Induced Phase Transition of FUS Liquid Droplets and Reversible Hydrogels into Irreversible Hydrogels Impairs RNP Granule Function. *Neuron* 88, 678-690.

Murphy, J.M., Henry, R.G., Langmore, S., Kramer, J.H., Miller, B.L., and Lomen-Hoerth, C. (2007). Continuum of frontal lobe impairment in amyotrophic lateral sclerosis. *Arch Neurol* 64, 530-534.

Neumann, M., Bentmann, E., Dormann, D., Jawaid, A., DeJesus-Hernandez, M., Ansorge, O., Roeber, S., Kretzschmar, H.A., Munoz, D.G., Kusaka, H., *et al.* (2011). FET proteins TAF15 and EWS are selective markers that distinguish FTLD with FUS pathology from amyotrophic lateral sclerosis with FUS mutations. *Brain* 134, 2595-2609.

Neumann, M., Mackenzie, I.R., Cairns, N.J., Boyer, P.J., Markesbery, W.R., Smith, C.D., Taylor, J.P., Kretzschmar, H.A., Kimonis, V.E., and Forman, M.S. (2007). TDP-43 in the ubiquitin pathology of frontotemporal dementia with VCP gene mutations. *J Neuropathol Exp Neurol* 66, 152-157.

Neumann, M., Rademakers, R., Roeber, S., Baker, M., Kretzschmar, H.A., and Mackenzie, I.R. (2009). A new subtype of frontotemporal lobar degeneration with FUS pathology. *Brain* 132, 2922-2931.

Neumann, M., Sampathu, D.M., Kwong, L.K., Truax, A.C., Micsenyi, M.C., Chou, T.T., Bruce, J., Schuck, T., Grossman, M., Clark, C.M., *et al.* (2006). Ubiquitinated TDP-43 in frontotemporal lobar degeneration and amyotrophic lateral sclerosis. *Science* 314, 130-133.

Neumann, M., Valori, C.F., Ansorge, O., Kretzschmar, H.A., Munoz, D.G., Kusaka, H., Yokota, O., Ishihara, K., Ang, L.C., Bilbao, J.M., *et al.* (2012). Transportin 1 accumulates specifically with FET proteins but no other transportin cargos in FTLD-FUS and is absent in FUS inclusions in ALS with FUS mutations. *Acta Neuropathol* 124, 705-716.

Nichols, R.C., Wang, X.W., Tang, J., Hamilton, B.J., High, F.A., Herschman, H.R., and Rigby, W.F. (2000). The RGG domain in hnRNP A2 affects subcellular localization. *Exp Cell Res* 256, 522-532.

Niedner, A., Muller, M., Moorthy, B.T., Jansen, R.P., and Niessing, D. (2013). Role of Loc1p in assembly and reorganization of nuclear ASH1 messenger ribonucleoprotein particles in yeast. *Proc Natl Acad Sci U S A* 110, E5049-5058.

Nishimoto, Y., Nakagawa, S., Hirose, T., Okano, H.J., Takao, M., Shibata, S., Suyama, S., Kuwako, K., Imai, T., Murayama, S., *et al.* (2013). The long non-coding RNA nuclear-enriched abundant transcript 1_2 induces paraspeckle formation in the motor neuron during the early phase of amyotrophic lateral sclerosis. *Mol Brain* 6, 31.

Nishimura, A.L., Zupunski, V., Troakes, C., Kathe, C., Fratta, P., Howell, M., Gallo, J.M., Hortobagyi, T., Shaw, C.E., and Rogelj, B. (2010). Nuclear import impairment causes cytoplasmic trans-activation response DNA-binding protein accumulation and is associated with frontotemporal lobar degeneration. *Brain* 133, 1763-1771.

- Niu, C., Zhang, J., Gao, F., Yang, L., Jia, M., Zhu, H., and Gong, W. (2012). FUS-NLS/Transportin 1 complex structure provides insights into the nuclear targeting mechanism of FUS and the implications in ALS. *PLoS One* 7, e47056.
- Noegel, A.A., Blau-Wasser, R., Sultana, H., Muller, R., Israel, L., Schleicher, M., Patel, H., and Weijer, C.J. (2004). The cyclase-associated protein CAP as regulator of cell polarity and cAMP signaling in *Dictyostelium*. *Mol Biol Cell* 15, 934-945.
- Nomura, T., Watanabe, S., Kaneko, K., Yamanaka, K., Nukina, N., and Furukawa, Y. (2014). Intranuclear aggregation of mutant FUS/TLS as a molecular pathomechanism of amyotrophic lateral sclerosis. *J Biol Chem* 289, 1192-1202.
- Nott, T.J., Craggs, T.D., and Baldwin, A.J. (2016). Membraneless organelles can melt nucleic acid duplexes and act as biomolecular filters. *Nat Chem* 8, 569-575.
- Nott, T.J., Petsalaki, E., Farber, P., Jervis, D., Fussner, E., Plochowietz, A., Craggs, T.D., Bazett-Jones, D.P., Pawson, T., Forman-Kay, J.D., *et al.* (2015). Phase transition of a disordered nuage protein generates environmentally responsive membraneless organelles. *Mol Cell* 57, 936-947.
- Ong, S.E., Mittler, G., and Mann, M. (2004). Identifying and quantifying in vivo methylation sites by heavy methyl SILAC. *Nat Methods* 1, 119-126.
- Orozco, D., and Edbauer, D. (2013). FUS-mediated alternative splicing in the nervous system: consequences for ALS and FTL. *J Mol Med (Berl)* 91, 1343-1354.
- Orozco, D., Tahirovic, S., Rentzsch, K., Schwenk, B.M., Haass, C., and Edbauer, D. (2012). Loss of fused in sarcoma (FUS) promotes pathological Tau splicing. *EMBO Rep* 13, 759-764.
- Ozdilek, B.A., Thompson, V.F., Ahmed, N.S., White, C.I., Batey, R.T., and Schwartz, J.C. (2017). Intrinsically disordered RGG/RG domains mediate degenerate specificity in RNA binding. *Nucleic Acids Res* 45, 7984-7996.
- Pahlich, S., Bschor, K., Chiavi, C., Belyanskaya, L., and Gehring, H. (2005). Different methylation characteristics of protein arginine methyltransferase 1 and 3 toward the Ewing Sarcoma protein and a peptide. *Proteins* 61, 164-175.
- Pahlich, S., Zakaryan, R.P., and Gehring, H. (2006). Protein arginine methylation: Cellular functions and methods of analysis. *Biochim Biophys Acta* 1764, 1890-1903.
- Pankiv, S., Clausen, T.H., Lamark, T., Brech, A., Bruun, J.A., Outzen, H., Overvatn, A., Bjorkoy, G., and Johansen, T. (2007). p62/SQSTM1 binds directly to Atg8/LC3 to facilitate degradation of ubiquitinated protein aggregates by autophagy. *J Biol Chem* 282, 24131-24145.
- Patel, A., Lee, H.O., Jawerth, L., Maharana, S., Jahnel, M., Hein, M.Y., Stoyanov, S., Mahamid, J., Saha, S., Franzmann, T.M., *et al.* (2015). A Liquid-to-Solid Phase Transition of the ALS Protein FUS Accelerated by Disease Mutation. *Cell* 162, 1066-1077.
- Patel, A., Malinowska, L., Saha, S., Wang, J., Alberti, S., Krishnan, Y., and Hyman, A.A. (2017). ATP as a biological hydrotrope. *Science* 356, 753-756.
- Polymenidou, M., and Cleveland, D.W. (2011). The seeds of neurodegeneration: prion-like spreading in ALS. *Cell* 147, 498-508.
- Qamar, S., Wang, G., Randle, S.J., Ruggeri, F.S., Varela, J.A., Lin, J.Q., Phillips, E.C., Miyashita, A., Williams, D., Ströhl, F., *et al.* (2018). FUS Phase Separation Is Modulated by a Molecular Chaperone and Methylation of Arginine Cation- π Interactions. *Cell* 173, 720-734.e715.

- Rabbitts, T.H., Forster, A., Larson, R., and Nathan, P. (1993). Fusion of the dominant negative transcription regulator CHOP with a novel gene FUS by translocation t(12;16) in malignant liposarcoma. *Nat Genet* 4, 175-180.
- Rademakers, R., Neumann, M., and Mackenzie, I.R. (2012). Advances in understanding the molecular basis of frontotemporal dementia. *Nat Rev Neurol* 8, 423-434.
- Raman, B., Guarnaccia, C., Nadassy, K., Zakhariyev, S., Pintar, A., Zanuttin, F., Frigyes, D., Acatrinei, C., Vindigini, A., Pongor, G., *et al.* (2001). N(omega)-arginine dimethylation modulates the interaction between a Gly/Arg-rich peptide from human nucleolin and nucleic acids. *Nucleic Acids Res* 29, 3377-3384.
- Ramaswami, M., Taylor, J.P., and Parker, R. (2013). Altered ribostasis: RNA-protein granules in degenerative disorders. *Cell* 154, 727-736.
- Rappsilber, J., Friesen, W.J., Paushkin, S., Dreyfuss, G., and Mann, M. (2003). Detection of Arginine Dimethylated Peptides by Parallel Precursor Ion Scanning Mass Spectrometry in Positive Ion Mode. *Analytical Chemistry* 75, 3107-3114.
- Rascovsky, K., Hodges, J.R., Knopman, D., Mendez, M.F., Kramer, J.H., Neuhaus, J., van Swieten, J.C., Seelaar, H., Dopper, E.G., Onyike, C.U., *et al.* (2011). Sensitivity of revised diagnostic criteria for the behavioural variant of frontotemporal dementia. *Brain* 134, 2456-2477.
- Ratti, A., and Buratti, E. (2016). Physiological functions and pathobiology of TDP-43 and FUS/TLS proteins. *J Neurochem* 138 Suppl 1, 95-111.
- Ravenscroft, T.A., Baker, M.C., Rutherford, N.J., Neumann, M., Mackenzie, I.R., Josephs, K.A., Boeve, B.F., Petersen, R., Halliday, G.M., Kril, J., *et al.* (2013). Mutations in protein N-arginine methyltransferases are not the cause of FTL-D-FUS. *Neurobiol Aging* 34, 2235 e2211-2233.
- Renton, A.E., Majounie, E., Waite, A., Simon-Sanchez, J., Rollinson, S., Gibbs, J.R., Schymick, J.C., Laaksovirta, H., van Swieten, J.C., Myllykangas, L., *et al.* (2011). A hexanucleotide repeat expansion in C9ORF72 is the cause of chromosome 9p21-linked ALS-FTD. *Neuron* 72, 257-268.
- Rexach, M., and Blobel, G. (1995). Protein import into nuclei: association and dissociation reactions involving transport substrate, transport factors, and nucleoporins. *Cell* 83, 638-692.
- Rho, J., Choi, S., Jung, C.R., and Im, D.S. (2007). Arginine methylation of Sam68 and SLM proteins negatively regulates their poly(U) RNA binding activity. *Arch Biochem Biophys* 466, 49-57.
- Rhoads, S.N., Monahan, Z.T., Yee, D.S., Leung, A.Y., Newcombe, C.G., O'Meally, R.N., Cole, R.N., and Shewmaker, F.P. (2018). The prion-like domain of FUS is multiphosphorylated following DNA damage without altering nuclear localization. *Mol Biol Cell*, mbcE17120735.
- Rogelj, B., Easton, L.E., Bogu, G.K., Stanton, L.W., Rot, G., Curk, T., Zupan, B., Sugimoto, Y., Modic, M., Haberman, N., *et al.* (2012). Widespread binding of FUS along nascent RNA regulates alternative splicing in the brain. *Sci Rep* 2, 603.
- Rohrer, J.D., Guerreiro, R., Vandrovicova, J., Uphill, J., Reiman, D., Beck, J., Isaacs, A.M., Authier, A., Ferrari, R., Fox, N.C., *et al.* (2009). The heritability and genetics of frontotemporal lobar degeneration. *Neurology* 73, 1451-1456.
- Rothstein, J.D. (2009). Current hypotheses for the underlying biology of amyotrophic lateral sclerosis. *Ann Neurol* 65 Suppl 1, S3-9.
- Rulten, S.L., Rotheray, A., Green, R.L., Grundy, G.J., Moore, D.A., Gomez-Herreros, F., Hafezparast, M., and Caldecott, K.W. (2014). PARP-1 dependent recruitment of the amyotrophic lateral sclerosis-associated protein FUS/TLS to sites of oxidative DNA damage. *Nucleic Acids Res* 42, 307-314.

Ryan, V.H., Dignon, G.L., Zerze, G.H., Chabata, C.V., Silva, R., Conicella, A.E., Amaya, J., Burke, K.A., Mittal, J., and Fawzi, N.L. (2018). Mechanistic View of hnRNPA2 Low-Complexity Domain Structure, Interactions, and Phase Separation Altered by Mutation and Arginine Methylation. *Mol Cell* 69, 465-479 e467.

Saha, S., and Hyman, A.A. (2017). RNA gets in phase. *J Cell Biol* 216, 2235-2237.

Saha, S., Weber, C.A., Nusch, M., Adame-Arana, O., Hoegge, C., Hein, M.Y., Osborne-Nishimura, E., Mahamid, J., Jahnel, M., Jawerth, L., *et al.* (2016). Polar Positioning of Phase-Separated Liquid Compartments in Cells Regulated by an mRNA Competition Mechanism. *Cell* 166, 1572-1584 e1516.

Scaramuzzino, C., Monaghan, J., Milioto, C., Lanson, N.A., Jr., Maltare, A., Aggarwal, T., Casci, I., Fackelmayer, F.O., Pennuto, M., and Pandey, U.B. (2013). Protein arginine methyltransferase 1 and 8 interact with FUS to modify its sub-cellular distribution and toxicity in vitro and in vivo. *PLoS One* 8, e61576.

Scekic-Zahirovic, J., Oussini, H.E., Mersmann, S., Drenner, K., Wagner, M., Sun, Y., Allmeroth, K., Dieterle, S., Sinniger, J., Dirrig-Grosch, S., *et al.* (2017). Motor neuron intrinsic and extrinsic mechanisms contribute to the pathogenesis of FUS-associated amyotrophic lateral sclerosis. *Acta Neuropathol* 133, 887-906.

Schindelin, J., Arganda-Carreras, I., Frise, E., Kaynig, V., Longair, M., Pietzsch, T., Preibisch, S., Rueden, C., Saalfeld, S., Schmid, B., *et al.* (2012). Fiji: an open-source platform for biological-image analysis. *Nat Methods* 9, 676-682.

Schwartz, J.C., Ebmeier, C.C., Podell, E.R., Heimiller, J., Taatjes, D.J., and Cech, T.R. (2012). FUS binds the CTD of RNA polymerase II and regulates its phosphorylation at Ser2. *Genes Dev* 26, 2690-2695.

Schwartz, J.C., Podell, E.R., Han, S.S., Berry, J.D., Eggan, K.C., and Cech, T.R. (2014). FUS is sequestered in nuclear aggregates in ALS patient fibroblasts. *Mol Biol Cell* 25, 2571-2578.

Schwartz, J.C., Wang, X., Podell, E.R., and Cech, T.R. (2013). RNA seeds higher-order assembly of FUS protein. *Cell Rep* 5, 918-925.

Seelaar, H., Kamphorst, W., Rosso, S.M., Azmani, A., Masdjedi, R., de Koning, I., Maat-Kievit, J.A., Anar, B., Donker Kaat, L., Breedveld, G.J., *et al.* (2008). Distinct genetic forms of frontotemporal dementia. *Neurology* 71, 1220-1226.

Seelaar, H., Klijnsma, K.Y., de Koning, I., van der Lugt, A., Chiu, W.Z., Azmani, A., Rozemuller, A.J., and van Swieten, J.C. (2010). Frequency of ubiquitin and FUS-positive, TDP-43-negative frontotemporal lobar degeneration. *J Neurol* 257, 747-753.

Sharma, A., Lyashchenko, A.K., Lu, L., Nasrabady, S.E., Elmaleh, M., Mendelsohn, M., Nemes, A., Tapia, J.C., Mentis, G.Z., and Shneider, N.A. (2016). ALS-associated mutant FUS induces selective motor neuron degeneration through toxic gain of function. *Nat Commun* 7, 10465.

Shelkovernikova, T.A., Robinson, H.K., Connor-Robson, N., and Buchman, V.L. (2013). Recruitment into stress granules prevents irreversible aggregation of FUS protein mislocalized to the cytoplasm. *Cell Cycle* 12, 3194-3202.

Shelkovernikova, T.A., Robinson, H.K., Troakes, C., Ninkina, N., and Buchman, V.L. (2014). Compromised paraspeckle formation as a pathogenic factor in FUSopathies. *Hum Mol Genet* 23, 2298-2312.

Shen, E., Henry, M., Weiss, V., Valentini, S., Silver, P., and Lee, M. (1998). Arginine methylation facilitates the nuclear export of hnRNP proteins. *Genes Dev* 12, 679-691.

Shin, Y., and Brangwynne, C.P. (2017). Liquid phase condensation in cell physiology and disease. *Science* 357.

- Shorter, J. (2017). Liquidizing FUS via prion-like domain phosphorylation. *EMBO J* 36, 2925-2927.
- Snowden, J.S., Hu, Q., Rollinson, S., Halliwell, N., Robinson, A., Davidson, Y.S., Momeni, P., Baborie, A., Griffiths, T.D., Jaros, E., *et al.* (2011). The most common type of FTL-D-FUS (aFTLD-U) is associated with a distinct clinical form of frontotemporal dementia but is not related to mutations in the FUS gene. *Acta Neuropathol* 122, 99-110.
- Suarez-Calvet, M., Neumann, M., Arzberger, T., Abou-Ajram, C., Funk, E., Hartmann, H., Edbauer, D., Kremmer, E., Gobl, C., Resch, M., *et al.* (2016). Monomethylated and unmethylated FUS exhibit increased binding to Transportin and distinguish FTL-D-FUS from ALS-FUS. *Acta Neuropathol* 131, 587-604.
- Sun, S., Ling, S.C., Qiu, J., Albuquerque, C.P., Zhou, Y., Tokunaga, S., Li, H., Qiu, H., Bui, A., Yeo, G.W., *et al.* (2015). ALS-causative mutations in FUS/TLS confer gain and loss of function by altered association with SMN and U1-snRNP. *Nat Commun* 6, 6171.
- Sun, Z., Diaz, Z., Fang, X., Hart, M.P., Chesi, A., Shorter, J., and Gitler, A.D. (2011). Molecular determinants and genetic modifiers of aggregation and toxicity for the ALS disease protein FUS/TLS. *PLoS Biol* 9, e1000614.
- Tan, A.Y., and Manley, J.L. (2009). The TET family of proteins: functions and roles in disease. *J Mol Cell Biol* 1, 82-92.
- Tan, A.Y., Riley, T.R., Coady, T., Bussemaker, H.J., and Manley, J.L. (2012). TLS/FUS (translocated in liposarcoma/fused in sarcoma) regulates target gene transcription via single-stranded DNA response elements. *Proc Natl Acad Sci U S A* 109, 6030-6035.
- Tang, J., Frankel, A., Cook, R.J., Kim, S., Paik, W.K., Williams, K.R., Clarke, S., and Herschman, H.R. (2000). PRMT1 Is the Predominant Type I Protein Arginine Methyltransferase in Mammalian Cells. *Journal of Biological Chemistry* 275, 7723-7730.
- Tanikawa, C., Ueda, K., Suzuki, A., Iida, A., Nakamura, R., Atsuta, N., Tohnai, G., Sobue, G., Saichi, N., Momozawa, Y., *et al.* (2018). Citrullination of RGG Motifs in FET Proteins by PAD4 Regulates Protein Aggregation and ALS Susceptibility. *Cell Rep* 22, 1473-1483.
- Thandapani, P., O'Connor, T.R., Bailey, T.L., and Richard, S. (2013). Defining the RGG/RG motif. *Mol Cell* 50, 613-623.
- Tradewell, M.L., Yu, Z., Tibshirani, M., Boulanger, M.C., Durham, H.D., and Richard, S. (2012). Arginine methylation by PRMT1 regulates nuclear-cytoplasmic localization and toxicity of FUS/TLS harbouring ALS-linked mutations. *Hum Mol Genet* 21, 136-149.
- Traut, T.W. (1994). Physiological concentrations of purines and pyrimidines. *Mol Cell Biochem* 140, 1-22.
- Tripsianes, K., Madl, T., Machyna, M., Fessas, D., Englbrecht, C., Fischer, U., Neugebauer, K.M., and Sattler, M. (2011). Structural basis for dimethylarginine recognition by the Tudor domains of human SMN and SPF30 proteins. *Nat Struct Mol Biol* 18, 1414-1420.
- Troakes, C., Hortobagyi, T., Vance, C., Al-Sarraj, S., Rogelj, B., and Shaw, C.E. (2013). Transportin 1 colocalization with Fused in Sarcoma (FUS) inclusions is not characteristic for amyotrophic lateral sclerosis-FUS confirming disrupted nuclear import of mutant FUS and distinguishing it from frontotemporal lobar degeneration with FUS inclusions. *Neuropathol Appl Neurobiol* 39, 553-561.
- Tsai, W.C., Gayatri, S., Reineke, L.C., Sbardella, G., Bedford, M.T., and Lloyd, R.E. (2016). Arginine Demethylation of G3BP1 Promotes Stress Granule Assembly. *J Biol Chem* 291, 22671-22685.

Tsai, W.C., Reineke, L.C., Jain, A., Jung, S.Y., and Lloyd, R.E. (2017). Histone arginine demethylase JMJD6 is linked to stress granule assembly through demethylation of the stress granule nucleating protein G3BP1. *J Biol Chem*.

Tsuiji, H., Iguchi, Y., Furuya, A., Kataoka, A., Hatsuta, H., Atsuta, N., Tanaka, F., Hashizume, Y., Akatsu, H., Murayama, S., *et al.* (2013). Spliceosome integrity is defective in the motor neuron diseases ALS and SMA. *EMBO Mol Med* 5, 221-234.

Udagawa, T., Fujioka, Y., Tanaka, M., Honda, D., Yokoi, S., Riku, Y., Ibi, D., Nagai, T., Yamada, K., Watanabe, H., *et al.* (2015). FUS regulates AMPA receptor function and FTLD/ALS-associated behaviour via GluA1 mRNA stabilization. *Nat Commun* 6, 7098.

Uhlmann, T., Geoghegan, V.L., Thomas, B., Ridlova, G., Trudgian, D.C., and Acuto, O. (2012). A method for large-scale identification of protein arginine methylation. *Mol Cell Proteomics* 11, 1489-1499.

Urwin, H., Josephs, K.A., Rohrer, J.D., Mackenzie, I.R., Neumann, M., Authier, A., Seelaar, H., Van Swieten, J.C., Brown, J.M., Johannsen, P., *et al.* (2010). FUS pathology defines the majority of tau- and TDP-43-negative frontotemporal lobar degeneration. *Acta Neuropathol* 120, 33-41.

van Blitterswijk, M., DeJesus-Hernandez, M., and Rademakers, R. (2012). How do C9ORF72 repeat expansions cause amyotrophic lateral sclerosis and frontotemporal dementia: can we learn from other noncoding repeat expansion disorders? *Curr Opin Neurol* 25, 689-700.

van den Bogaart, G., Meinema, A.C., Krasnikov, V., Veenhoff, L.M., and Poolman, B. (2009). Nuclear transport factor directs localization of protein synthesis during mitosis. *Nat Cell Biol* 11, 350-356.

Van Langenhove, T., van der Zee, J., and Van Broeckhoven, C. (2012). The molecular basis of the frontotemporal lobar degeneration-amyotrophic lateral sclerosis spectrum. *Ann Med* 44, 817-828.

Vance, C., Rogelj, B., Hortobagyi, T., De Vos, K.J., Nishimura, A.L., Sreedharan, J., Hu, X., Smith, B., Ruddy, D., Wright, P., *et al.* (2009). Mutations in FUS, an RNA processing protein, cause familial amyotrophic lateral sclerosis type 6. *Science* 323, 1208-1211.

Vance, C., Scotter, E.L., Nishimura, A.L., Troakes, C., Mitchell, J.C., Kathe, C., Urwin, H., Manser, C., Miller, C.C., Hortobagyi, T., *et al.* (2013). ALS mutant FUS disrupts nuclear localization and sequesters wild-type FUS within cytoplasmic stress granules. *Hum Mol Genet* 22, 2676-2688.

Vanderweyde, T., Apicco, D.J., Youmans-Kidder, K., Ash, P.E.A., Cook, C., Lummertz da Rocha, E., Jansen-West, K., Frame, A.A., Citro, A., Leszyk, J.D., *et al.* (2016). Interaction of tau with the RNA-Binding Protein TIA1 Regulates tau Pathophysiology and Toxicity. *Cell Rep* 15, 1455-1466.

Vanderweyde, T., Yu, H., Varnum, M., Liu-Yesucevitz, L., Citro, A., Ikezu, T., Duff, K., and Wolozin, B. (2012). Contrasting pathology of the stress granule proteins TIA-1 and G3BP in tauopathies. *J Neurosci* 32, 8270-8283.

Vossenaar, E.R., Zendman, A.J., van Venrooij, W.J., and Pruijn, G.J. (2003). PAD, a growing family of citrullinating enzymes: genes, features and involvement in disease. *Bioessays* 25, 1106-1118.

Walport, L.J., Hopkinson, R.J., Chowdhury, R., Schiller, R., Ge, W., Kawamura, A., and Schofield, C.J. (2016). Arginine demethylation is catalysed by a subset of JmjC histone lysine demethylases. *Nat Commun* 7, 11974.

Wang, A., Conicella, A.E., Schmidt, H.B., Martin, E.W., Rhoads, S.N., Reeb, A.N., Nourse, A., Ramirez Montero, D., Ryan, V.H., Rohatgi, R., *et al.* (2018a). A single N-terminal phosphomimic disrupts TDP-43 polymerization, phase separation, and RNA splicing. *EMBO J*.

Wang, J., Choi, J.M., Holehouse, A.S., Lee, H.O., Zhang, X., Jahnel, M., Maharana, S., Lemaitre, R., Pozniakovskiy, A., Drechsel, D., *et al.* (2018b). A Molecular Grammar Governing the Driving Forces for Phase Separation of Prion-like RNA Binding Proteins. *Cell*.

Wang, J.T., Smith, J., Chen, B.C., Schmidt, H., Rasoloson, D., Paix, A., Lambrus, B.G., Calidas, D., Betzig, E., and Seydoux, G. (2014). Regulation of RNA granule dynamics by phosphorylation of serine-rich, intrinsically disordered proteins in *C. elegans*. *Elife* 3, e04591.

Wang, W.Y., Pan, L., Su, S.C., Quinn, E.J., Sasaki, M., Jimenez, J.C., Mackenzie, I.R., Huang, E.J., and Tsai, L.H. (2013). Interaction of FUS and HDAC1 regulates DNA damage response and repair in neurons. *Nat Neurosci* 16, 1383-1391.

Warda, A.S., Freytag, B., Haag, S., Sloan, K.E., Gorlich, D., and Bohnsack, M.T. (2016). Effects of the Bowen-Conradi syndrome mutation in EMG1 on its nuclear import, stability and nucleolar recruitment. *Hum Mol Genet* 25, 5353-5364.

Webby, C.J., Wolf, A., Gromak, N., Dreger, M., Kramer, H., Kessler, B., Nielsen, M.L., Schmitz, C., Butler, D.S., Yates, J.R., 3rd, *et al.* (2009). Jmjd6 catalyses lysyl-hydroxylation of U2AF65, a protein associated with RNA splicing. *Science* 325, 90-93.

Weber, S.C., and Brangwynne, C.P. (2012). Getting RNA and protein in phase. *Cell* 149, 1188-1191.

Wegmann, S., Eftekharzadeh, B., Tepper, K., Zoltowska, K.M., Bennett, R.E., Dujardin, S., Laskowski, P.R., MacKenzie, D., Kamath, T., Commins, C., *et al.* (2018). Tau protein liquid-liquid phase separation can initiate tau aggregation. *EMBO J*.

Wheaton, M.W., Salamone, A.R., Mosnik, D.M., McDonald, R.O., Appel, S.H., Schmolck, H.I., Ringholz, G.M., and Schulz, P.E. (2007). Cognitive impairment in familial ALS. *Neurology* 69, 1411-1417.

Winton, M.J., Igaz, L.M., Wong, M.M., Kwong, L.K., Trojanowski, J.Q., and Lee, V.M. (2008). Disturbance of nuclear and cytoplasmic TAR DNA-binding protein (TDP-43) induces disease-like redistribution, sequestration, and aggregate formation. *J Biol Chem* 283, 13302-13309.

Wisniewski, J.R., Hein, M.Y., Cox, J., and Mann, M. (2014). A "proteomic ruler" for protein copy number and concentration estimation without spike-in standards. *Mol Cell Proteomics* 13, 3497-3506.

Wolozin, B. (2012). Regulated protein aggregation: stress granules and neurodegeneration. *Mol Neurodegener* 7, 56.

Wooderchak, W.L., Zang, T., Zhou, Z.S., Acuna, M., Tahara, S.M., and Hevel, J.M. (2008). Substrate profiling of PRMT1 reveals amino acid sequences that extend beyond the "RGG" paradigm. *Biochemistry* 47, 9456-9466.

Yamaguchi, A., and Kitajo, K. (2012). The effect of PRMT1-mediated arginine methylation on the subcellular localization, stress granules, and detergent-insoluble aggregates of FUS/TLS. *PLoS One* 7, e49267.

Yamazaki, T., Chen, S., Yu, Y., Yan, B., Haertlein, T.C., Carrasco, M.A., Tapia, J.C., Zhai, B., Das, R., Lalancette-Hebert, M., *et al.* (2012). FUS-SMN protein interactions link the motor neuron diseases ALS and SMA. *Cell Rep* 2, 799-806.

Yang, L., Gal, J., Chen, J., and Zhu, H. (2014). Self-assembled FUS binds active chromatin and regulates gene transcription. *Proc Natl Acad Sci U S A* 111, 17809-17814.

Yang, L., Zhang, J., Kamelgarn, M., Niu, C., Gal, J., Gong, W., and Zhu, H. (2015). Subcellular localization and RNAs determine FUS architecture in different cellular compartments. *Hum Mol Genet* 24, 5174-5183.

- Yang, Y., and Bedford, M.T. (2013). Protein arginine methyltransferases and cancer. *Nat Rev Cancer* 13, 37-50.
- Yang, Z., and Klionsky, D.J. (2010). Eaten alive: a history of macroautophagy. *Nat Cell Biol* 12, 814-822.
- Yasuda, K., Clatterbuck-Soper, S.F., Jackrel, M.E., Shorter, J., and Mili, S. (2017). FUS inclusions disrupt RNA localization by sequestering kinesin-1 and inhibiting microtubule detyrosination. *J Cell Biol* 216, 1015-1034.
- Yasuda, K., Zhang, H., Loisel, D., Haystead, T., Macara, I.G., and Mili, S. (2013). The RNA-binding protein Fus directs translation of localized mRNAs in APC-RNP granules. *J Cell Biol* 203, 737-746.
- Yoneda, Y., Imamoto-Sonobe, N., Yamaizumi, M., and Uchida, T. (1987). Reversible inhibition of protein import into the nucleus by wheat germ agglutinin injected into cultured cells. *Exp Cell Res* 173, 586-595.
- Yoshizawa, T., Ali, R., Jiou, J., Fung, H.Y.J., Burke, K.A., Kim, S.J., Lin, Y., Peeples, W.B., Saltzberg, D., Soniat, M., *et al.* (2018). Nuclear Import Receptor Inhibits Phase Separation of FUS through Binding to Multiple Sites. *Cell* 173, 693-705.e622.
- Yu, Y., Chi, B., Xia, W., Gangopadhyay, J., Yamazaki, T., Winkelbauer-Hurt, M.E., Yin, S., Eliasse, Y., Adams, E., Shaw, C.E., *et al.* (2015). U1 snRNP is mislocalized in ALS patient fibroblasts bearing NLS mutations in FUS and is required for motor neuron outgrowth in zebrafish. *Nucleic Acids Res* 43, 3208-3218.
- Yu, Y., and Reed, R. (2015). FUS functions in coupling transcription to splicing by mediating an interaction between RNAP II and U1 snRNP. *Proc Natl Acad Sci U S A* 112, 8608-8613.
- Zhang, K., Donnelly, C.J., Haeusler, A.R., Grima, J.C., Machamer, J.B., Steinwald, P., Daley, E.L., Miller, S.J., Cunningham, K.M., Vidensky, S., *et al.* (2015). The C9orf72 repeat expansion disrupts nucleocytoplasmic transport. *Nature* 525, 56-61.
- Zhang, X., and Cheng, X. (2003). Structure of the Predominant Protein Arginine Methyltransferase PRMT1 and Analysis of Its Binding to Substrate Peptides. *Structure* 11, 509-520.
- Zhang, Z.C., and Chook, Y.M. (2012). Structural and energetic basis of ALS-causing mutations in the atypical proline-tyrosine nuclear localization signal of the Fused in Sarcoma protein (FUS). *Proc Natl Acad Sci U S A* 109, 12017-12021.
- Zhou, Y., Liu, S., Liu, G., Ozturk, A., and Hicks, G.G. (2013). ALS-associated FUS mutations result in compromised FUS alternative splicing and autoregulation. *PLoS Genet* 9, e1003895.
- Zu, T., Liu, Y., Banez-Coronel, M., Reid, T., Pletnikova, O., Lewis, J., Miller, T.M., Harms, M.B., Falchook, A.E., Subramony, S.H., *et al.* (2013). RAN proteins and RNA foci from antisense transcripts in C9ORF72 ALS and frontotemporal dementia. *Proc Natl Acad Sci U S A* 110, E4968-4977.
- Zurita Rendon, O., Silva Neiva, L., Sasarman, F., and Shoubbridge, E.A. (2014). The arginine methyltransferase NDUFAF7 is essential for complex I assembly and early vertebrate embryogenesis. *Hum Mol Genet* 23, 5159-5170.

7 PUBLICATION RECORD

Hofweber, M.*, Hutten, S.* , Bourgeois, B., Spreitzer, E., Niedner-Boblenz, A., Schifferer, M., Ruepp, M.-D., Simons, M., Niessing, D., Madl, T., *et al.* (2018). Phase Separation of FUS Is Suppressed by Its Nuclear Import Receptor and Arginine Methylation. *Cell* 173, 706-719.e713 #

* these authors contributed equally to this work

Elsevier holds the copyright (2018) for this article published in *Cell* and permits the usage of text and figures in this dissertation.

Mulholland, C.B., Smets, M., Schmidtman, E., Leidescher, S., Markaki, Y., **Hofweber, M.**, Qin, W., Manzo, M., Kremmer, E., Thanisch, K., *et al.* (2015). A modular open platform for systematic functional studies under physiological conditions. *Nucleic Acids Res* 43, e112.

Kruger, T., **Hofweber, M.**, and Kramer, S. (2013). SCD6 induces ribonucleoprotein granule formation in trypanosomes in a translation-independent manner, regulated by its Lsm and RGG domains. *Mol Biol Cell* 24, 2098-2111.

8 ACKNOWLEDGEMENT

First, I thank my supervisor Dr. Dorothee Dormann, for giving me the opportunity to join her lab for my Ph.D. studies. Furthermore, I am very grateful for her guidance as well as constant advice and support during my thesis. Moreover, I am very thankful for the chance to present our work at conferences.

I thank Dr. Saskia Hutten for the great teamwork for paper submission, sharing her knowledge and helpful discussions. Moreover, I am grateful for her assistance and patience in microscopy.

I also thank our collaborators: Prof. Dr. Tobias Madl, Dr. Benjamin Bourgeois, Prof. Dr. Dierk Niessing, Dr. Annika Niedner-Boblenz, Dr. Marc-David Ruepp, Prof. Dr. Mikael Simons, Dr. Martina Schifferer, and Emil Spreitzer for excellence communication, exchange of materials and collaboration.

I thank the members of my thesis advisory committee, Prof. Dr. Dr. h.c. Christian Haass and Prof. Dr. Axel Imhof for their time and helpful suggestions.

Furthermore, I thank all other past and present members of the Dormann lab for sharing protocols, helpful discussions, good lab spirit and celebrations. Special thanks goes to Dr. Helena Ederle for many happy conversations and sharing here experiences made during her Ph.D. studies.

I also thank Andrea Wilytsch and Ralf Bigiel, the good spirits of the department, for assistance in bureaucracy.

Finally, I thank my family, especially my parents, for their constant support and encouragement. Last but not least I thank my girlfriend Andrea for her support and enduring my moods.

9 EIDESSTATTLICHE VERSICHERUNG/AFFIDAVIT

Hiermit versichere ich an Eides statt, dass ich die vorliegende Dissertation "Pathomechanisms driving Phase Separation and Aggregation of the Fused in Sarcoma Protein in Neurodegenerative Diseases" selbstständig angefertigt habe, mich außer der angegebenen keiner weiteren Hilfsmittel bedient und alle Erkenntnisse, die aus dem Schrifttum ganz oder annähernd übernommen sind, als solche kenntlich gemacht und nach ihrer Herkunft unter Bezeichnung der Fundstelle einzeln nachgewiesen habe.

München, 06/12/2018

Mario Hofweber

I hereby confirm that the dissertation "Pathomechanisms driving Phase Separation and Aggregation of the Fused in Sarcoma Protein in Neurodegenerative Diseases" is the result of my own work and that I have only used sources or materials listed and specified in the dissertation.

Munich, 06/12/2018

Mario Hofweber

10 DECLARATION OF COPYRIGHT AND CONTRIBUTIONS

Mario Hofweber wrote the thesis text, performed most experiments and prepared most of the figures (see section “2 Results - Declaration of copyright and contributions by other researchers” for detailed listing of exceptions).

Munich, _____

Saskia Hutten, postdoctoral researcher in the research group of Dorothee Dormann, conducted and analyzed sedimentation assays, semi-permeabilized cell assays and cytosolic anchoring experiments (see section “2 Results - Declaration of copyright and contributions by other researchers” for detailed listing).

Munich, _____

Dorothee Dormann, supervisor and lab head, developed the design of the project and coordinated involved collaborators (*e.g.* communication with collaborators, exchange of recombinant proteins and expression vectors). Dorothee Dormann is furthermore the senior/corresponding author of the in parallel prepared and by now in *Cell* published study ‘Phase Separation of FUS Is Suppressed by Its Nuclear Import Receptor and Arginine Methylation’ based on the majority of the results presented in this Ph.D. thesis and therefore functions as a representative for contributing co-authors:

- 1) Benjamin Bourgeois and Emil Spreitzer who purified and provided recombinant TNPO1 and performed ITC and NMR experiments and corresponding analysis (see section “2 Results - Declaration of copyright and contributions by other researchers” for detailed listing).

- 2) Annika Niedner-Boblenz who performed and analyzed radioactive filter-binding assays and Electrophoretic Mobility Shift Assays (EMSA) (see section “2 Results - Declaration of copyright and contributions by other researchers” for detailed listing).
- 3) Martina Schifferer who performed TEM imaging (see section “2 Results - Declaration of copyright and contributions by other researchers” for detailed listing).

Munich,
